THERMOMECHANICAL PROCESSING OF IN 601 AND SS 304

Thesis

Submitted in partial fulfilment of the requirements for the degree of

Doctor of Philosophy

by

Preetish Crimson Dsilva

(MT13F05)

DEPARTMENT OF METALLURGICAL AND MATERIALS ENGINEERING

NATIONAL INSTITUTE OF TECHNOLOGY KARNATAKA SURATHKAL, MANGALORE – 575025

MAY 2024

DECLARATION

I hereby declare that the Research Thesis titled **"Thermomechanical Processing of IN 601 and SS 304"** which is being submitted to the **National Institute of Technology Karnataka, Surathkal** in partial fulfilment of the requirements for the award of the **Degree of Doctor of Philosophy** in **Department of Metallurgical and Materials Engineering**, is a bonafide report of the research work carried out by me. The material contained in this Research Thesis has not been submitted to any University or Institution for the award of any degree.

Register Number: **138033MT13F05**

Name of Research Scholar: **Preetish Crimson Dsilva**

Signature of the Research Scholar: 

Department of Metallurgical and Materials Engineering

Place: NITK, Surathkal

Date: 04-May-2024

CERTIFICATE

This is to certify that the Research Thesis titled **"Thermomechanical Processing of IN 601 and SS 304"** submitted by **Mr. Preetish Crimson Dsilva (138033MT13F05)** as the record of research work carried out by him, is accepted as the Research Thesis submission in partial fulfilment of the requirements for the award of degree of **Doctor of Philosophy.**

Research Guide

Dr. Subray R. Hegde

Professor

Chairman - DRPC

Department of Metallurgical and Materials Engineering

Date: 04-May-2024

Chairman - DRPC
Dept. of Metallurgical and Materials Engineering
National Institute of Technology Karntaka, Surathkal
Post Srinivasnagar, Mangaluru - 575 025
Karnataka, India

ACKNOWLEDGEMENT

I would like to extend my heartfelt gratitude to my research guide Dr. Subray R. Hegde, Associate Professor, Department of Metallurgical and Materials Engineering. His constant guidance, exposure to real life engineering problems and motivation to learn new things every day during this research work was exciting. He has been instrumental in defining the research work that focuses on industrial application. I shall be forever indebted to him. Thank you.

I would like to offer special thanks to my RPAC panel members Prof. Uday Bhat K. and Dr. Ramesh M. R. for their valuable suggestions and reviews given during my research work, which has helped me in providing better shape to the project.

I express my gratitude to former heads Prof. K Narayan Prabhu, Prof. Jagannath Nayak, Prof. Uday Bhat K., Prof. Anandhan Srinivasan, and current head Dr. Ravishankar K S, Department of Metallurgical and Materials Engineering, NITK, Surathkal for giving me an opportunity to take up the research work in the Department.

I would like to extend special gratitude to my colleague and team-mate Mr. Basavaraj for his special contribution to my research work and providing moral support during my research work. I thank Prof. Sushil Mishra of Department of Mechanical Engineering, IIT Bombay for permitting me to use their FESEM and EBSD facility and his team of Dr. Jitesh Vasavada and Mr. Satyaprakash for training/ helping me to operate the machine. I thank Prof. Narayan Prabhu for allowing me to use his facilities of thermocouples, microhardness tester. I am grateful to Prof. Uday Bhat K for TEM facility; Dr. Ravishankar for Tensile testing facility and Dr. Rahman for advanced XRD facility.

I owe my thanks to all staff members of the Department of Metallurgical and Material Engineering, especially to Mrs. Sharmila for her constant help in administrative and documentation works, Mr. Sundar, Mr. Dinesh, Mr. Ismail Sab Nadaf, Mr. Lokesh, Mr. Yashwanth, and Mr. Satish for assistance during my experimental work. I appreciate and thank all the teaching and non-teaching staff of the Department of Metallurgical and Materials engineering for their co-operation and help rendered during the research work.

I am grateful to my teammates Pavankumar Sondar, Rakshan J K and Ranjith for their support in experiments and discussions related to research work. I would like to thank my friends Dr. Prashanth Huilgol, Mr. Gurudath, Dr. Palaksha Acharya, Dr. Anjan B. N, Dr. Pavan Pujar, Dr. Prabhu Kumar and Dr. Jayalakhmi for their valuable support and suggestions.

Dedication

I dedicate this dissertation to my family. I love you deeply with all my heart. To my wife Evita, you have been a supporter of all my endeavors. Your partnership, steadfastness, and love sustain me. Thank you for your patience as I pursued and completed this degree. To my parents, thank you for your constant support, encouragement, and belief in me during my doctoral research work. Love you all.

ABSTRACT

Present study investigates isothermal annealing behaviour of prior-cold-worked Inconel 601 (aka, IN 601) and Stainless-Steel 304 (aka, SS 304) sheets. The study comprehensively covers the annealing response of the materials over wide cold-reduction and temperature ranges. Using structural characterization and mechanical testing, the study tracks strain-hardening, strain-aging, recovery, and recrystallization stages of the sheets as a function of degree of cold-reduction and annealing temperature. By tracking the thermomechanical behaviour of the experimental materials, the study searches the possibility of producing fine-elongated grains in recrystallized-form such that the creep-resistance of wrought alloys should improve without compromising on the strength, toughness, and fatigue-resistance.

Using X-Ray diffraction analysis, hardness measurements, and tensile tests, the study reveals that, irrespective of the degree of cold-reduction, both IN 601 and SS 304 consistently exhibit strain-aging during low-temperature exposures as the experimental-results confirm that the prior-coldworked sheets display non-monotonic increasing-decreasing trend in hardness and strength with increased annealing temperature. The investigation reveals that the 'recovery-stage' is preceded by 'strain-aging-stage' during which the alloys exhibit superior strength and hardness than the strain-hardened and recovered states. Discontinuous-yielding observed during the loading-unloading type tensile tests suggest that the peak-hardening due to strain-aging during low-temperature annealing is likely caused by dislocation-pinning of interstitial carbon. Based on the thermomechanical experimental-results, the current work proposes a thermomechanical processing map for each alloy that integrates 'strain-hardening' and 'strain-aging' stages with 'recovery' and 'recrystallization' stages.

Additionally, microstructural analysis and SEM-EBSD analysis presented in this work indicate that, by suitably controlling strain-hardening and the recrystallization-annealing, a refined microstructure comprising high aspect-ratio grains having high-angle grain-boundaries can be obtained in IN 601 sheets that may improve both fatigue and creep properties. However, SS 304 does not form elongated grains during the

recrystallization likely due to the low stacking fault energy of the material that promotes twinning and leads to formation of polygonal equiaxed grains.

Keywords: IN 601; SS 304; sheet-metal; strain-aging; recrystallization; elongated grains.

CONTENTS

1. INTRODUCTION 1

2. LITERATURE REVIEW 5

2.1 Thermomechanical Processing 6

2.2 Strain-Aging Phenomena 8

2.3 Effect of Grain Size on Mechanical Properties 9

2.4 Effect of Grain-Size on Creep-Behaviour 10

2.5 Effect of Grain-Shape on Creep-Behaviour 13

2.5.1 Thoria Dispersed Nickel Alloys 14

2.5.2 Zirconia Grain Stabilized (ZGS) Platinum 15

2.5.3 Dispersion Hardened Platinum (DPH) 16

2.6 Superalloy Inconel 601 16

2.7 Austenitic Stainless Steels 18

2.7.1 Martensitic Transformation of ASSs 19

2.7.2 Influence of SFE in Plastic-Deformation of ASSs 20

2.7.3 Types of SIM and Mechanism 23

2.7.4 Factors influencing the amount of Martensite formed during Cold Rolling 24

2.7.5 Effect of SIM on Mechanical Property 25

2.7.6 Low-Temperature Hardening of ASSs 26

2.7.7 Martensite-Reversion 27

2.7.8 Recovery and Recrystallization 28

2.7.9 Summary 29

3. PROPOSED WORK 31

3.2 Ideation 32

3.3 Research Objectives 33

4. MATERIALS AND METHODS 35
5. RESULTS AND DISCUSSION OF IN 601 41
5.1 Effect of Cold-Reduction 41
5.2 Effect of Annealing 45
5.3. Discussion 54
6. RESULTS AND DISCUSSION OF SS 304 59
6.1 Effect of Cold-Reduction 59
6.2 Effect of Annealing 63
6.3 Discussion 78
7. SUMMARY AND CONCLUSION 81
REFERENCES 85
PUBLICATIONS 95
BIODATA 97

List of Figures

Figure 2.1: Schematic Deformation Mechanism Map of a metallic material. 12
Figure 2.2: Deformation mechanism map of Ni-based superalloy, MAR-M200 12
Figure 2.3: Effect of grain aspect ratio (GAR) in oxide dispersion strengthened nickel alloys at 1093°C: (a) yield-strength; (b) 100 h rupture stress; (c) stress for minimum creep-rate of $l0^{-4}$ /h 15
Figure 2.4: Variation of fracture mode with GAR in MA 6000 nickel alloy creep tested at 950°C under 230 MN/m^2 15
Figure 2.5: High Temperature service temperatures for heat resistant metals, based on 100 hr stress rupture strength 17
Figure 2.6: Time-temperature-transformations in ASSs for various heat treatments between room temperature and melting point 20
Figure 2.7: Variation of martensite formation with temperature and true strain for 304. 24
Figure 2.8: Stability of SIM for different temperatures 28
Figure 3.1: Schematic of; a) fine-equiaxed grains, b) coarse-equiaxed grains, c) elongated grains. 32
Figure 5.1: Longitudinal microstructures of IN 601 sheets showing flattening of equiaxed grains during cold-rolling; (a) as-annealed, (b) 50% cold-rolled, and (b) 80% cold-rolled. 41
Figure 5.2: Curves showing variations in, (a) grain aspect ratio, and (b) hardness, of cold-rolled IN 601 sheets with an increase in the cold-reduction. 42
Figure 5.3: XRD profiles of as-annealed and cold-rolled IN 601 sheets showing significant variations in the relative peak-intensities with increased cold-reduction. . 42
Figure 5.4: IPF maps of IN 601 sheets for: a) 0%, b) 10%, c) 30%, d) 50%, and e) 70% cold-reduction, showing crystallographic-orientations relative to Rolling Direction (RD) and Transverse Direction (TD). 43
Figure 5.5: EBSD rotation-angle map of: a) 30%, and b) 50% cold-reduced sheets showing increased high-angle (> 15°) rotation with increased cold-reduction. 44

Figure 5.6: Tensile behaviour of cold-rolled IN 601 sheets along the rolling direction. 45
Figure 5.7: Longitudinal microstructures (500X) of cold-rolled and isothermally annealed IN 601 sheets; the microstructural variation is presented as a matrix with cold-reductions (10% - 80%) arranged along rows and annealing temperatures ($0.4T_m$ - $0.8T_m$) as columns. 46
Figure 5.8: Hardness variations of cold-rolled IN 601 sheets with annealing temperature. 47
Figure 5.9: Tensile behaviour of 30%, 50% and 70% cold-rolled IN 601 after isothermal-annealing at $0.4T_m$, $0.5T_m$, $0.6T_m$, $0.7T_m$, and $0.8T_m$ 50
Figure 5.10: Mechanical behaviour of cold-rolled IN 601 as a function of annealing temperature. 51
Figure 5.11: XRD profiles of 10%, 30%, 50% and 70% cold-rolled IN 601 sheets after isothermal annealing at (a) $0.4T_m$, (b) $0.5T_m$, (c) $0.7T_m$, and (d)$0.8T_m$. 52
Figure 5.12: IPF maps of: a) 50%, b) 70%, and c) 80% reduced sheets following $0.7T_m$ annealing. 53
Figure 5.13: Grain boundary maps of: a) 50%, and d) 80% reduced sheets following $0.7T_m$ annealing. 54
Figure 5.14: Stress-Strain curve of $0.6T_m$ and $0.7T_m$ exposed specimen showing discontinuous yielding. 55
Figure 5.15: Thermomechanical Processing Map of IN 601. 57
Figure 6.1: Longitudinal microstructures of IN 601 sheets showing flattening of equiaxed grains during cold-rolling; (a) as-annealed, (b) 50% cold-rolled, and (b) 70% cold-rolled. 59
Figure 6.2: Curves showing variations in, (a) grain aspect ratio, and (b) hardness, of cold-rolled SS 304 sheets with increasing degree of cold reduction. 60
Figure 6.3: XRD profiles of as-received and 10% to 70% cold-reduced SS 304 showing crystallographic texturing and increased SIM with increased reduction. 61
Figure 6.4: IPF maps of SS 304 sheets cold-rolled to: a) 30%, b) 50%, and c) 70%, showing crystallographic-orientations relative to Rolling Direction (RD) and Transverse Direction (TD). 62

Figure 6.5: EBSD Phase Fraction Maps of cold-rolled SS 304 sheets showing increased SIM with increased reduction; a) 30%, b) 50%, and c) 70%. 63
Figure 6.6: Microstructural matrix of SS 304 that is cold rolled by 10 % to 70 % reductions (shown in rows) followed by isothermal annealing for 1 hour at 0.3Tm to 0.7Tm (shown in columns). 65
Figure 6.7: Hardness-profiles of cold-rolled SS 304 sheets with annealing temperature. 66
Figure 6.8: Engineering stress-strain curves of 10% and 30% reduced SS 304 after annealing at various temperatures; AR refers to as-rolled. 68
Figure 6.9: Engineering Stress-strain curves of 50% and 70% reduced SS 304 after annealing at various temperatures; AR refers to as-rolled. 69
Figure 6.10: Mechanical properties of cold-rolled and annealed SS 304: a) hardness, b) tensile strength, c) ductility, and d) yield strength. 70
Figure 6.11: XRD profiles of 10%, 30%, 50%, and 70% deformed SS 304 sheets; a) before annealing, and b) after annealing at $0.3T_m$. 71
Figure 6.12: XRD profiles of 10%, 30%, 50%, and 70% deformed SS 304 sheets; a) before annealing, and b) after annealing at $0.3T_m$. 72
Figure 6.13: Gaussian α′ phase-fraction profiles of SS 304. 73
Figure 6.14: EBSD Phase Fraction Maps of SS 304 sheets that are cold-rolled to: 30%, 50%, and 70% (a, b, and c), followed by annealing at $0.3T_m$ (d, e, and f) and $0.6T_m$ (g, h, and i) showing strain-induced martensitic transformation and reversion. 75
Figure 6.15: EBSD IPF Maps of 10%, 30%, 50% and 70% cold-rolled SS 304 that are annealed at room temperature (as-rolled), $0.3T_m$, and $0.6T_m$; cold-reductions are arranged as rows and annealing temperatures are arranged as columns; (RD, TD) rolling and transverse directions. 76
Figure 6.16: Thermomechanical Processing Map of SS 304. 79

List of Tables

Table 2.1: Chemical composition and SFE of some ASSs (Padilha et al., 2003). 22
Table 4.1: Chemical composition of SS 304 and IN 601 (in wt. %). 37
Table 4.2: Experimental-Matrix for thermomechanical processing of IN 601, SS 304 sheets. 38
Table 5.1: Mechanical properties of cold-worked IN 601 sheets. 45
Table 6.1: Gaussian α′ phase-fraction (%) analysis of as-rolled and annealed SS 304. 73
Table 6.2: EBSD Phase fraction (%) analysis of α′-martensite in cold-rolled and annealed SS 304. 77

NOMENCLATURE

PDAS	Primary Dendrite Arm Spacing
SDAS	Secondary Dendrite Arm Spacing
DS	Directionally Solidified
GAR	Grain Aspect Ratio
BCC	Body Centred Cubic
HCP	Hexagonal Close Packed
FCC	Face Centred Cubic
ODS	Oxide Dispersion Strengthened
ZGS	Zirconia Grain Stabilized Platinum
DPH	Dispersion Hardened Platinum
IN	Inconel
SS	Stainless Steel
SEM	Secondary Electron Microscope
EDS	Energy Dispersive X-Ray Spectroscopy
XRD	X-Ray Diffraction
EBSD	Electron Back Scatter Diffraction
ASS	Austenitic Stainless Steel
SFE	Stacking Fault Energy
SIM	Strain Induced Martensite
M_d	Deformation Temperature
M_s	Austenite to Martensite transformation temperature.
γ	Austenite
MC	Metal carbide
α'	BCC Martensite
ε	HCP Martensite
TMP	Thermomechanical Processing
T_m	Homologous Melting temperature (K)
TEM	Transmission Electron Microscope
HV	Vickers Micro-Hardness
IPF	Inverse Pole Figure

1. INTRODUCTION

This chapter provides a broad overview of structure-property correlations of structural metallic materials and eventually converges to thermomechanical processing for controlling the microstructure of wrought alloys in achieving superior strength, fatigue-resistance, creep-resistance. Thus, the chapter provides relevant context to the research problem and establishes the aim of the research work.

Mechanical properties of structural engineering materials are influenced in general by four levels of structures, viz., atomic structure, crystal structure, microstructure, and macrostructure. Arguably, the microstructure imposes the greatest influence on the properties of wrought materials that form the major constituent of vast variety of engineering structures. The cost, quality, fabrication, performance, and service-life of the components used in structural applications are highly influenced by the microstructure. It is generally known that microstructure greatly dictates structural strength of an engineering material. However, it is important to note that microstructure influences both static and dynamic mechanical properties of any engineering material. Strength, hardness, ductility, and toughness are key static mechanical properties as they are measures of materials' instantaneous responses to external loading.

Fatigue-resistance and creep-resistance are considered dynamic properties as these are measures of delayed responses to applied loading and the loading can be static or dynamic in nature. In general, the fatigue-strength, along with static-strength, ductility, and toughness, can be improved by refining the microstructure with fine-equiaxed grains. However, creep is a time dependant deformation phenomenon that becomes active when the materials operate at elevated temperatures. Traditionally, grain-coarsening heat-treatment is applied to improve the creep-resistance of wrought-alloys while columnar-grains along the stress-axis are produced by directional-solidification of cast-alloys. The objective here is to minimize the transverse grain-boundaries in the components considering that the in-service diffusional-creep is a grain-boundary phenomenon. The idea of minimizing the grain-boundaries for achieving superior creep resistance is extended to eliminate the grain-boundaries altogether. Such an idea is successfully adopted in developing single-crystal turbine blades for jet-engines. Thus,

microstructure needs to be suitably engineered for structures depending on type of loading, loading-cycles, thermal-cycles, operating-environment, operating-temperature, duration of service, etc. Common microstructural-features of wrought materials include grains, grain boundaries, a continuous primary-phase called matrix, secondary strengthening phases such as, in-situ formed intermetallic precipitates, externally added hard particle dispersions, etc., and tertiary phases in the form of unwanted inclusions that are trapped within the matrix during manufacturing processes. Of all these, a striking microstructural-feature of a wrought-material is polycrystalline grains. These grains are essentially fine crystals formed by the nucleation of atomic clusters of unit cells that grow crystallographically in three dimensions during mechanical-processing or melt-processing. It is important to recognise here that each grain is a single crystal with orthotropic properties. However, a wrought polycrystalline material possesses large number of fine grains arranged randomly and thus assuming average isotropic properties in bulk. As two adjacent grains possess two different crystallographic-orientations, an internal-surface or interface is naturally formed between them in the form of grain boundaries. These boundaries between adjacent grains, in fact, is a crystallographic defect having three-dimensional surface features.

Often, grain-boundaries are considered mechanically weak and energetically active regions and are preferentially attacked when a metallographic specimen is chemically or electrochemically etched. When observed under metallurgical microscope, grains appear as crystallites with distinctly visible grain-boundaries. Thus, shape and size of grains can be easily observed, quantified, and correlated with the gross mechanical properties of the materials. For instance, the wrought materials used for general structural applications possess uniform granular microstructure whose grains are equiaxed in shape and typically 5-50 μm in size. Within this range it is well-established by Hall-Petch relationship that grain-size has an inverse relationship with the structural-strength. In other words, the finer the grains the stronger the material. Additionally, it is also known that chemically homogeneous and fine-uniform microstructure imparts superior toughness and fatigue-resistance to the structural materials. The concept of grain-refinement is greatly applied in designing wrought-processes in various forms to produce strong structural components that can be used to build superior engineering structures (Dieter and Bacon 1988; Morris 2001; Lasalmonie and Strudel 1986).

However, cast-materials typically possess coarse unequiaxed grains made of dendrite-colonies with significant compositional-heterogeneity between the dendrite-cores and inter-dendritic regions. Their grain-size may vary from few microns to few inches depending on the processing parameters and component dimensions. For cast-materials, compositional-homogeneity, shapes of dendritic grains, orientations of grain-boundaries, and nature of secondary phases, strongly influence mechanical properties rather than mere grain-size.

In particular, fineness and orientations of dendrites are important parameters for the structure-property correlations. While crystallographic orientation of a dendrite is expressed relative to the direction of the stress-axis, dendritic-features are quantified in terms of primary and secondary dendrite arm spacing (PDAS, SDAS). It is not uncommon to correlate SDAS with the gross tensile strength of a conventionally-cast (CC) structure. For improving the creep-resistance of cast-alloys, directionally solidified (DS) and single-crystal (SX) structures are successfully developed and used in gas-turbines. In fact, for advanced meso-mechanics based prognostic methodologies, microstructural features such as, shape, size volume fraction, and distribution of trans-granular and intergranular hard particles/precipitates, are suitably used along with grain-size, grain-shape, grain-orientation, and dendritic features. For the assessment of property-performance-life of the materials used in critical applications such as, hot-sections of jet engines, these microstructural-features are extensively used as key-parameters.

The above description provides a general understanding of microstructures and importance of microstructural engineering in advanced structural materials that operate in arduous conditions. Interestingly enough, in most part, the microstructural details discussed above confined to advanced cast-structures. For wrought-structures, thus far, grain-size has been the most important microstructural feature. Major research and development efforts of wrought-alloys across the globe generally directed towards grain-refinement for achieving superior strength and improving other room-temperature mechanical properties. Irrespective of the processing methodologies used, microstructural-engineering of wrought-alloys is heavily focused at reducing the grain-size. Fine-grained materials are proven to improve static-strength and fatigue-resistance especially for structures that operate at ambient-temperature. However, for structures

that operate at elevated-temperatures, coarser grains aid creep-resistance and hence help in extending the service-life.

In fact, engineering developments in controlling the grain-shape in DS and SX structures has been a break-through in the gas turbine industry as they significantly improve the performance and service-lives of critical components. Yet, the very concept of property-improvement by controlling the 'grain-shape' rather than 'grain-size' is either ignored or less-attended for wrought materials. This research-work intends to explore that research space by keenly studying the thermomechanical processing of wrought-alloys. As the first step, this work tracks the static-recrystallization behaviour of two commercially important alloys by thermomechanically processing them over wide ranges of cold-reduction and annealing temperatures. Using suitable testing and characterization methods, this work introduces 'thermomechanical processing maps' that show various regimes of metallurgical phenomena. Thus, the work explores the possibility of controlling the shape of the grains in wrought materials by scanning thermomechanical processing parameters to produce fine-elongated grains having high grain aspect ratio (GAR) in recrystallized form for improving the creep-properties relative to their equiaxed counterparts. In other words, this work aims at comprehensively understanding the metallurgical phenomena occurring during the thermomechanical processing, and searches for an opportunity to design elongated-recrystallized grains in wrought-alloys analogous to the columnar-grains in directionally solidified cast-alloys.

2. LITERATURE REVIEW

This section provides an overview of structure-property correlation, influence of grain morphology, and effect of cold-working followed by annealing. The section provides the effect of grain-size and grain-shape and past attempts in modifying the grain-shape to improve the creep resistance of high temperature materials. Specific details of thermomechanical processing and associated transformations are also provided for stainless steels and IN 601.

Mechanical properties of structural metallic-materials are directly influenced by the chemical-composition, crystal-structure, microstructure, grain-size, presence and distribution of secondary and tertiary phases, etc. Altering the chemical-composition by alloying with substitutional or interstitial solutes can cause solid-solution strengthening and precipitation-hardening. Thus, properties of a structural material can be optimized by limiting the fractions of alloying-elements. This way, several grades of materials are designed for constructing engineering structures that would operate at given conditions for required applications. Crystal-structure plays a crucial role in the mechanical behaviour of a material. Materials with body-centred cubic (BCC), face-centred cubic (FCC), and hexagonal close-packed (HCP) crystal structures exhibit different mechanical behaviours. Owing to higher active slip systems, FCC materials often have good ductility, while BCC metals tend to be stronger, and HCP materials are less ductile. Thus, crystallographic arrangement of atoms influences materials properties. Typically, heat-treatments involve solid-state phase-transformations to obtain suitable crystal-structures for inducing required properties (Heckel 1997; Verlinden et al. 2007).

Crystallographic defects such as, vacancies, dislocations, stacking-faults, twins, and grain-boundaries inherently influence the mechanical behaviour of materials(Clemens and Scheu 2008). A combination of thermal-processing and mechanical-processing is widely used for altering the crystal-structure and designing the microstructure for realizing required properties. Traditionally, cold-working followed by recrystallization-annealing or hot-working is adapted for designing suitable microstructure in wrought-materials. The former causes static-recrystallization while the later causes dynamic-recrystallization in the materials and hence refined microstructure with compositional-

homogeneity and uniform grain-size is obtained. Recently, severe plastic deformation (SPD) is being tried out to produce ultra-fine grains in metallic materials for gaining superior strength. Thus, required properties are obtained by designing required crystal-structure and microstructure by optimizing the thermomechanical processing and hence a structure-property correlation is established for each material (Segal 2005; Verlinden et al. 2007).

2.1 Thermomechanical Processing

Thermomechanical processing is a manufacturing method that combines temperature and mechanical deformation to shape engineering structures. It finds widespread application in processing metals and alloys. By precisely controlling deformation and heat-treatment, this technique strives to attain accurate microstructures and mechanical properties. With its adaptability, thermomechanical processing customizes materials properties to match specific requirements of applications. Through meticulous design of plastic-deformation, processing-temperature, and cooling parameters, manufacturers attain suitable mechanical properties in billets, bars, tubes, channels, sheets, wires, other industrial structures. This processing in general referred to as wrought-processing and the materials used are referred to as wrought-materials (Babu 2022).

Cold-Working techniques including, forming, rolling, forging, drawing, extrusion, etc., profoundly influence the mechanical properties. Cold-Rolling is a mechanical processing method of materials performed below the recrystallization temperature. The cold-rolling process modifies the microstructure by elongating and aligning grains along the rolling direction. This results in property variations across different orientations. Just like any other cold-working process, cold-rolling increases the dislocation density within the grains, which hinder the movement of other dislocations. Consequently, this leads to increased strength and hardness. Moreover, cold rolling can induce specific crystallographic orientations, yielding a textured microstructure. This texture influences material anisotropy and properties along distinct crystallographic axes (Mittemeijer 2011; Verlinden et al. 2007).

Cold-Rolling significantly amplifies the yield strength, tensile strength, and hardness due to increased dislocation density and pile-up, networking, and kink-formation of dislocations. This results from both grain boundary strengthening and work hardening.

However, while it increases the strength, it often diminishes ductility. Residual stresses arise from cold rolling and can influence materials behaviour during subsequent processing or service(Wang and Gong 2002). Furthermore, the increased dislocation density and grain deformation bolster hardness, rendering the material more resilient against indentation and wear. However, excessive cold rolling can exacerbate brittleness, especially in materials with limited ductility, potentially causing cracking and fracture (Verlinden et al. 2007).

For general metallic materials, it is well established that cold-working increases strength due to a phenomenon called strain-hardening. This involves the accumulation of energy within the material in the form of internal stress-fields due to the presence of dislocations. As the cold-reduction process intensifies, there is a greater multiplication, interconnection, and accumulation of these dislocations, resulting in higher internal stresses. Consequently, the hardness and strength are enhanced through strain-hardening. When a strain-hardened material is exposed to elevated temperatures, a series of changes occurs. These include recovery, recrystallization, and grain growth, driven by the thermodynamic aim of reducing internal energy. Annealing provides the necessary thermal activation for these processes. Consequently, hardness and strength would decrease with increasing annealing-time and annealing-temperature. During the recovery stage, a minor reduction in hardness might be observed due to annihilation of dislocations. Subsequently, a significant decline in both hardness and strength is expected during the recrystallization phase due to the formation of new stress-free grains. If the alloy is exposed to higher temperatures or held at the recrystallization temperature for an extended period, a further deterioration in mechanical properties is likely due grain-coarsening. This way, thermomechanical processing brings in changes in the internal structure and corresponding change in the properties. While cold-working followed by annealing can cause static recrystallization, simultaneous application of heating and deformation in hot-working can cause dynamic-recrystallization. Thus, the final microstructure of the materials can be tailored by properly sequencing and controlling the thermomechanical processing parameters (Mittemeijer 2011; Semiatin. S. L. 2005; Verlinden et al. 2007).

2.2 Strain-Aging Phenomena

Cotrell and Bilby introduced the notion of "Atmosphere" in 1949 to elucidate the role of impurities in the plastic deformation of alloys (Cottrell and Bilby 1949). This concept, later termed the "Cottrell Atmosphere," describes a small cluster of impurity atoms enveloping dislocations within crystals. Impurity atoms, particularly interstitials such as carbon, nitrogen, and boron segregate near dislocation, driven by the stress-field generated by the dislocations. Consequently, this stress-induced segregation of impurity atoms around dislocations results in the creation of the Cottrell atmosphere. This Cottrell Atmosphere significantly influences the mechanical properties as these clusters hinder the movement of dislocations during thermomechanical processing (Mittemeijer 2011). This phenomenon is referred to as strain-aging. During hot-working, the continuous deformation and immobilization of newly formed dislocations by impurity atoms are known as the Portevin-LeChatelier (PLC) effect (Mittemeijer 2011; Verlinden et al. 2007). This causes serration in the stress-strain curves and the phenomenon is referred to as dynamic strain aging. Various studies have documented instances of dynamic strain aging in different grades of steel, both at high and low temperatures. Notably, interactions between carbon and chromium at high temperatures and carbon and nickel at low temperatures have been observed (Hall 1970).

The impact of dynamic strain aging becomes evident through discontinuous plastic flow during deformation at specific temperature and strain rate ranges (Hähner 1993; Hähner and Rizzi 2003). Low-temperature dynamic strain aging occurs at temperatures below 400 K and is characterized by the serrated yield behavior observed during slow-rate tensile testing (Hänninen et al. 2003; Singh and Sahu 2019; Sourabh and Singh 2022). Reports indicate that static strain aging in pipeline steel occurs when pre-strained (less than 5% cold rolled) steel is heated at around 400 K, leading to serrated yield behavior during room temperature tensile tests (Lee et al. 2018; Zhao et al. 2012). This finding corroborates the connection between strain aging and the Cottrell atmosphere formed at low temperatures. Similar aging phenomena have been observed in various stainless steels and some superalloys, attributed to the presence of the Cottrell atmosphere (Koyama et al. 2013; Stewart and Jonas 2004; Wesselmecking et al. 2022). Subsequent research after Cotrell's original work provided further evidence for this phenomenon. Given that the phenomenon operates at the atomic level, advanced

techniques such as atomic probe tomography have been employed to visually confirm the existence of the atmosphere (Aboulfadl et al. 2015).

2.3 Effect of Grain Size on Mechanical Properties

It is well-established that key mechanical properties such as, strength, hardness, ductility, toughness, ductile-to-brittle transition, fatigue-strength, and creep-behaviour of polycrystalline wrought materials are all influenced by grain-size(Ahmad and Channa 2013; Lasalmonie and Strudel 1986). The stress-strain behaviour of these materials is directly correlated with the grain-size. A general understanding from this correlation is that the finer the grains the stronger the material.

A general relationship between the yield-strength and average grain-size of a material is expressed using the famous Hall-Petch equation. This relationship suggests that, over the range of conventional grain-sizes (5-100 μm), the yield strength of a polycrystalline material increases with the reciprocal root of the grain size as expressed below (Morris 2001; Lasalmonie and Strudel 1986)

$$\boldsymbol{\sigma_y = \sigma_o + kd^{-1/2}} \tag{2.1}$$

where, $\boldsymbol{\sigma_y}$ is the yield-strength, $\boldsymbol{\sigma_o}$ is the frictional stress representing the overall resistance of the crystal lattice to dislocation motion, **k** is the locking parameter or strengthening coefficient which measures the relative hardening contribution of the grain boundaries, and **d** is the average grain-size.

The Hall-Petch relationship is effectively utilised in suitably adjusting the grain-size for a given application (Dieter and Bacon 1988). From the above relationship, it is clear that grain-refinement improves the tensile behaviour of materials. In fact, grain refinement is an effective and economical strengthening mechanism of structural materials. In addition to the yield-strength, grain refinement improves various other mechanical properties, as listed below.

a. Unlike other strengthening methods, grain refinement strengthens materials with improved toughness and ductility.(Calcagnotto et al. 2010; Hansen 2004).
b. Grain refinement lowers ductile-to-brittle transition and improves the impact toughness (Armstrong 1970; Calcagnotto et al. 2010).
c. Grain refinement increases the indentation hardness (Armstrong 1970)

d. Grain refinement improves the fatigue-strength and the fracture-toughness (Armstrong 1970; Calcagnotto et al. 2010;).

Though it is not stated, it is important to note that all the above points are applicable for ambient temperature services of structures. However, for extended elevated-temperature services, grain refinement is not beneficial as fine-grained materials are highly susceptible to creep.

2.4 Effect of Grain-Size on Creep-Behaviour

Benefits of refined-microstructure comprising fine-grains as mentioned in previous section are applicable for ambient temperature services of structures. However, for elevated temperature services grain-refinement is not beneficial. At moderate to high temperatures the presence of grain-boundaries weakens a material for the following reasons (Armstrong 1970).

a) Grain boundaries enhance diffusion process by acting as sources and sinks of vacancies,
b) Extent of grain boundary sliding or shearing increases as the grain size decreases,
c) Grain boundaries are sources of dislocations,
d) Grain boundaries are preferred sites for the nucleation and growth of cracks or cavities.

Dependence of steady-state creep of materials on operating temperature, applied stress, and grain-size is given by Mukherjee-Bird-Dorn (MBD) relationship (Kassner 2015; Mukherjee 2002; Zhao et al. 2018)

$$\acute{\varepsilon}_{ss} = \left(\frac{AbDG}{kT}\right).\left(\frac{b}{d}\right)^{p}.\left(\frac{\sigma}{G}\right)^{n} \qquad (2.2)$$

where, $\boldsymbol{\varepsilon'_{ss}}$ is the stead-state creep strain-rate,

A is a materials constant, **T** is the operating temperature,
b is the Berger's vector, **d** is the average grain-size,
D is the diffusion coefficient, **σ** is the applied stress,
G is the shear modulus, **p** is the grain-size coefficient,
k is the Boltzmann's constant; **n** is the stress exponent.

Creep behaviour of a metallic material is comprehensively presented graphically in the form of Deformation Mechanism Map (DMM) in which steady-state creep-rates are shown as contours in normalized-stress (ratio of tensile-stress to shear-modulus) homologous-temperature (ratio of operating-temperature to melting-temperature in kelvin) plot. A typical DMM is presented schematically in Figure 2.1, and DMM of MAR-M200, a commercial alloy is presented in Figure 2.2. These maps commonly show two main regimes, Diffusional Creep, and Dislocation-Creep (aka, Power-Law Creep). The diffusional creep is further divided in to two regimes, grain-boundary diffusional creep (aka, Coble Creep) and lattice diffusional creep (aka, Nabarro-Herring Creep). Thus, there are three important creep regimes showing dominant creep mechanisms depending on the operating temperature and the stress (Kawasaki and Langdon 2013).

For dislocation-controlled Power-Law Creep that operates at high-temperature and high-stress regime, values of **p** and **n** are about 4.5 and 0 respectively. For lattice-diffusion-controlled Nabarro-Herring Creep that operates at high temperature and low-stress regime, **p** and **n** are 1 and 2 respectively. For grain-boundary diffusion-controlled Coble-Creep that operates in low-temperature and low-stress regime, **p** and **n** are 1 and 3 respectively (Meyers and Chawla 2008). While grain-size has no relevance to the creep-rate in PLC, the diffusion controlled Nabarro-Herring creep and Coble creep mechanisms have inverse relationships with grain-size.

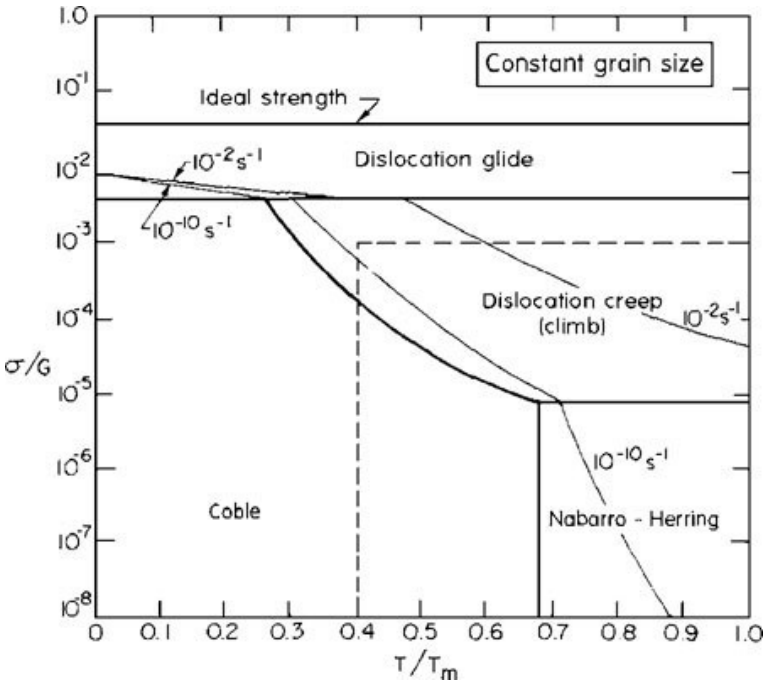

Figure 2.1: Schematic Deformation Mechanism Map of a metallic material (Kawasaki and Langdon 2013)**.**

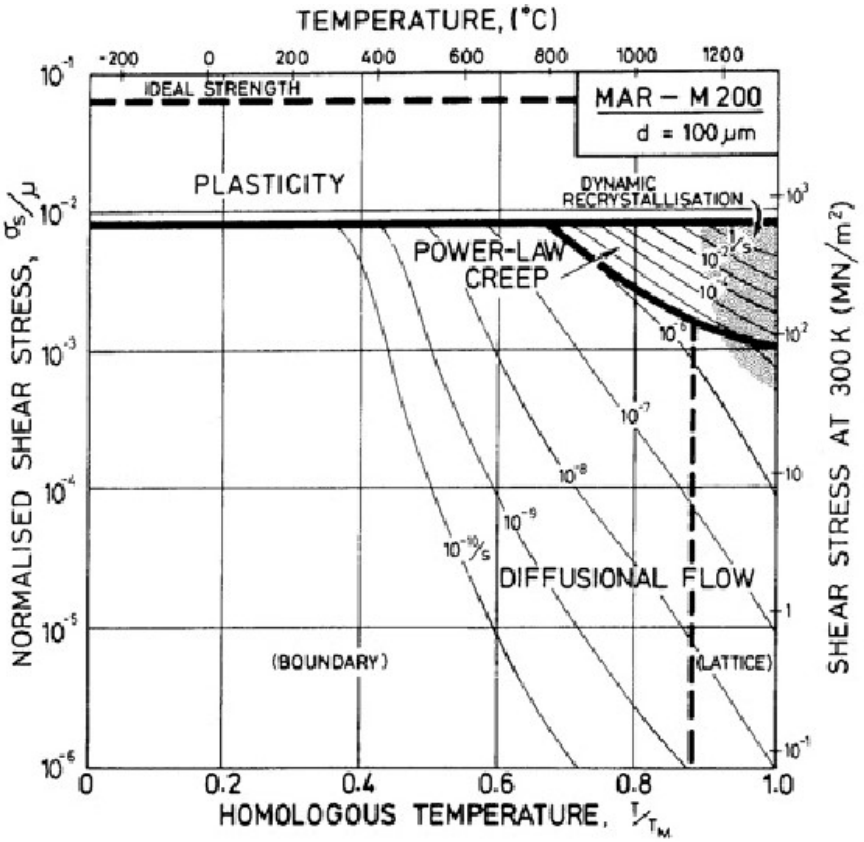

Figure 2.2: Deformation mechanism map of Ni-based superalloy, MAR-M200 (Asadi et al. 2012)**.**

This suggests that the finer the grains the higher the creep-rate, and the lower the creep-life. Considering that high-temperature structures are generally made to operate in the Coble creep (CC) regime, the creep-rate is inversely proportional to the grain-size-cubed (d^3). In other words, grain-coarsening reduces the creep-rate substantially. For example, if the grain-size is doubled by any grain-coarsening heat-treatment, the creep-rate reduces by 8 times. Thus, the service life of the structure should increase significantly.

It is important to note that as the grain-size increases, the number of transverse grain-boundaries to the stress-axis reduces. This is important for the diffusional creep as the creep-strain accumulation occurs by atomic diffusion from the longitudinal grain-boundaries to the transverse grain boundaries when the long-axis of the material is subjected to tensile-stress. Due to high thermal activation, for (Nabarro-Herring Creep) NHC this diffusional mass-transport occurs through the lattice, while for CC this diffusional transport occurs along the grain-boundaries. Thus, net diffusional path increases when the grain-size is increased. As the diffusional path or the diffusion distance has a parabolic relationship with the diffusion time, the creep-strain accumulation rate decreases when the grain-size is increased. Thus, the steady-state creep rate decreases. This leads to delayed cavitation and delayed on-set of tertiary-creep and thus, increased creep-life. Therefore, the service life of the component increases significantly.

2.5 Effect of Grain-Shape on Creep-Behaviour

Grain-coarsening is one method of increasing the diffusional-distance between the longitudinal-grain-boundaries to the transverse grain-boundaries. In principle, the same can be achieved by elongated grains with high aspect-ratio along the tensile stress-axis of a component. In fact, this idea is applied in directionally solidified gas-turbine blades having columnar-grains and improved creep-resistance (Biswas et al. 2022; Burgel et al. 2004; Glenny et al. 1975)**.** However, it is important to note that such idea of modifying the grain-shape is successfully applied in cast-alloys. For wrought alloys, there are limited attempts in designing elongated or flattened grains.

A study reported that grain-shape has significant effect on improving the strength and creep resistance (Wilcox and Clauer 1972). Elongated-grains provides additional

diffusion time and path for atoms and vacancy movement along the grain boundary; and hence creep resistance improves threefold specially in Coble-Creep regime. It is common in oxide dispersion strengthened (ODS) materials to produce elongated grain during cold-working process typically cold-rolling. However, it is important to note that ODS alloys following cold working do not recrystallize in general. As the oxide dispersion hinders the grain boundary migration, nucleation and growth of new crystals are supressed and there by elongated grains are locked in place. In ODS alloys it is found that creep depends not only on grain size but also on the Grain Aspect Ratio (GAR = L/l) is the ratio of average dimension of grains parallel to the tensile stress direction (L) to the dimension perpendicular to the tensile stress direction (l) (Lasalmonie and Strudel 1986). The contribution of grain boundary sliding to the deformation process is reduced when the grains are elongated parallel to the applied stress (Malakondaiah & Rama Rao, 1985; Nabarro & De Villiers, 1995).

2.5.1 Thoria Dispersed Nickel Alloys

Wilcox & Clauer, 1972 observed in Thoria dispersed nickel alloys that high temperature yield-strength as well as creep-resistance increase with grain aspect ratio as shown in Figure 2.3. When a material with elongated grains is used with longer grain axis along the stress axis, diffusion path becomes much longer than the equiaxed counterparts. Thus, diffusional creep is significantly retarded as GAR is increased. However, GAR beyond 20 is not beneficial as there is no further improvement in the creep life. For grains with high aspect ratio, it has been also observed that fracture mode varies from intergranular mode for short grains to trans-granular mode for long grains. Along with improved rupture life, a transition from intergranular to trans-granular fracture was observed (Figure 2.4) in Inconel MA6000 alloy when the grain aspect ratio exceeded a critical value of about 20 (Arzt and Singer 1984; Nabarro and De Villiers 1995).

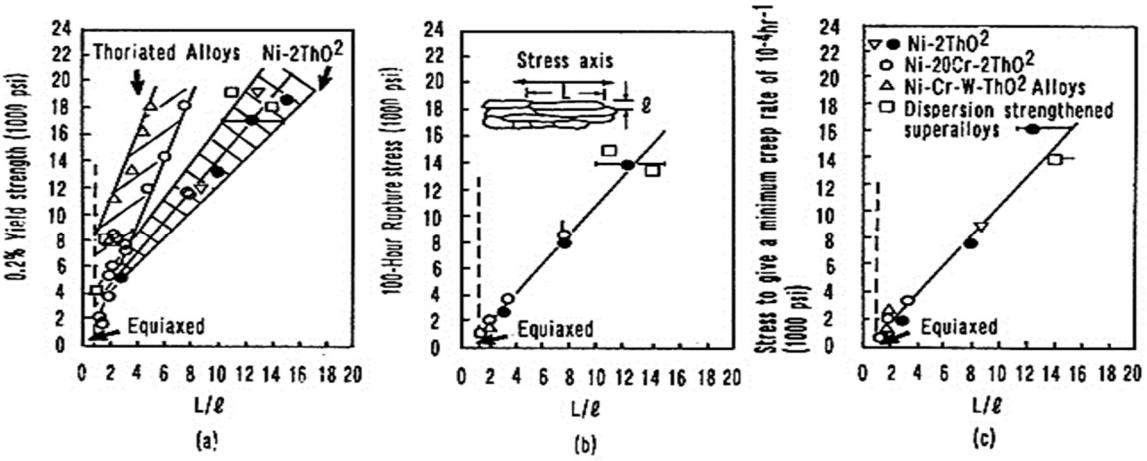

Figure 2.3: Effect of grain aspect ratio (GAR) in oxide dispersion strengthened nickel alloys at 1093°C: (a) yield-strength; (b) 100 h rupture stress; (c) stress for minimum creep-rate of 10^{-4} /h (Wilcox and Clauer 1972)**.**

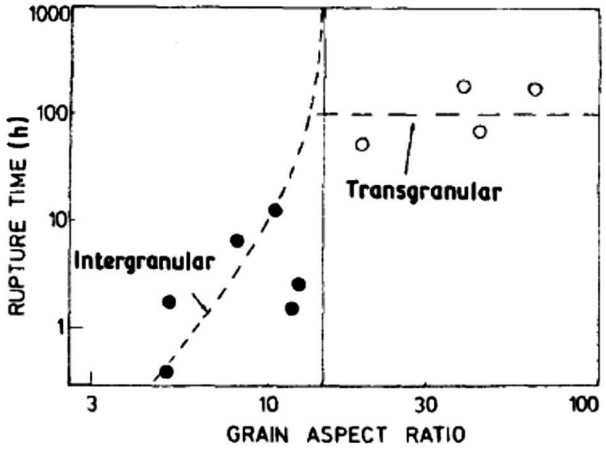

Figure 2.4: Variation of fracture mode with GAR in MA 6000 nickel alloy creep tested at 950°C under 230 MN/m^2 (Arzt and Singer 1984).

2.5.2 Zirconia Grain Stabilized (ZGS) Platinum

Johnson Matthey, a premier precious metal supplying company has developed Zirconia Grain Stabilized (ZGS) platinum. This is essentially oxide dispersion strengthening of platinum and platinum-rhodium alloys. Zirconia dispersion in precious metals restricts deformation at high temperatures by resisting grain growth and significantly improving properties over conventional platinum and its alloys. ZGS platinum contains fine, evenly dispersed particles of zirconia throughout their matrix. These particles slow down the processes of degradation by pinning dislocation networks formed during

thermomechanical processing, thereby inhibiting the movement of these dislocations to the grain boundaries. Due to effective restriction of degradation of microstructure ZGS materials have extended operating lives, compared to conventional platinum group metals. Another benefit of ZGS materials is the improved resistance to intergranular contamination through retention of the high aspect-ratio grain structure (Morris and McGrath 2013).

2.5.3 Dispersion Hardened Platinum (DPH)

This technology is developed by Heraeus, a German precious metal supplying company (Fischer et al. 2001; Teichmann et al. 2011). Alloying elements such as, zirconium, yttrium and, in some cases, cerium are added to the platinum in elemental form during the melting process followed by casting. In the next step of forming operations, the semi-finished products such as sheets, tubes and bars are subjected to an annealing process in an oxidising medium that causes internal oxidation. Finely dispersed oxide precipitates are formed from the alloying elements. The annealing process is adjusted to ensure that the reactive elements are completely converted to oxides. The platinum DPH materials have significantly improved properties due to highly elongated grains. Even welded components manufactured from them display high strength, good ductility, resistance to thermal cycling, corrosion resistance, and low notch sensitivity. The DPH platinum and alloys are superior to previous ODS platinum materials. They are used in glass melting and other industrial applications. It is important to mention here that weldability of ODS strengthened platinum materials is poor due to segregation of oxides in the fusion zone. Additionally, the oxide dispersions are considered contaminants in precious metal industry. It is extremely difficult to remove the contaminations from the precious metals. Thus, the recycling of precious metals is affected due to the oxide-dispersion (Fischer et al. 2001).

2.6 Superalloy Inconel 601

Superalloys are special alloys, and due to their excellent chemical and mechanical degradation resistance find applications at temperatures above 540 °C. Unlike any other class of alloys, superalloys are used in load-bearing applications at high-temperatures relative to their incipient melting temperatures (Figure 2.5). In principle, superalloys

are an extension of austenitic stainless steels since FCC phase constitutes the matrix phase. They are broadly classified into; a) Iron-Nickel base, b) Nickel-base and c) Cobalt-base (Donachie and Donachie 2002; Geddes et al. 2010; Kishawy and Hosseini 2019; Reed 2006; William et al. 1987).

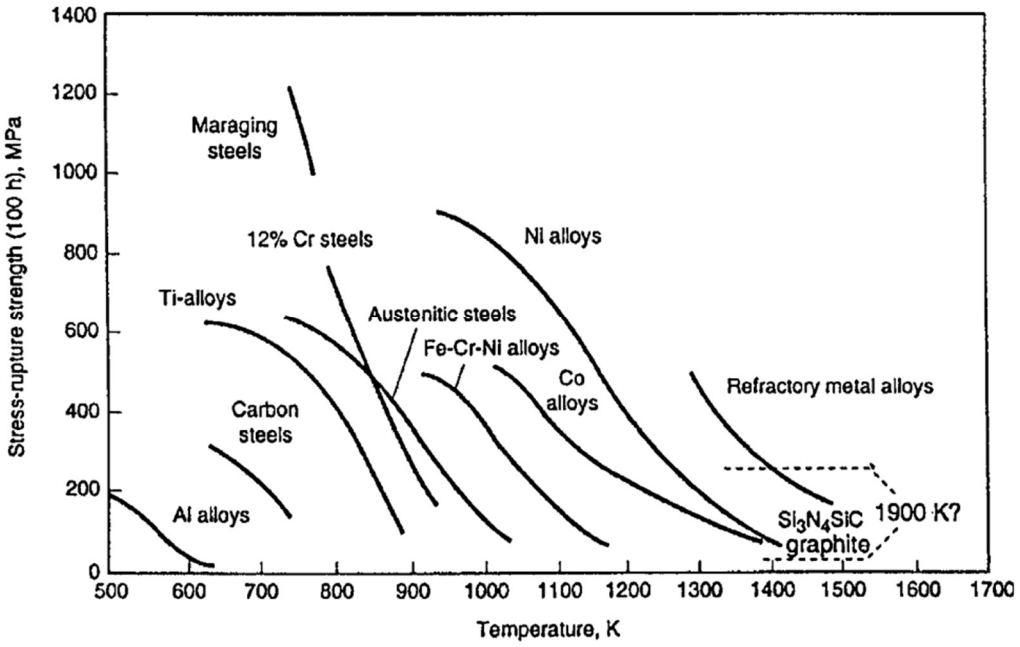

Figure 2.5: High Temperature service temperatures for heat resistant metals, based on 100 hr stress rupture strength (Fuchs 2005).

The alloying elements determine the microstructure of the superalloys and thereby influence the strengthening of mechanical properties. Nickel based superalloys are typically used for critical applications such as aerospace, power generation, steam turbines, nuclear power plants, rocket engines, chemical industry, where functional stability is required in high temperature and corrosive environments. FCC crystal structure along with solid solution strengthening by addition of Cr, Fe, Cr, Al, Ti, Nb, W, V enables metallurgical stability in severe conditions. Nickel which is used as the base metal has low diffusivity, oxidation resistance, high ductility, toughness, and good formability providing the multiple processing techniques to achieve desired specialized application (Fuchs 2005; Nowotnik 2016). In particular, austenitic Ni-based Inconel 601 is an excellent heat resisting alloy. It is solid solution strengthened by the ternary system of Ni–Cr–Fe forming a uniform single phase solid solution at all temperatures

below melting temperature (Lai 2007). Excellent formability has allowed this alloy to be used extensively in wrought form for high temperature applications such as gas turbines, process-heaters, steam-generator tubes, thermal reactor, thermal processing equipment, thermocouple protection tubes, etc. (Davis 1997, 2000; Donachie and Donachie 2002; Lai 2007; Reed 2006; Reed and Rae 2014; William et al. 1987).

In comparison with the widely popular Inconel 600 (Ni–15-17Cr–8Fe), Inconel 601 (Ni–20-25Cr–20Fe) has higher Fe and Cr content. This increases the solid solution strengthening and addition of Al further improves creep, oxidation, and corrosion resistance (Geddes et al. 2010; Mehta et al. 2014). Therefore, Inconel 601 is an ideal material for applications that involve high temperature oxidation and corrosive environment. Structurally, Inconel 601 is a highly stable FCC solid solution consisting of Nickel in the range of 58-63 along with Chromium in 21-25, Iron in range of 12-14, Aluminium in 1.0-1.7 and other elements such as copper, silicon, titanium, and manganese in small amounts. Typical microstructure consists of γ matrix along with chromium carbides and titanium nitrides in very small amounts. High temperature stability is achieved by absence of embrittling intermetallic phases. Therefore, Inconel 601 does not undergo embrittlement when exposed to high temperatures for extended duration (Nowotnik 2016). Formation of chromium oxide (Cr_2O_3) in conjunction with internal oxidation of Aluminium provides highly adherent oxidation protection on the external surface on IN 601 (Buscail et al., 2011).

2.7 Austenitic Stainless Steels

Austenitic stainless steels (ASSs) are solid solution strengthened alloys with metastable austenite that do not undergo any phase transformation during normal heat-treatment process due the stability of austenitic phase. ASSs comprise Fe-Cr-Ni as key elemental-compositions and have low stacking fault energy (SFE). In annealed condition, ASSs have comparatively low yield strength of 200 MPa and the microstructure is characterised by annealing twins (Spencer et al. 2004). Figure 2.6 gives an overview of the transformations taking place for ASS at different temperatures. Strengthening can be achieved through strain (or work) hardening whereby dislocation motion is hindered by increasing the dislocation density through plastic deformation. Greater the amount of strain induced through plastic deformation higher is the stress required to further

deform the metal (Milad et al. 2008) Strengths in excess of 2 GPa can be achieved through strain hardening of ASSs (Spencer et al. 2004).

2.7.1 Martensitic Transformation of ASSs

The deformation behaviour of ASSs is both special and complex. During plastic deformation of ASSs at ambient temperature, strain induced martensite (SIM) is formed. By deforming at low temperatures, a combination of high strength and ductility can be achieved, which is called as transformation induced plasticity (Shen et al. 2012). This transformation is rendered complex due to various factors affecting the stability of the austenite phase. The amount and type of martensite formed depends on stacking fault energy (SFE), deformation temperature, strain, strain rate, state of stress, grain size and composition. However, among these SFE and deformation temperatures are the major factors. SIM forms easily for steels with unstable austenite (γ) and improves the mechanical strength. However, a highly stable austenite (γ) limits the strain-hardening of the steel (Milad et al. 2008; Padilha et al. 2003; Talonen and Hänninen 2004). A graphical representation of time-temperature-transformations in ASSs is given in Figure 2.6.

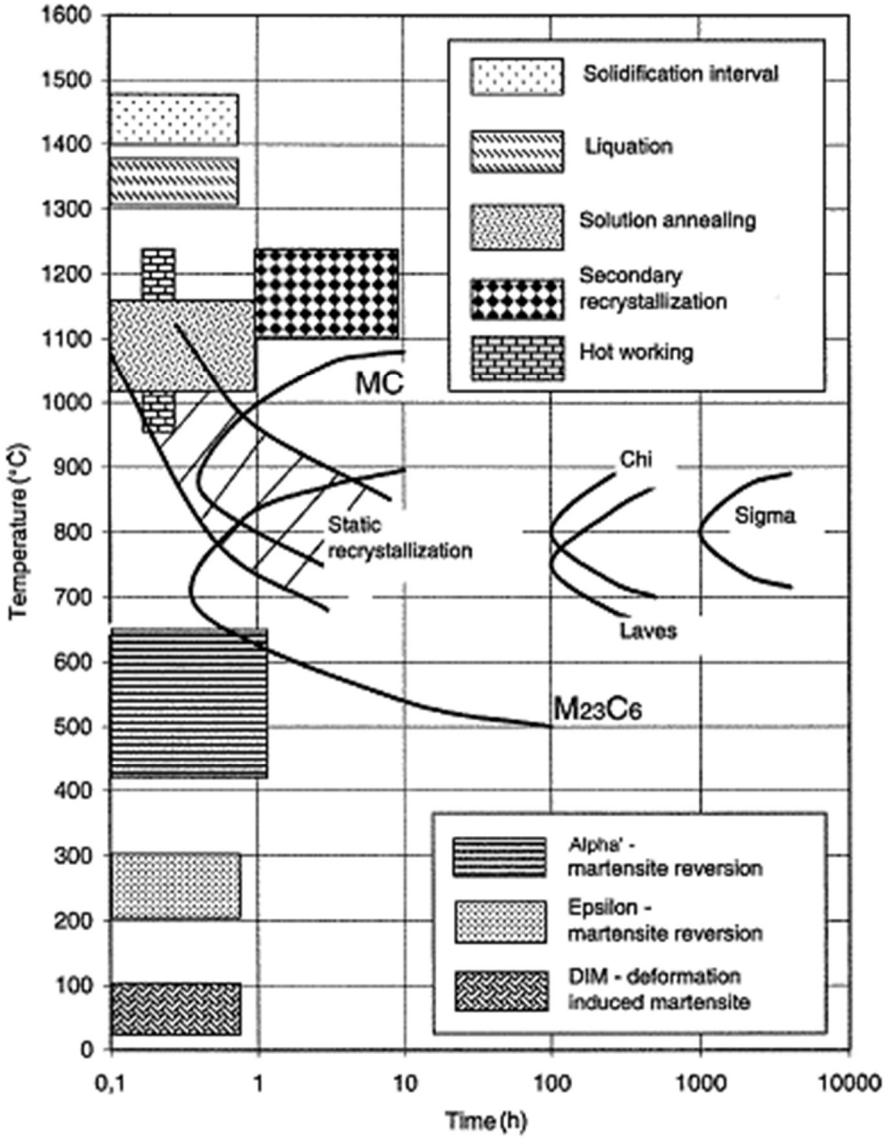

Figure 2.6: Time-temperature-transformations in ASSs for various heat treatments between room temperature and melting point (Padilha et al. 2003).

2.7.2 Influence of SFE in Plastic-Deformation of ASSs

In FCC metals the deformation mechanism and mechanical properties are dependent on their SFE, which depends on the composition. For steels, SFE generally ranges from 10 to 100 mJ/m^2 (Schramm and Reed 1975)as shown in Table 2.1. SFE is increased by elements such as Nickel and carbon thereby promoting dislocation cross slip, while chromium, manganese, and silicon tend to decrease SFE favouring planar slip (Singh 1985).SFE determines whether a material deforms by martensitic transformation,

twinning or dislocation glide. Stacking faults precede twins and ε-martensite. Martensite transformation occurs at SFE less than 18 mJ/m^2, by twinning in the SFE range of 18-45 mJ/m^2 and by dislocation glide when SFE exceeds 45 mJ/m^2 (Shen et al. 2012). Stacking fault energy of ASSs is a function of alloy composition and temperature, and is evaluated using the following empirical equation (Schramm, Reed, 1975):

$$\boldsymbol{SFE\ (mJ/m^2) = -53 + 6.2(\%Ni) + 0.7(\%Cr) + 3.2(\%Mn) + 9.3(\%Mo)} \quad \textbf{(2.3)}$$

Research has shown that, Type 301 stainless steel grade, due to its lowest stability has highest strain-hardening rate and forms the greatest amount of strain induced martensite. Grades 310 and 321 are considered most stable, while grade 304 has medium range of stability (Kumar et al. 2004; Milad et al. 2008). The Table 2.1 provides composition and SFE values for some of the common ASS grades. As the SFE increases, principal deformation mode changes from formation of ε-martensite, through deformation-twinning, to slipping. For 304 SS which has lower SFE (9.2- 32.5), mixture of ε-martensite and mechanical twins form as an intermediate phase before the formation of α′-martensite. SS 316 has higher SFE and hence, during deformation, mechanical twins are formed followed by α′-martensite (Hadji and Badji 2002). Lowering the temperature decreases the SFE in ASSs, therefore formation of strain-induced martensite occurs readily at 77 K. But at ambient temperatures large strains are required due to lack of driving force (Spencer et al. 2004). Rolling at sub-zero temperatures produced large amounts of martensite (Coleman and West 1976).

Formation of martensite depending on the stability of austenite, generally occurs between the temperatures M_s and M_d. The M_s is the temperature below which austenite transforms to α′-martensite instantly on cooling and M_d is the temperature below which deformation stresses can initiate martensitic transformation (Mangonon and Thomas 1970a; Padilha et al. 2003). M_s is calculated using the equation of Eichelmann and Hull (Padilha et al. 2003).

$$\boldsymbol{M_S\ (^\circ C\ ) = 1305 - [1667(\%C + \%N) + 28(\%Si) + 33(\%Mn) + 42(\%Cr) + 61(\%Ni)]} \quad \textbf{(2.4)}$$

Amount of martensite formed on cooling ASS even up to 4°K is little. Therefore, straining is necessary to impart higher strength through martensite transformation (Spencer et al. 2004). The $M_{d30/50}$ temperature, at which 50% α′-martensite will form at 30% true-strain under tensile condition has been suggested by Angel T. (Padilha et al. 2003).

$$\boldsymbol{M_{d30/50}}\,(°\boldsymbol{C}) = \mathbf{413} - [\mathbf{462}(\%\boldsymbol{C} + \%\boldsymbol{N}) + \mathbf{9.2}(\%\boldsymbol{Si}) + \mathbf{8.1}(\%\boldsymbol{Mn}) + \mathbf{13.7}(\%\boldsymbol{Cr}) + \mathbf{9.5}(\%\boldsymbol{Ni}) + \mathbf{18.5}(\%\boldsymbol{Mo})] \quad \textbf{(2.5)}$$

Therefore, steels such as 301 and 304 which have higher M_d temperature easily form SIM at room temperatures whereas 316 and 321 grades with lower M_d temperatures do not form SIM at room temperatures. For SS 304, the M_s < 4 °K and M_d ~ 293 °K (& Thomas G, 1970).

Table 2.1: Chemical composition and SFE of some ASSs (Padilha et al., 2003).

Type	C	Mn	Si	Cr	Ni	Mo	Other	SFE (mJ/m^2)
301	<0.15	<2.0	<1.0	16.0-18.0	6.0-8.0	----	----	<16
304	<0.8	<2.0	<1.0	18.0-20.0	8.0-10.0	-----	----	9.2- 32.5
304L	<0.03	<2.0	<1.0	18.0-20.0	8.0-12.0	----	----	9.2- 41.8
316	<0.8	<2.0	<1.0	16.0-18.0	10.0-14.0		----	34.6-80.7
316L	<0.03	<2.0	<1.0	16.0-18.0	10.0-14.0	----	----	34.6-80.7
321	<0.8	<2.0	<1.0	17.0-19.0	9.0-12.0	----	Ti >5x %C	14.7-41.1
347	<0.8	<2.0	<1.0	17.0-19.0	9.0-13.0	----	Nb>10x%C	14.7-47.3
370	0.08-0.12	1.6-2.0	0.25-0.45	14.5-15.5	15.0-16.0	1.05-1.4	Ti=0.35-0.45	65.0-76.5

2.7.3 Types of SIM and Mechanism

Two types of strain induced martensite are formed based on amount of strain, ε-martensite (hcp, paramagnetic) and α′-martensite (bcc, ferromagnetic). ASSs become ferromagnetic after formation of α′- martensite. In initial stages of deformation shear bands are formed which consist of stacking-faults, mechanical-twins and ε-martensite. These shear bands intersect with each other forming potential nucleation sites for SIM. These intersections are sensitive to SFE as well as temperature and strain-rate and increase with decreasing SFE (Hadji and Badji 2002; Hedayati et al. 2010; Reed 1962; Staudhammer et al. 1983; Talonen and Hänninen 2004).

The ε-martensite forms directly from γ phase prior to α′-martensite at low deformation levels (≤ 10%). In low SFE ASSs such as SS 301 and SS 304, ε-martensite forms by an easy shift of atoms to HCP structure (Staudhammer et al. 1983). The formation of ε-phase takes place by the dissociation of dislocations into partials (P. Mangonon & Thomas G, 1970).The ε-martensite consists of overlapping stacking faults and heavily faulted crystal structure, due to which the XRD peaks are wide and have low intensity (Talonen and Hänninen 2004). The volume fraction of ε-phase reaches a maximum with increasing deformation and then decreases as α′-phase starts nucleating (Mangonon and Thomas 1970b). The ε-martensite bands are fine in nature having a typical thickness of ~100 nm in the $(0001)_{\varepsilon}$ direction. The α′-martensite that nucleates from ε is also very fine and the typical size of α′ laths is ≤300 nm (Spencer et al., 2004). As deformation increases α′-martensite nucleates at intersection of shear band components i.e. two ε-bands and at ε with grain-boundaries or twin boundaries. With increasing cold-reduction, α′-martensite laths are formed by repeated nucleation and coalescence/stacking of needle-shaped α′ embryos (Staudhammer et al. 1983). The transformation follows the sequence γ→ε→α′. At high levels of deformation ε-martensite and γ-austenite phase decrease as α′-martensite grows at their expense to become the major phase. For 316 ASS, with higher SFE the transformation mode follows the sequence of γ → mechanical twinning → α′. The α′ nucleates at the intersection of deformation twins (Hadji and Badji 2002; Shen et al. 2012)

2.7.4 Factors influencing the amount of Martensite formed during Cold Rolling

The amount of strain induced martensite depends on the stability of γ-phase and rolling conditions including, strain, strain-rate, and temperature. For low austenite stability and low deformation temperatures the ductility and amount of martensite formed is high. The transformation curve of % α′-martensite vs % cold rolling has a sigmoidal shape. The amount of α′-martensite formed can be greatly enhanced by cold working at sub-zero temperatures as compared to ambient temperatures for the same amount of strain, since SFE decreases (Al-Fadhalah, 2015; Coleman & West, 1976; Hedayati et al., 2010; Naghizadeh & Mirzadeh, 2016; Ravi Kumar et al., 2010; Singh, 1985).

Ravi Kumar et al., 2010 obtained SIM of 56% for cold rolling of 90% for SS 304 at room temperature. The low volume fraction of α′-martensite at room temperature conditions is attributed to adiabatic heating of the material during cold working at higher strains and strain-rates due its inability to fully dissipate the heat. This reduces the driving force required for martensitic transformation (Kumar et al. 2004, Shen et al. 2012). Figure 2.5 shows variation of martensite with temperature and true strain for SS 304.

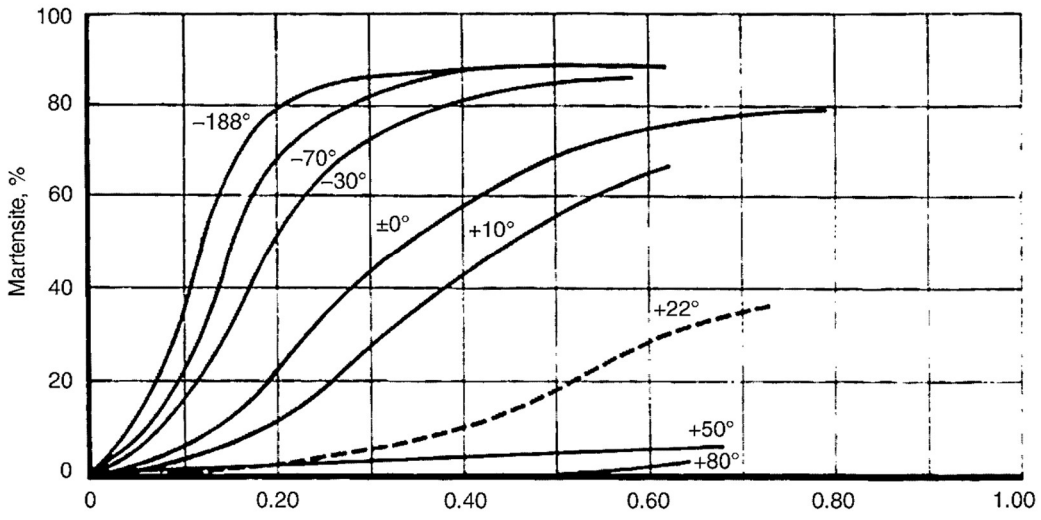

Figure 2.7: Variation of martensite formation with temperature and true strain for 304 (McGuire 2008)**.**

Staudhammer et al. (1983) observed a crossover in terms of % strain for relation between amount of α′ and strain rates. For lower strains (<0.25) more α′ was produced

at higher strain rate (10^3 s^{-1}), while at higher strains (>0.25) α′ produced was higher for low strain rates (10^{-3} s^{-1}). The martensite formation decreases with increase in strain rate, due to increase in heat generation in the material during deformation. This adiabatic heating promotes non-planar slip and suppresses martensite formation due to reduction in nucleation sites (Shen et al. 2012; Staudhammer et al. 1983). With respect to grain size, (Sundara Raman and Padmanabhan 1994) in their experiments with SS 304LN observed greater ductility due higher α′-martensite content for coarser grains owing to higher density of shear-bands as compared to fine grained samples. In experiments by Hadji & Badji (2002) for SS 304 they reported that the amount of α′-martensite formed increases with decreasing grain size, since increase in grain size provides less-number of nucleation sites. In the case of SS 316 having higher SFE, the formation of α′-martensite is independent of grain size.

2.7.5 Effect of SIM on Mechanical Property

SIM has pronounced effect on mechanical properties of ASSs. Depending on the amount of α′-martensite formed cold working of ASSs is able to increase the yield and tensile strengths and hardness of the steels, with subsequent decrease in ductility. The volume fraction of α′ determines the magnitude of strengthening imparted in the steels (Mangonon and Thomas 1970b). The decrease in ductility of steels was found to be sharp initially for cold-rolling upto 30%, beyond which the rate of decrease was lower (Milad et al. 2008) TMP involving severe cold-rolling and annealing has been able to produce ASSs with high strength and improved ductility with submicron-grained microstructure (Hedayati et al. 2010). It was possible to increase the Vickers hardness from 200 for as-received to 600 for 90% cold-reduced (at 0°C) sample. Also, the strength was increased from 300 to 1825 MPa. The ratio of the average tensile strength to the average Vickers hardness in different percentages of cold rolling was found to be three for steels of AISI 304 and 304L respectively (Hedayati et al. 2010; Milad et al. 2008).

Spencer et al. (2004) have shown that the martensite acts as a reinforcing phase in the FCC-BCC composite due to its ability to sustain higher stresses than the austenite under external loading when deformed at 300 K. The strengthening effect is due to the fine scale of martensite since the amount of carbon in martensite is insufficient to impart

strength. The martensitic phase deforms in ductile nature along with the austenitic phase although it has higher flow stress than austenite. Singh, 1985 in his work with SS 304 and SS 321, has shown that hardening in ASS is achieved not only by martensitic transformation in the FCC phase but also by deformation-bands. These deformation bands contain mechanical-twins and are stable for annealing temperatures of up to 800°C.

2.7.6 Low-Temperature Hardening of ASSs

One interesting behaviour that has been observed is the hardening of austenitic steels having SIM when they are subsequently heated to temperatures of 200-450 °C. The increase in hardness was observed in general for strains of 15% or more and it was optimum for the aging temperature of 300-400°C. Also, most of the increase in hardness occurs for the first one hour of aging (Singh 1985).This bake-hardening strengthening phenomena has been studied extensively to understand the mechanism of hardening (Karjalainen et al. 2008). Chukhleb & Martynov (1959) were the first to explain the possible cause for increase in mechanical properties. They proposed that carbides precipitate in the retained austenite followed by nucleation of α′. They argued that the increase in the material hardness is due to increased α′ amount. (Mangonon and Thomas 1970a) reported increase in α′ for SS 304 but ruled out formation of carbides due to low carbon content (0.07 %). The α′ formed during aging were observed to have different orientation and lenticular shape unlike lath-like structure of SIM. In the above work, martensite formed during stress relieving at 400 °C, and was shown to have been thermally nucleated by shear process similar to martensite formation in Fe-C and Fe-Ni-C steels. Mukhopadhyay et al. (1995) observed increase of α′ on cooling after aging. It was attributed to increase in M_s temperature due to depletion of chromium and carbon after precipitation of carbides. Rathbun et al., (2000) found no change in martensite volume during strain aging and suggested the strengthening of α′-martensite by short-range redistribution of carbon into dislocations and phase boundaries. Hardening due to increase in α′ content has also been reported by Gauzzi et al. (2006), Lee et al. (2010) and Jeong et al. (2012) for SS 304. Apart from increase of α′ content, Lee et al. (2010) and Jeong et al. (2012) also observed hardening of martensite and deformed austenite phases. Hardening of phases was attributed to diffusion of carbon atoms into

dislocations and twins in α′-martensite and austenite phases and precipitation of carbides ($M_{23}C_6$) at dislocations. However, similar hardening behaviour has been reported for SS 201 grade with low martensite content of 1-5% (Karjalainen et al. 2008) and for 321 grade austenitic steel which does not form any SIM (Singh, 1985). Yield strength increase of about 100 MPa and more can be achieved in commercial ASSs without affecting ductility and formability (Karjalainen et al. 2008).

2.7.7 Martensite-Reversion

Singh (1985) in his work has reported on the stability of the various deformation induced phases for different annealing temperatures. The ε phase is found to be stable upto 200 °C, α′ upto 400 °C and deformation bands are stable upto temperatures of 800°C. Above 200 °C the ε phase reverts back to γ phase by recombination of partials to form whole dislocations (Mangonon and Thomas 1970a). During ageing at 500 °C and above, reversion occurs leading to softening due to decrease in α′ content. The α′ phase is not stable at high temperatures and it undergoes reversion to form fine grained austenite after annealing. This reversion occurs by formation of subgrains and nucleation of γ within α′. Higher the amount of α′ faster is the rate of softening and hence greater the degree of recrystallization. The reversion to austenite phase follows the sequence of ε→γ and α′→γ, without the formation of any intermediate phase (Singh 1985). Generally, reversion to austenite phase takes place at temperatures of 500-750°C, below recrystallization temperature accompanied by grain refining (Al-Fadhalah 2015; Padilha et al. 2003; Ravi Kumar et al. 2010). Figure 2.6 shows variation of SIM for different annealing temperatures.

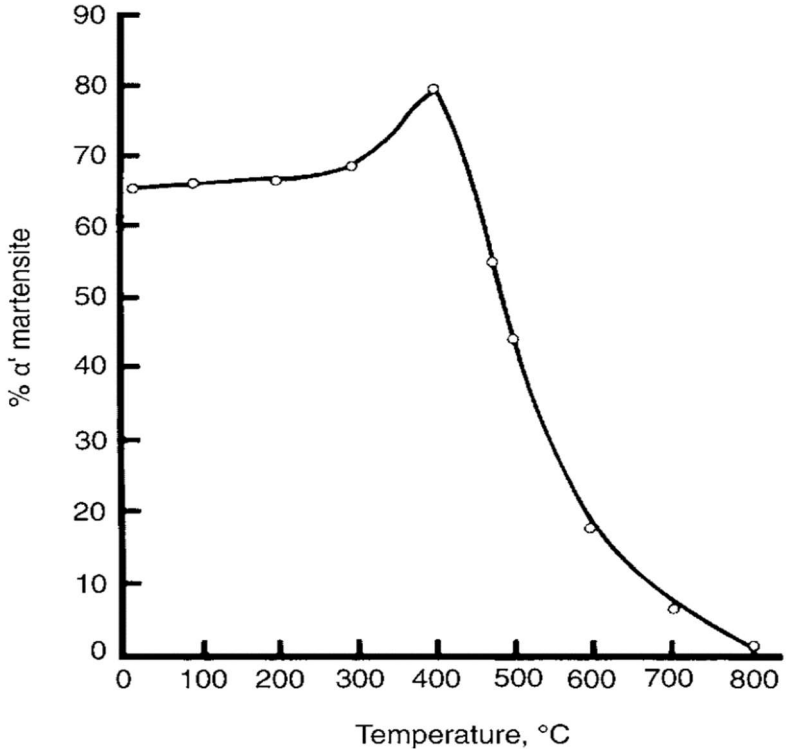

Figure 2.8: Stability of SIM for different temperatures (McGuire 2008)**.**

2.7.8 Recovery and Recrystallization

Recovery plays a minor role in low SFE steels having low austenite stability such as AISI 304 and softening occurs mainly due to recrystallization. Whereas, in austenitic steels with higher SFE, recovery takes place prior to recrystallization (Padilha et al. 2003). Recrystallization of ASSs is influenced by several factors and due to this, specifying a particular recrystallization temperature is difficult. These factors include composition, prior heat treatment, cold working conditions (% strain, temperature, mode, and strain rate) and heat treatment parameters including holding time and heating rate. In general, recrystallization occurs at temperatures of 100 °C above the martensite reversion temperature. Recrystallization occurs only in the cold worked retained γ regions and not in the reversed γ. Recrystallization begins on deformation bands and around the grain boundaries. Factors (lower SFE and higher amount of SIM) that increase stored energy during cold deformation also contribute to decrease the recrystallization temperature (Padilha et al. 2003). By annealing at lower temperatures, it is possible to obtain fine grained microstructure and achieve optimum mechanical

properties by controlling the reversion annealing parameters (Naghizadeh and Mirzadeh, 2016).

2.7.9 Summary

From the literature survey it is clear that the thermomechanical processing of austenitic stainless steels (ASSs), especially that of SS 304, is quite complex due to the strain-induced martensitic transformation and reversion. However, being a Ni-based M-type material, Inconel 601 is much simpler to design thermomechanical processing due to lack of any strain-induced transformation.

Apart from cast-alloys, historically, attempts to design elongated-grains along the tensile stress axis are limited to oxide dispersion strengthened (ODS) wrought alloys. Considering that the oxide dispersions pin-down and hinder grain-boundary migration, cold-rolled ODS alloys were used at sufficiently elevated temperatures without undergoing recrystallization. Thus, superior strength as well as creep-resistance were achieved.

The literature survey indicates that there have been no published reports about designing elongated grains in wrought materials in recrystallized condition. Considering that cold-worked ODS structures may pose problems in welding, punching, forming and fabrication, it is worth exploring the possibility of producing fine-elongated in wrought alloys without any dispersion.

3. PROPOSED WORK

This chapter provides a preamble to the research problem and states the ideation of producing elongated recrystallized-grains in wrought-materials. Once the context of the research problem is established, the chapter states the methodology and objectives of the thesis.

3.1 Preamble

It is well-established that refined microstructure having fine-equiaxed grains imparts superior strength, plasticity, toughness, and fatigue-resistance to the wrought-alloys that are used to construct structural components for ambient temperature services. For the same reason, grain-refinement in cast-structures, typically by inoculation during the solidification, is practiced for cast-alloys. However, conventionally cast and directionally solidified components that serve at elevated temperatures require coarse and columnar grains respectively. Both coarse-grains and columnar-grains minimize the transverse grain-boundary density along the loading direction. For elevated temperature applications such cast structures show minimal creep. In single crystals, creep-rate is further reduced due to the absence of grain-boundaries.

The idea of increasing the grain-boundary distance or reducing the transverse grain-boundary density in wrought-structures, for high temperature applications, is conventionally achieved by coarsening the grains by heat-treatment. However, this reduces the strength and toughness of the material significantly. Further increase in the creep-resistance of the wrought-alloys can be achieved in principle, by designing elongated grains along the stress-axis. From the literature work it is clear that obtaining elongated grains in oxide-dispersion strengthened (ODS) alloys is quite possible as they do not recrystallize easily due to dislocation-pinning and grain-boundary-pinning by oxide-dispersion. Thus, cold-worked structure is almost frozen during service life (Wilcox and Clauer 1972).

Using the above idea, platinum based proprietary alloys, Zirconia Grain Stabilized (ZGS) Platinum and Dispersion Hardened Platinum (DPH) have been developed that possess elongated grains and superior high temperature strength and creep resistance. However dispersed oxides in these alloys present drawbacks for sheet-metal

applications, such as, segregation during welding and low tool-life of punching-dies(Fischer et al., 2001; Morris & McGrath, 2013; Teichmann et al., 2011). Producing elongated or flattened grains by cold-rolling is quite-easy and natural. But such structure is thermodynamically unstable. The same cannot be used for the elevated temperature applications since the thermal exposure may cause recrystallization during the service. Fine-equiaxed-recrystallized grains may then increase the creep-rate in elevated temperature service. Therefore, the elongated or flattened grains with high aspect-ratio should be in stable-recrystallized form such that no significant structural change occurs during the elevated temperature exposures. However, producing elongated grains in recrystallized form is challenging and is not tried before. This work makes such attempt and aims at producing elongated grains along the rolling-direction in thin-sheets of about 1-2 mm thickness.

3.2 Ideation

Existing approach of improving creep-resistance is grain coarsening or by modifying the microstructure from (a) to (b) as shown in Figure 4.1. The idea proposed in this work is to engineer the microstructure from (a) to (c). The proposed ideation is, wrought alloy sheets to be subjected to controlled cold-rolling followed by controlled recrystallization-annealing to cause discrete nuclei that would have limited growth in the through-thickness direction and maximum growth in the rolling direction. This way, in principle. long grains with a high aspect ratio can be designed for thin sheets. If the thickness of the sheet is comparable to the grain-size, this idea can become a reality. In other words, the thinner the sheet the higher the possibility of producing elongated or flattened grains.

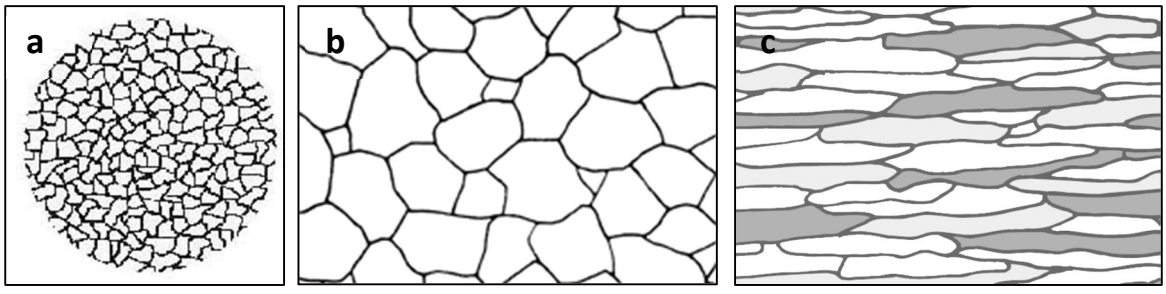

Figure 3.1: Schematic of; a) fine-equiaxed grains, b) coarse-equiaxed grains, c)elongated grains.

As the first step, the idea of producing elongated-recrystallized grains is being tried for thin-sheets rather than bulk-structures. The methodology proposed here is, cold-rolling of sheet-metals followed by isothermal-annealing. However, the processing-window for controlling the nucleation and grain-growth needs to be determined practically. Thus, the static-recrystallization behaviour of a particular wrought-alloy needs to be mapped. This can be achieved by cold-rolling the metal-sheets to wide-ranges of reduction and subjecting the same to isothermal-annealing over a wide temperature-range. Considering that the thickness of the sheets is limited, for certain combination of cold-reduction and annealing temperature, recrystallized-structure with un-equiaxed grains along the rolling direction is anticipated. Considering that secondary phases such as, intermetallic precipitates, oxide-dispersion, hard-particles, etc may interfere in the recrystallization and grain-growth kinetics, pure-metals or simple m-type alloys having a single-phase microstructure such as Stainless Steel 304 and Inconel 601 are ideal experimental materials for the proposed work. The rationale for choosing the experimental materials and experimental methods is stated in detail in the next section. The research objectives are stated concisely as follows.

3.3 Research Objectives

1. Map recrystallization behaviour of Stainless Steel 304 and Inconel 601 sheets by performing cold-rolling and isothermal-annealing experiments followed by mechanical testing and structural-characterization.

2. Identify and optimize the processing window in each material to obtain elongated-grains with high aspect-ratio in the recrystallized form.

3. Propose a thermomechanical process to obtain the best combination of mechanical strength and creep resistance in wrought alloys.

4. MATERIALS AND METHODS

This chapter provides the morale for the materials-selection and the experimental methods applied in the research work. Following the procurement of the experimental materials, compositional-analysis, specimen-preparation, and processing-methods, the chapter provides a detailed account of the mechanical-testing procedure and structural-characterization techniques adopted for achieving the research objectives.

This work intends to comprehensively cover the effects of all possible metallurgical phenomena occurring in wrought alloys during thermomechanical processing. On one-hand, pure-metals having simplest microstructure would have been ideal materials for the study. However, pure metals are seldom used for structural applications. On the other hand, heavily alloyed structural-materials possessing complex microstructures are not ideal for this work as they may contain highly refined grains and multiple secondary-phases. Thus, tracking microstructural change with the processing steps becomes challenging for advanced commercial materials. Since the very objective of this work is to track the grain-size and grain-shape during thermomechanical processing, compositionally complex, microstructurally simple, and commercially important alloys are suitable for the present work.

Stainless Steel (aka, SS 304) is arguably the most important stainless-steel grade that is widely used for structural applications. The austenitic structure containing significant Ni and Cr additions make this material strong, tough, and corrosion resistant. Thus, SS 304 finds wide application in constructing structures that are used in: corrosive atmospheres, fatigue-loading conditions, and elevated-temperature services. Being the most popular and widely used commercial grade, stainless-steel 304 (SS 304) became a natural choice. It is important to note that the very austenitic structure of the SS 304 served as a precursor in designing Nickel and Nickel-Iron based superalloys that can operate at much elevated temperatures for extended periods often in corrosive environments. Thus, Inconel 601 (IN 601) was chosen as the second experimental material as this grade fulfils the very objective of the work as described below.

1. Both SS 304 and IN 601 are solid-solution strengthened wrought-alloys having comparable microstructures comprising only one phase, solid-solution strengthened austenitic γ phase. However, both the materials are widely used in arduous engineering applications involving, corrosion, fatigue, and creep.
2. Fe, Ni, and Cr are the three major alloying elements in both SS 304 and IN 601. Being a Ni-based alloy, and having marginally higher Cr content, IN 601 is slightly superior to SS 304 in thermal stability, environmental resistance and mechanical properties. Thus, IN 601 can be considered as a Ni-based counterpart of Fe-based SS 304.
3. Considering that both SS304 and IN 601 are m-type materials, hard-intermetallic precipitates as the secondary phases are absent. This should help in grain-boundary migration during recrystallization and grain-growth stages. Thus, both the alloys provide possibilities of producing elongated grains.
4. SS 304 is well-known for strain-induced martensitic transformations while IN 601 is not known to display any phase-transformation during processing. This difference in the experimental materials should influence the correlations between the microstructure and the properties.

Therefore, m-type commercial wrought-alloys, SS 304 and IN 601, that possess comparable granular microstructures, were consciously chosen for tracking their microstructural-variations with thermomechanical processing-steps. Following mechanical-testing and structural-characterization, a rational comparison of their structure-property correlations can be made. While forging, extrusion, rolling, drawing are all wrought-processes for shaping alloys, rolling is the simplest method of mechanical-processing. The degree of deformation of flat-rolled products can be expressed as percentage reduction by computing the difference in the thickness relative to the original thickness of the rolled products. Thus, cold-rolling of alloy-sheets to various degrees of reduction followed by isothermal-exposures at various temperatures is chosen as the experimental-method. This way, the work-hardening followed by static recrystallization behaviour of the alloys is tracked using suitable mechanical-testing and structural-characterization tools. Thus, the structure-property correlations can be established rather accurately. In general, ‘Annealing’ is elevated-heating of a

metal/alloy/glass followed by slow-cooling. The terms, 'Stress-Relieving Annealing' and 'Recrystallization Annealing' are also commonly used for the heat-treatment of both steels and nonferrous materials. In particular, for structural steels, 'Annealing Heat-Treatment' refers to isothermal-holding in austenitizing temperature-range followed by slow-cooling to soften the material by transforming austenite into pearlite. However, in published literature as well as industrial practice, the term 'Annealing' is commonly used for the isothermal-heating of a material. Therefore, irrespective of low-temperature or high-temperature exposure, the term 'Annealing' is commonly used in the thesis.

SS 304 and IN 601 sheets of thickness 3 mm were procured in mill-annealed condition from a local vendor. Chemical compositions of the procured materials were confirmed by spark emission spectroscopy. Table 4.1 provides the measured compositions of the experimental materials against the materials-specifications.

Table 4.1: Chemical composition of SS 304 and IN 601 (in wt. %).

Material		Ni	Cr	Mn	Si	C	Al	Cu	S & P	Fe
SS 304	Spec	8/12	18/20	< 2	< 1	<0.08	Nil	Nil	< 0.03	Bal.
	Measured	8.2	18.3	1.06	0.26	0.06	-	-	-	Bal.
IN 601	Spec	58/63	21/25	< 1	< 0.5	<0.10	1/1.7	< 1	<0.015	Bal.
	Measured	60	22	0.68	0.26	0.06	1.7	-	0.01	Bal.

Using an in-house rolling-mill, as-received sheets were cold-rolled at ambient temperature to various degrees of thickness reductions, 10 % to 80 % with increments of 10 %. The cold-rolled sheets were then subjected to isothermal annealing treatments for 1 hour at various homologous temperatures, $0.3T_m$ - $0.8T_m$ with increments of $0.1T_m$. The melting point T_m is taken as 1723 K and 1623 K for SS 304 and IN 601 respectively (Davis 1998; Donachie and Donachie 2002). Thus, the experimental matrix comprising a wide range of cold-reduction and 1h isothermal annealing over a wide temperature range was designed as shown in Table 4.2.

Table 4.2: Experimental-Matrix for thermomechanical processing of IN 601, SS 304 sheets.

Reduction (%)	Annealing Temperature					
10, 20, 30, 40, 50, 60, 70, 80	$0.3T_m$	$0.4T_m$	$0.5T_m$	$0.6T_m$	$0.7T_m$	$0.8T_m$

As-received, cold-rolled, and annealed sheets were sectioned both transversely and longitudinally to obtain about 20 mm X 20 mm size coupons for microstructural analysis and hardness measurement. The specimens were mounted using an acrylic cold-mount and ASTM E3 standard metallographic specimen preparation procedure was applied such that fine-polished longitudinal sections were made available for the microstructural analysis as well as microhardness measurements. SS 304 metallographic specimens were electrochemically etched using 60% nitric acid in distilled water at 1.1 V. Inconel 601 specimens were electrolytically etched using oxalic acid at 5 V.

Microstructural observations were carried out using a Zeiss Axio Lab A1 optical microscope. One representative micrograph per specimen was selected and the grain size analysis was carried out as per ASTM E112 by linear intercept method using combine cord patterns in Zeiss AxioVision software. Selected microstructures as grey-scale images were converted into binary images using the software. Average grain-size along the longitudinal and transverse directions were measured separately by liner-intercept method using horizontal and vertical pattern respectively, and their ratio was expressed as the grain aspect ratio (GAR).

Hardness measurements were made as per ASTM E384 using a Shimadzu HMV-G20ST digital Micro-Vicker's hardness tester with 0.3 kgf load for 15 second dwell time. The mounted, ground, and polished metallographic specimens were used for the hardness measurements. Thus, indentations were made on the longitudinal planes of the specimens normal to the through-thickness direction. For the statistical distribution, 5 reliable hardness readings were noted down for each specimen. For the tensile tests, cold-rolled and the annealed sheets were sectioned to obtain about 12 mm X 75 mm size strips with the long axis aligned along the rolling direction. Standard flat tensile specimens of gauge-length 32 mm and gauge width 6 mm were cut out of the strips by

wire electric discharge machining as per ASTM standard E8/E8M. Tensile tests of the flat-specimens were performed at 3.125 x 10^{-2} /s strain-rate using a Shimadzu AG-X Plus 100 kN universal testing machine as per ASTM E8/E8M and engineering stress-strain curves were generated.

For the XRD analysis, 20 mm x 10 mm size specimens were sectioned with the long axis aligned along the rolling direction. Considering that the longitudinal sections of the specimens varied with the degree of cold-reduction, the flat surfaces were fine-polished and XRD profiles were obtained from the flat-surfaces. X-Ray diffraction analysis of the polished-specimens was carried-out using monochromatic Cu-Kα radiation in a Rigaku Miniflex 600 X-Ray Diffractometer at 20°/min scan-speed between 40°-100° 2θ angles. The XRD peaks were identified and indexed using X'Pert High Score Plus software equipped with ICDD database. Origin 9.0 software was used for phase-quantification by Gaussian peak-fitting method to obtain areas under the peaks.

Considering that the research-work intends to track the grain-size and grain-shape of the sheets with the processing-sequence, it was decided to carryout EBSD analysis for tracking the granular microstructure rather than studying the crystallographic texture of the rolled-sheets. For the EBSD analysis, 10 mm X 10 mm coupon-specimens were sectioned from the rolled and annealed sheets such that the long axis aligned along the rolling direction. The coupons were sectioned longitudinally, and the longitudinal sections were ground as per the standard metallographic specimen preparation procedure. The ground specimens were fine-polished using 0.05 μm colloidal alumina suspension. To remove the deformed layer from the ground surfaces, the fine-polished specimens were subjected to electrolytic polishing using methanol (170 mL) (absolute) and hydrochloric acid (30 mL) solution at 30 volts for 20 seconds. The specimens were then mounted on a Zeiss Gemini Field Emission Scanning Electron Microscope (FESEM) fitted with Oxford EBS fast CCD detector. EBSD scans of the electropolished longitudinal sections of the specimens were performed at 0.3 μm steps using 20 kV accelerating voltage. TSL OIM software was used for analysing the scanned data and generating Inverse Pole Figure (IPF), and Grain Boundary Orientation Maps.

5. RESULTS AND DISCUSSION OF IN 601

This section presents the results and associated analysis of cold-rolling experiments, annealing experiments, hardness measurements, tensile tests, XRD analysis, EBSD analysis of IN 601. The section provides a comprehensive summary of the thermomechanical processing of the experimental material and proposes a Recrystallization Map of IN 601 based on the experimental results.

5.1 Effect of Cold-Reduction

Figure 5.1 compares the longitudinal-section microstructures of as-annealed, 50% cold-rolled, and 80% cold-rolled IN 601 sheets. As-annealed sheets show equiaxed grains of about 130 μm average grain-size having crystallographic twins and non-metallic inclusions within the grains. The longitudinal section of the rolled sheet shows grain-elongation along the rolling direction suggesting that the equiaxed grains are flattened into pancake like structure during cold-rolling. Thus, the flattened grains appear elongated along the rolling-direction whose aspect ratio (length to width ratio) depends on the degree of cold-reduction.

The effects of cold working on the grain aspect ratio and the hardness of the sheet are presented in Figure 5.2. The grain aspect ratio and typical hardness of as-annealed IN 601 sheets are 1:1 and 220 HV respectively. Both the grain aspect ratio and the hardness increase monotonically with increase in the degree of cold-reduction due to strain-hardening effect. The GAR and hardness values reach 18:1 and 486 HV respectively for the sheet cold-rolled to 80% reduction.

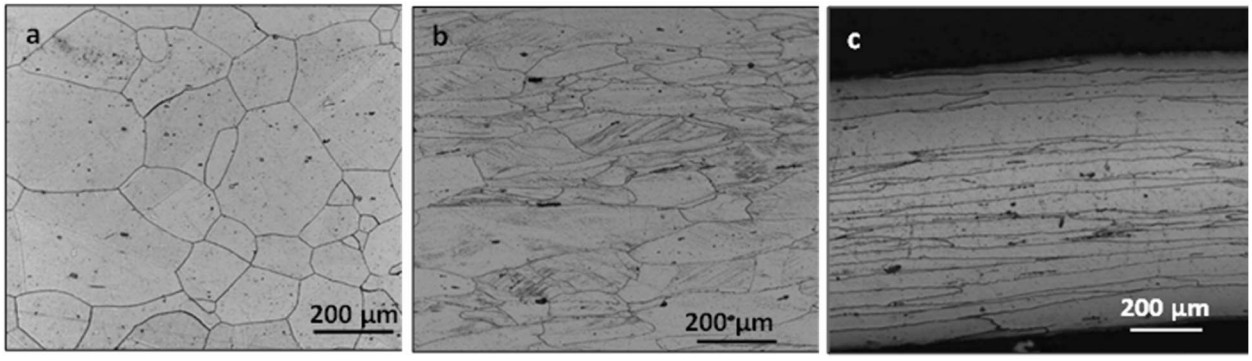

Figure 5.1: Longitudinal microstructures of IN 601 sheets showing flattening of equiaxed grains during cold-rolling; (a) as-annealed, (b) 50% cold-rolled, and (b) 80% cold-rolled.

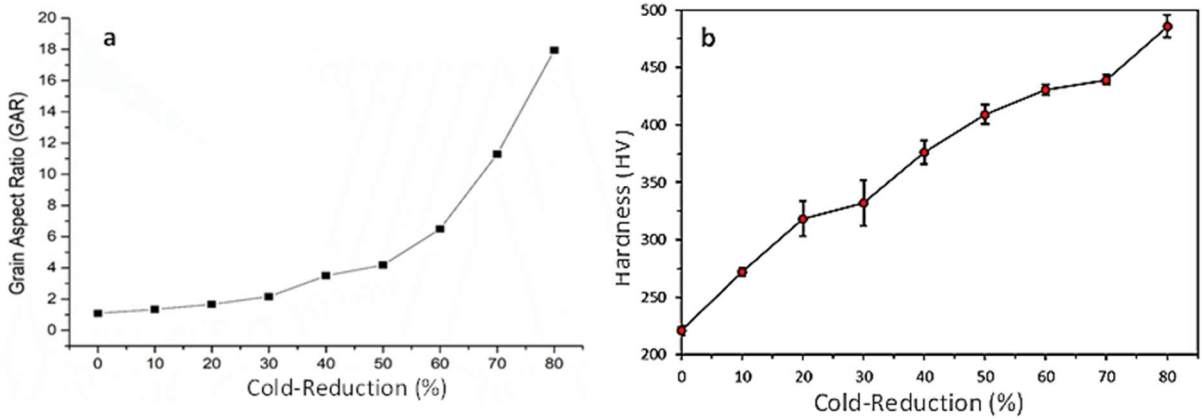

Figure 5.2: Curves showing variations in, (a) grain aspect ratio, and (b) hardness, of cold-rolled IN 601 sheets with an increase in the cold-reduction.

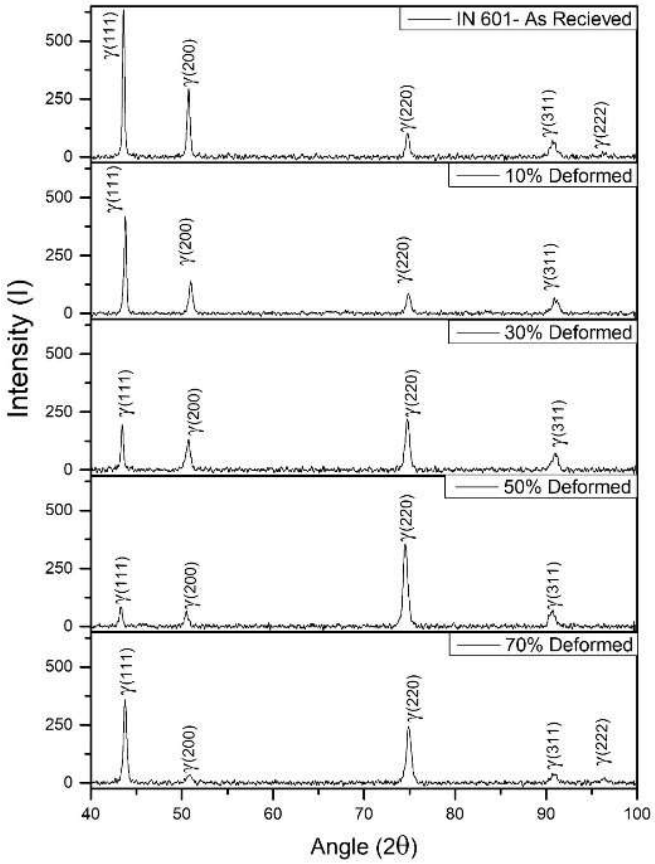

Figure 5.3: XRD profiles of as-annealed and cold-rolled IN 601 sheets showing significant variations in the relative peak-intensities with increased cold-reduction.

XRD profiles of as-annealed and cold-rolled IN 601 sheets are presented in Figure 5.3. The peaks are all indexed indicating that the sheets possess only the FCC γ-phase and that there is no phase transformation occurring during the cold-working. However, it is

notable that the relative intensities of γ-peaks vary systematically with increase in the cold-reduction suggesting that IN 601 sheets show crystallographic texture during cold-rolling.

Figure. 5.4 presents the IPF Maps of IN 601 sheets in as-annealed and cold-rolled conditions. It is clear from the IPF maps that the randomly oriented grains in the annealed sheet show (101) and (111) orientations dominantly along the rolling direction when cold-rolled up to 50% reduction. However, the grains are severely deformed during higher cold reductions. EBSD rotation-angle maps of 30% and 50% cold-reduced sheets show increased high-angle rotations with increased cold-reduction causing crystallographic textures in cold-rolled sheets (Figure. 5.5).

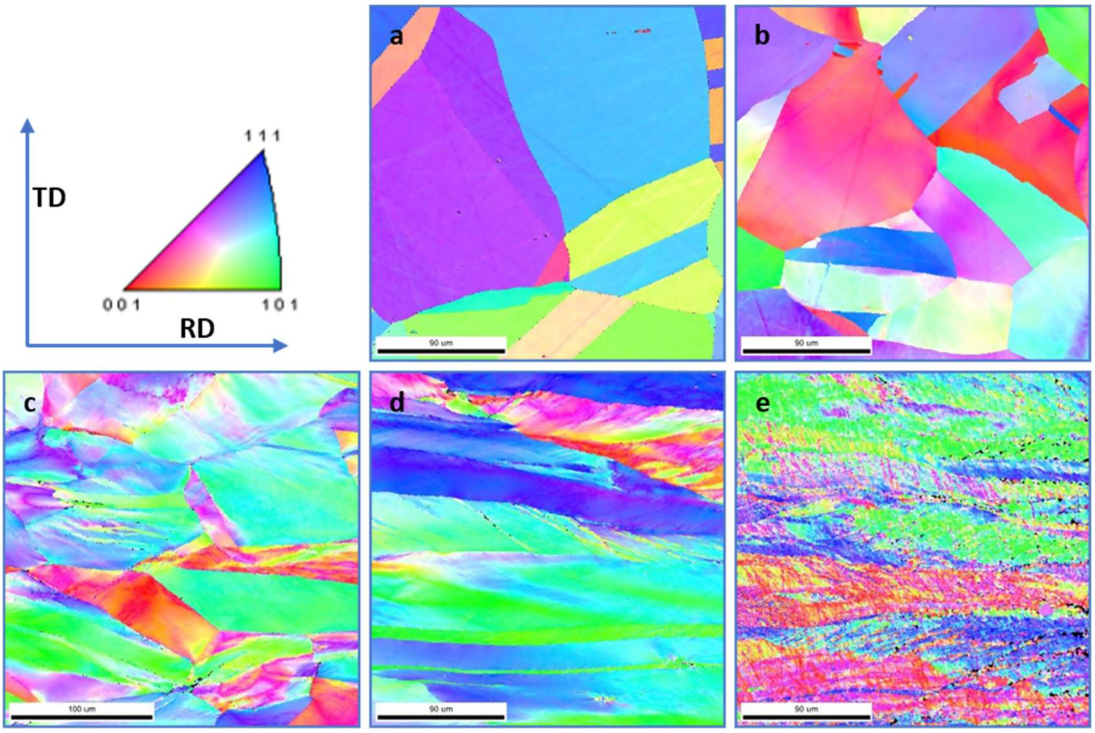

Figure 5.4: IPF maps of IN 601 sheets for: a) 0%, b) 10%, c) 30%, d) 50%, and e) 70% cold-reduction, showing crystallographic-orientations relative to Rolling Direction (RD) and Transverse Direction (TD).

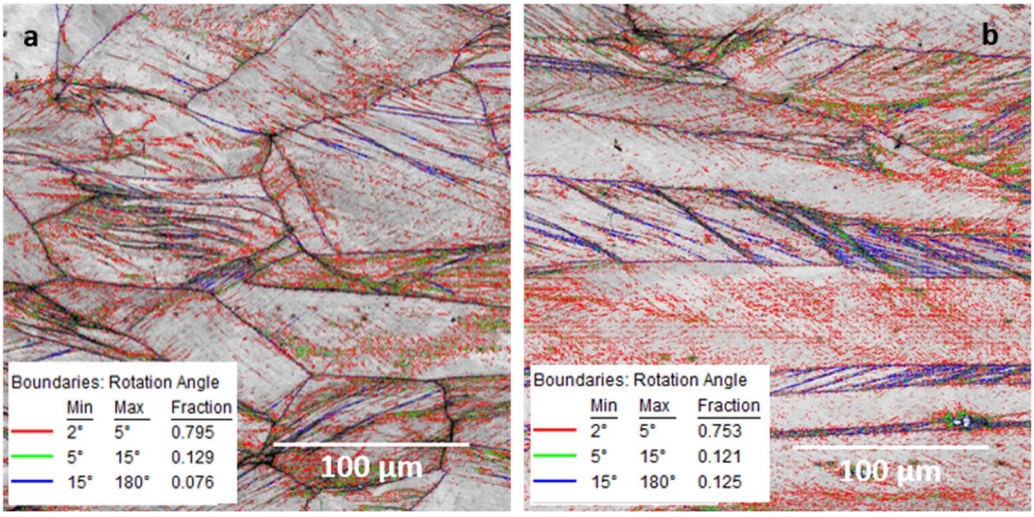

Figure 5.5: EBSD rotation-angle map of: a) 30%, and b) 50% cold-reduced sheets showing increased high-angle (> 15°) rotation with increased cold-reduction.

Tensile behaviour of cold-rolled IN 601sheets along the rolling direction is presented in Figure 5.6. It is clear from the engineering stress-strain curves that both the yield-strength (σ_y) and the ultimate tensile strength (σ_{uts}) of IN 601 sheets increase while the ductility decreases monotonically with increased cold-reduction. The increase in the tensile strength with the increase in the cold reduction is steady and linear in most part. However, the yield strength increases quite sharply up to 30% reduction and merges with the tensile strength for increased cold reduction. Accordingly, the ductility drops sharply with cold reduction between 0% and 30% reduction. However, drop in the ductility in excess of 30% reduction is rather steady. Thus, the tensile test results suggest that cold rolling of IN 601 causes a dramatic increase in the strength and sharp decrease in the ductility up to 30% reduction. This information should be of significant value for designing efficient mechanical processes of IN 601 such that the processing defects can be minimized, and that the equipment can be safeguarded against excessive stresses. Table 3 provides a comprehensive picture of the mechanical properties of cold-worked IN 601. It is important to note that variations in the tensile properties match very well with the variation in the hardness. There is a direct correlation between the hardness (HV) and the yield strength (MPa) of the cold-worked IN 601. Thus, an empirical formula for converting the hardness of IN 601 into the tensile strength can be proposed for IN 601 as, Tensile Strength (MPa) = 2.5 x Hardness (in HV).

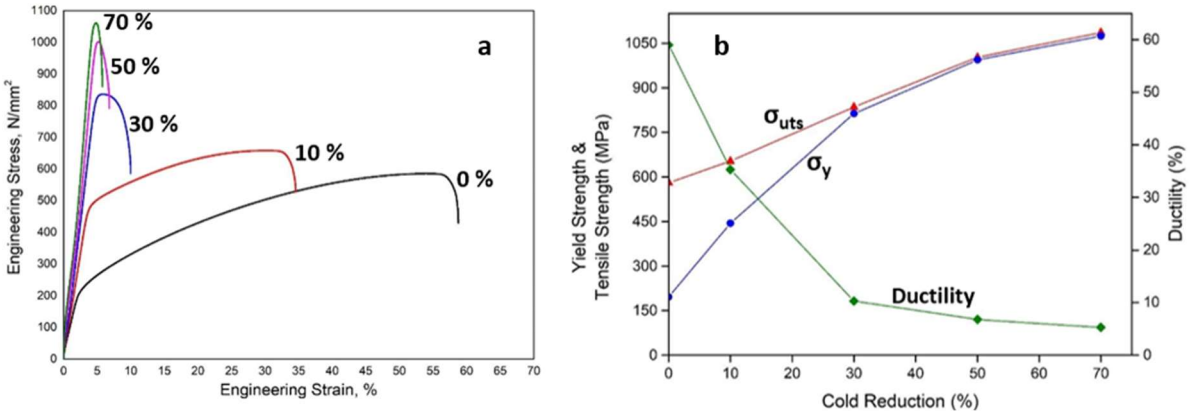

Figure 5.6: Tensile behaviour of cold-rolled IN 601 sheets along the rolling direction.

Table 5.1: Mechanical properties of cold-worked IN 601 sheets.

Cold-Reduction (%)	Yield Strength σ_y (MPa)	Tensile Strength σ_{uts} (MPa)	Ductility (%)	Hardness (HV)	σ_y/σ_{uts}	σ_{uts}/HV
0	196	580	59	224	0.34	2.59
10	444	653	35.3	270	0.68	2.42
30	813	835	10.3	332	0.97	2.52
50	994	1002	6.8	409	0.99	2.45
70	1074	1086	5.3	439	0.99	2.47

5.2 Effect of Annealing

Microstructures of thermomechanically processed IN 601 sheets are presented comprehensively in Figure 5.7 in the form of a matrix of degree of cold-reduction and annealing temperature. The microstructural matrix confirms that 10% and 20% cold-reduced specimens do not show any indication of microstructural change irrespective of the annealing temperature. However, 30% cold-reduced specimen shows a gradual change in the microstructure with increasing annealing temperature, and $0.8T_m$ annealed specimen indicates the on-set of recrystallization. The 40% and 50% cold-reduced specimen shows similar trend with a shift in the on-set of recrystallization to $0.7T_m$ annealing. The 50% cold-reduced specimen indicates a further shift in the on-set of recrystallization to $0.6T_m$. The 60%, 70%, and 80% cold-reduced specimens show highly etched slip-bands after annealing at $0.5T_m$ and $0.6T_m$ suggesting that the nucleation might have been initiated at these temperatures especially at the slip-bands

and the grain-boundaries. However, these specimens show completely recrystallized grains after annealing at $0.7T_m$ and $0.8T_m$.

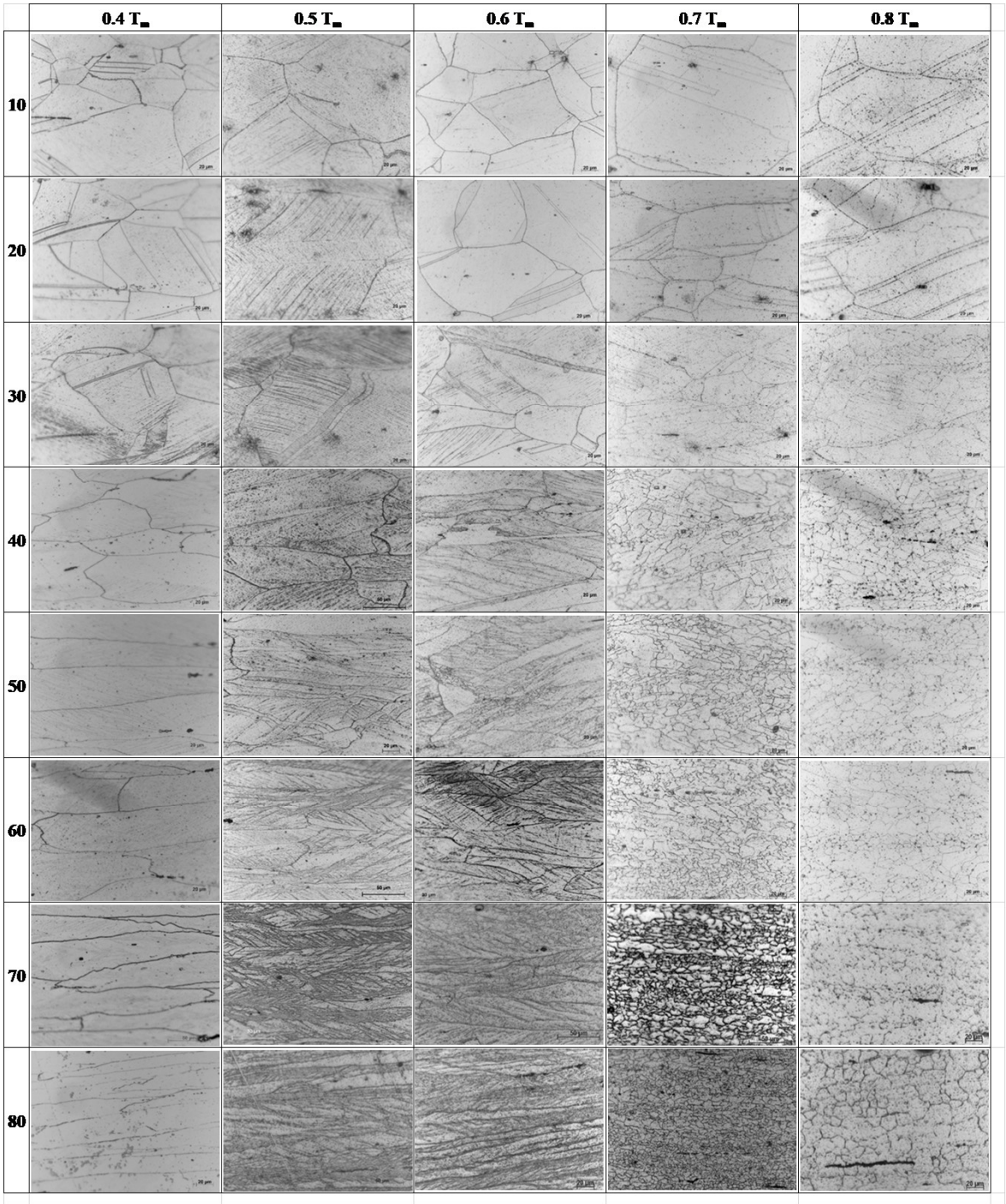

Figure 5.7: Longitudinal microstructures (500X) of cold-rolled and isothermally annealed IN 601 sheets; the microstructural variation is presented as a matrix with cold-reductions (10% - 80%) arranged along rows and annealing temperatures ($0.4T_m$ - $0.8T_m$) as columns.

Figure 5.8 presents the hardness profiles of cold-reduced IN 601 sheets as a function of annealing temperature. It should be noted that the hardness of the material was 224 HV before cold-rolling. However, after cold-rolling, the hardness increases monotonically with increased cold-reduction from 224 HV to about 475 HV. Thus, the hardness values of cold-rolled sheets at the room temperature (~ $0.2T_m$) should be considered as the reference points. It is generally expected that the hardness profiles of cold-rolled material should decrease monotonically with increase in the annealing temperature as the thermal activation during the isothermal annealing of the work-hardened alloy should enable, recovery, recrystallization, and grain-growth. However, the cold-rolled and annealed IN 601 sheets consistently displays an increasing-decreasing trend in the hardness profile irrespective of the degree of cold-reduction.

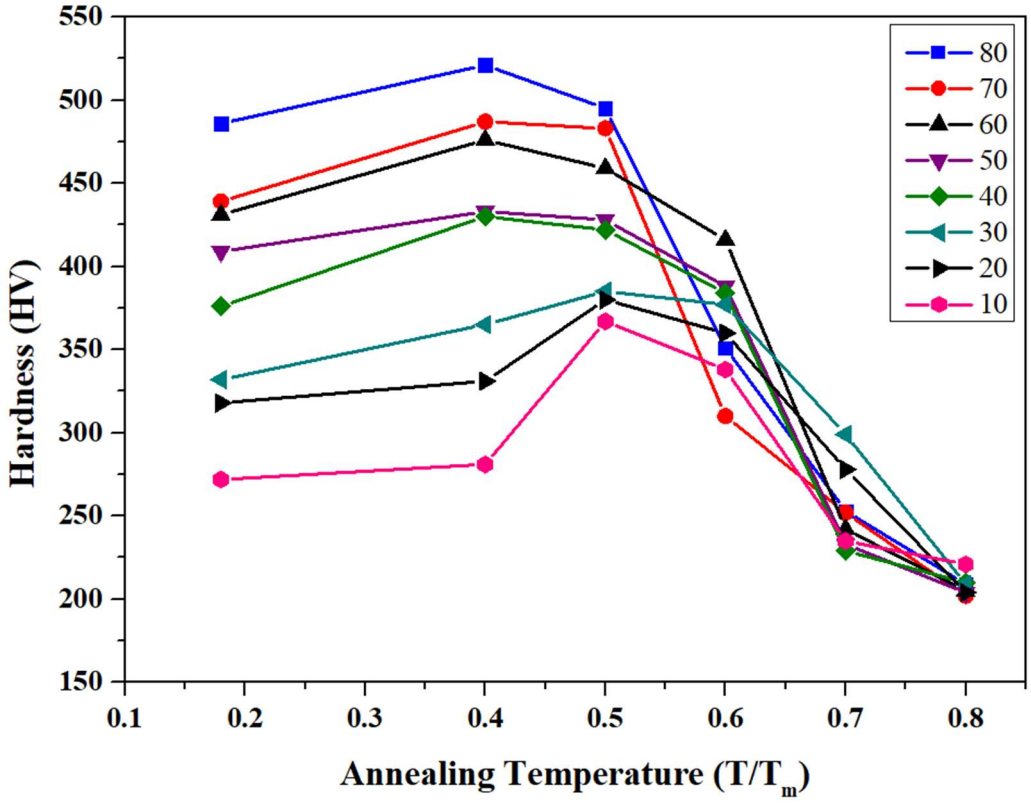

Figure 5.8: Hardness variations of cold-rolled IN 601 sheets with annealing temperature.

The 10%, 20% and 30% cold-worked sheets attain the peak-hardness after $0.5T_m$ annealing, while the peak-hardness shifts to $0.4T_m$ for highly cold-worked sheets.

Following the peak-hardness, there is a gradual decrease in the hardness profile between $0.5T_m$ and $0.6T_m$ annealing. The hardness profile dips sharply after annealing between $0.6T_m$ and $0.7T_m$. This trend in the hardness profile can be attributed to the recovery and recrystallization phenomena occurring during the annealing. However, consistently increased hardness during the low temperature annealing of the cold-rolled alloy is not obvious. This suggests that an interesting phenomenon occurs in the cold-worked IN 601 prior to the recovery stage during annealing. This phenomenon can only be termed as 'aging' at this stage.

The hardness profiles and the microstructural features of the cold-rolled and isothermally annealed sheets can be generalized into three groups; (a) 10% - 30% cold-rolled sheets that show peak-hardness between $0.5T_m$ and $0.55T_m$ and do not fully recrystallize during annealing up to $0.8T_m$, (b) 40% - 60% cold-rolled sheets that show peak-hardness between $0.45T_m$ and $0.5T_m$ and recrystallize during annealing at $0.7T_m$ and, (c) 70% - 80% cold-rolled sheets that show peak-hardness between $0.4T_m$ and $0.45T_m$ and recrystallize between $0.6T_m$ and $0.7T_m$. The cold-rolled sheets representing these three groups should provide a comprehensive picture of the tensile behaviour of cold-rolled and annealed IN 601.

Tensile stress-strain curves of 30%, 50% and 70% cold-reduced sheets along the rolling-direction are presented in Figure 5.9. The stress-strain curves presented in the figure confirm that there is an increasing-decreasing trend in the tensile-strength of cold-rolled (CR), $0.4T_m$, exposed, and $0.5T_m$ exposed specimens. The tensile strength decreases while the ductility increases monotonically with increasing annealing temperatures, $0.6T_m$, $0.7T_m$, and $0.8T_m$. This tensile behaviour of IN 601 is similar for 30%, 50% and 70% cold-reduced sheets. However, the 50% and 70% cold-reduced sheets show a segregation in the stress-strain curves. Up to $0.5T_m$ annealing, yield-strength, tensile strength and ductility of the sheets are very close to that of cold-rolled sheet. However, the strength drops and the ductility increases drastically when 50% and 70% cold-reduced sheets are annealed above $0.5T_m$. This abrupt change in the tensile behaviour should be attributed to the recrystallization phenomenon occurring in these sheets. It is important to note that the stress-strain curves of 30% cold-reduced sheets vary gradually with the annealing temperature likely because these sheets do not recrystallize up to $0.8T_m$ as confirmed by the microstructures presented in Figure 5.7.

Additionally, interesting yield phenomenon is noticed in the 70% cold reduced samples annealed at 0.6 T_m and 0.7 T_m, where discontinuous yielding is observed. This phenomenon is due to the Cottrell atmosphere likely because the alloy (IN 601) comprises of interstitial carbon. For this reason, the yield phenomenon is quite remarkable and appears similar to that of mild steel. However, discontinuous yielding is observed in other specimens as well, but it is quite subtle.

By clubbing the results of hardness measurement and the tensile tests, a comprehensive picture of the mechanical behaviour of cold-rolled and annealed IN 601 is provided in Figure 5.10. The tensile behaviour matches with the hardness profile. There is an increasing-decreasing trend in the hardness and the strength of the cold-worked IN 601 as a function of annealing temperature. The ductility curve is quite peculiar as 30% cold-rolled sheets show gradually increasing ductility with increase in the annealing temperature, while 50% and 70% cold-rolled sheets show a sudden increase in the ductility after annealing at $0.6T_m$. This behaviour suggests that the sheets that are cold-rolled by 50% and above recrystallize in most part during annealing at $0.6T_m$.

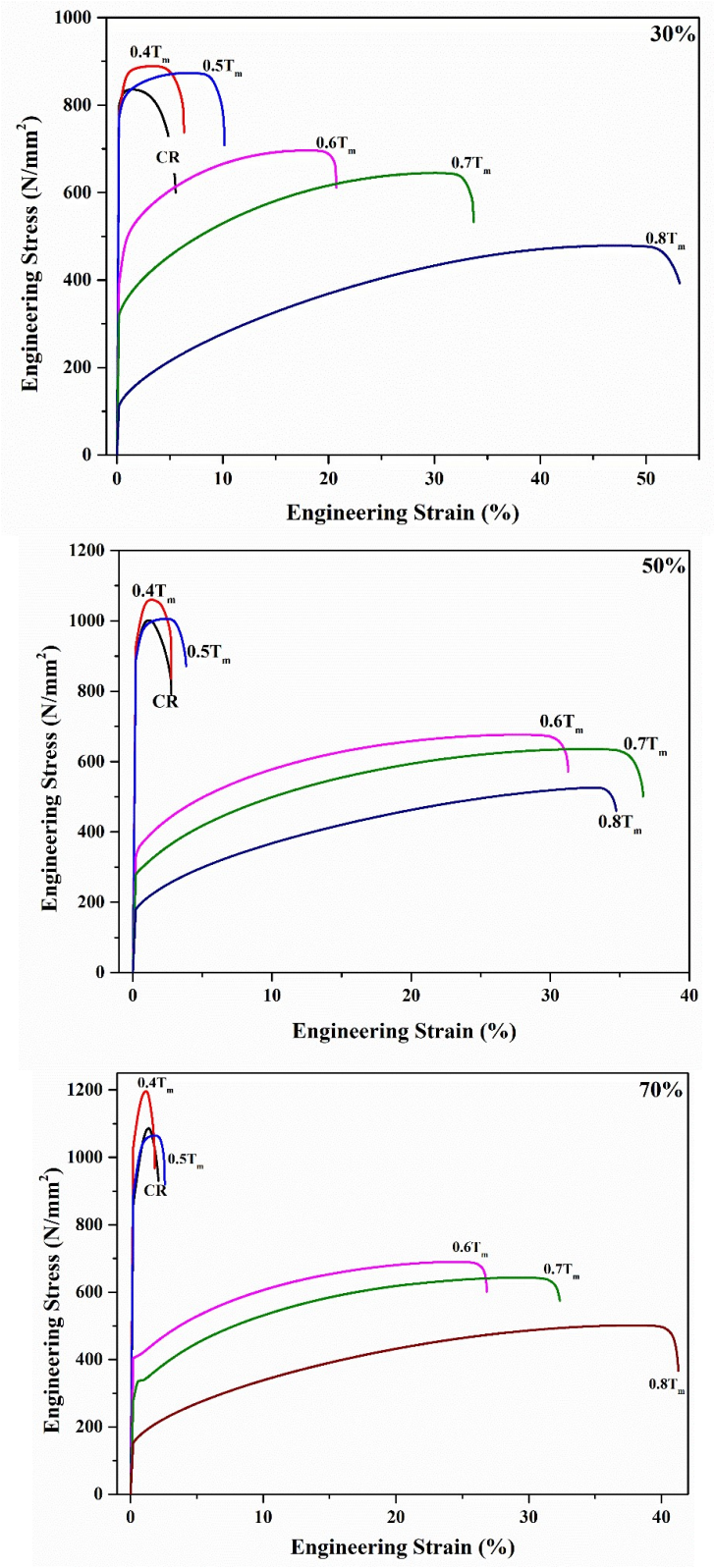

Figure 5.9: Tensile behaviour of 30%, 50% and 70% cold-rolled IN 601 after isothermal-annealing at $0.4T_m$, $0.5T_m$, $0.6T_m$, $0.7T_m$, and $0.8T_m$.

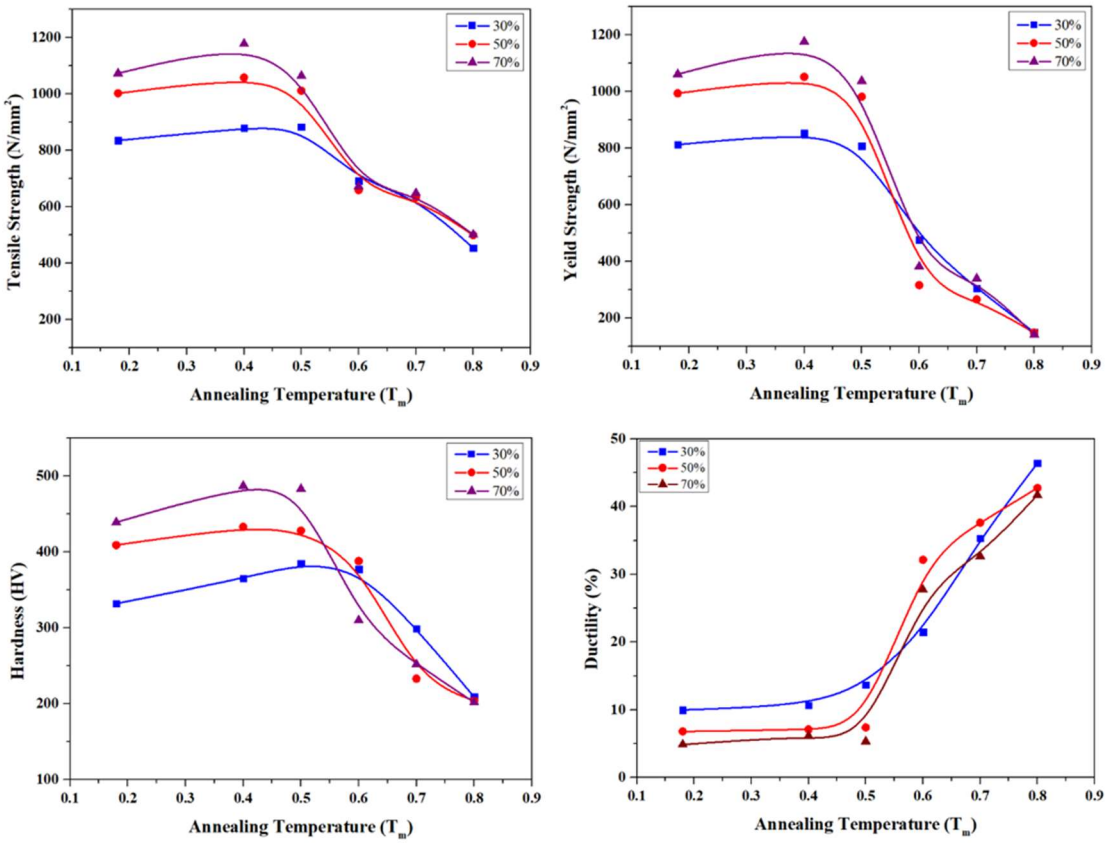

Figure 5.10: Mechanical behaviour of cold-rolled IN 601 as a function of annealing temperature.

Figure 5.11 presents the XRD profiles of cold-rolled IN 601 sheets following isothermal-annealing at $0.4T_m$, $0.5T_m$, $0.7T_m$, and $0.8T_m$. The XRD profiles of $0.4T_m$ and $0.5T_m$ annealed sheets shown in Figures 5.11(a) and 5.11(b) are comparable to that of as-rolled sheets shown in Figure 5.3. This suggests that there is neither a notable crystallographic change nor any phase-transformation occurring during the low-temperature annealing of strain-hardened IN 601. In Figure 5.9(c), 10% and 30% cold-rolled sheets do not show any significant change in the profile. However, 50% and 70% cold-reduced sheets after $0.7T_m$ annealing indicate that the crystallographic texture reverted to the random-orientation. The XRD results when corroborated with the microstructures and the mechanical behaviour suggest that, there is neither strain-induced transformation nor precipitation occurring during the processing of IN 601, and the recrystallization temperature of IN 601 lies between $0.5T_m$ and $0.7T_m$.

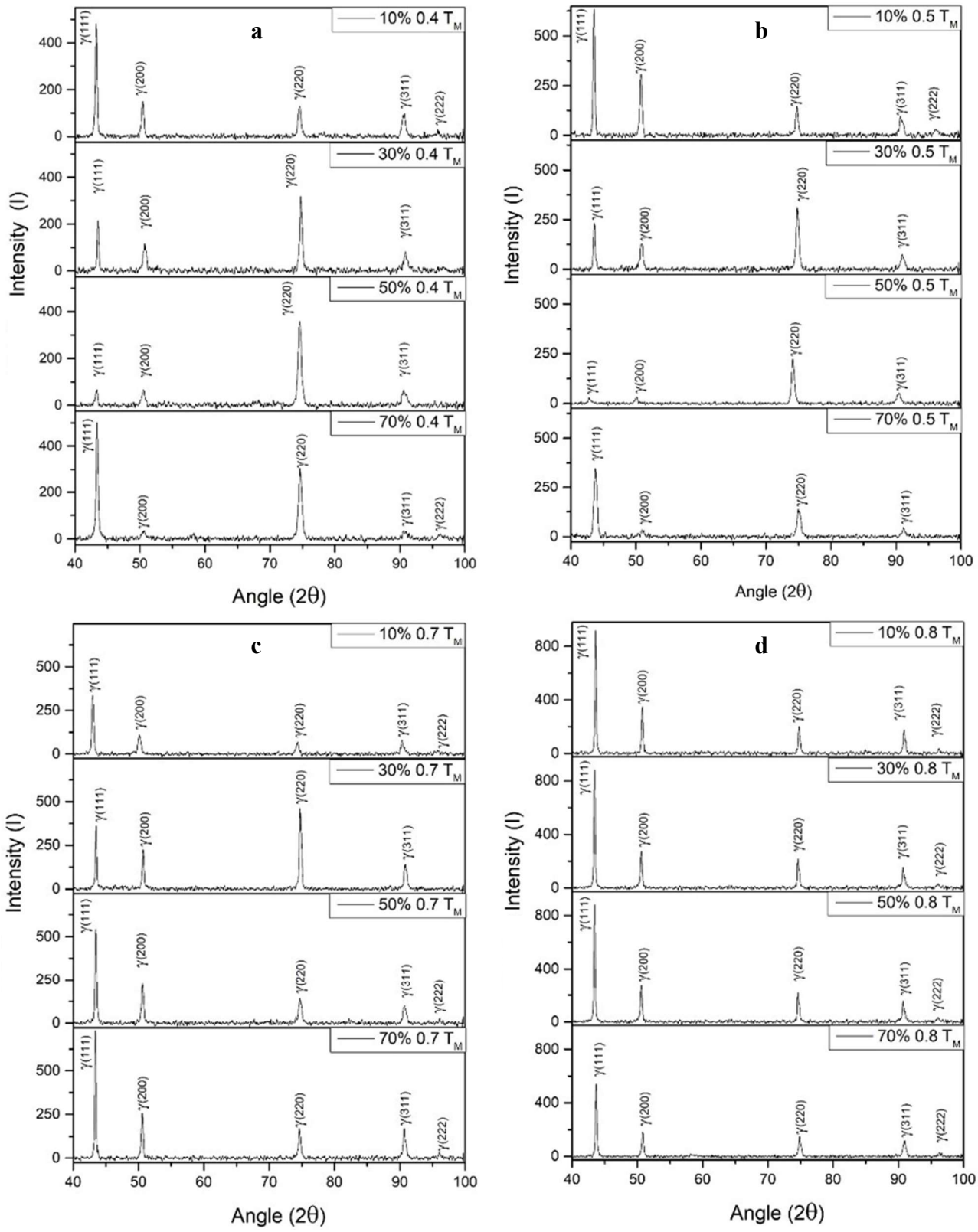

Figure 5.11: XRD profiles of 10%, 30%, 50% and 70% cold-rolled IN 601 sheets after isothermal annealing at (a) $0.4T_m$, (b) $0.5T_m$, (c) $0.7T_m$, and (d)$0.8T_m$.

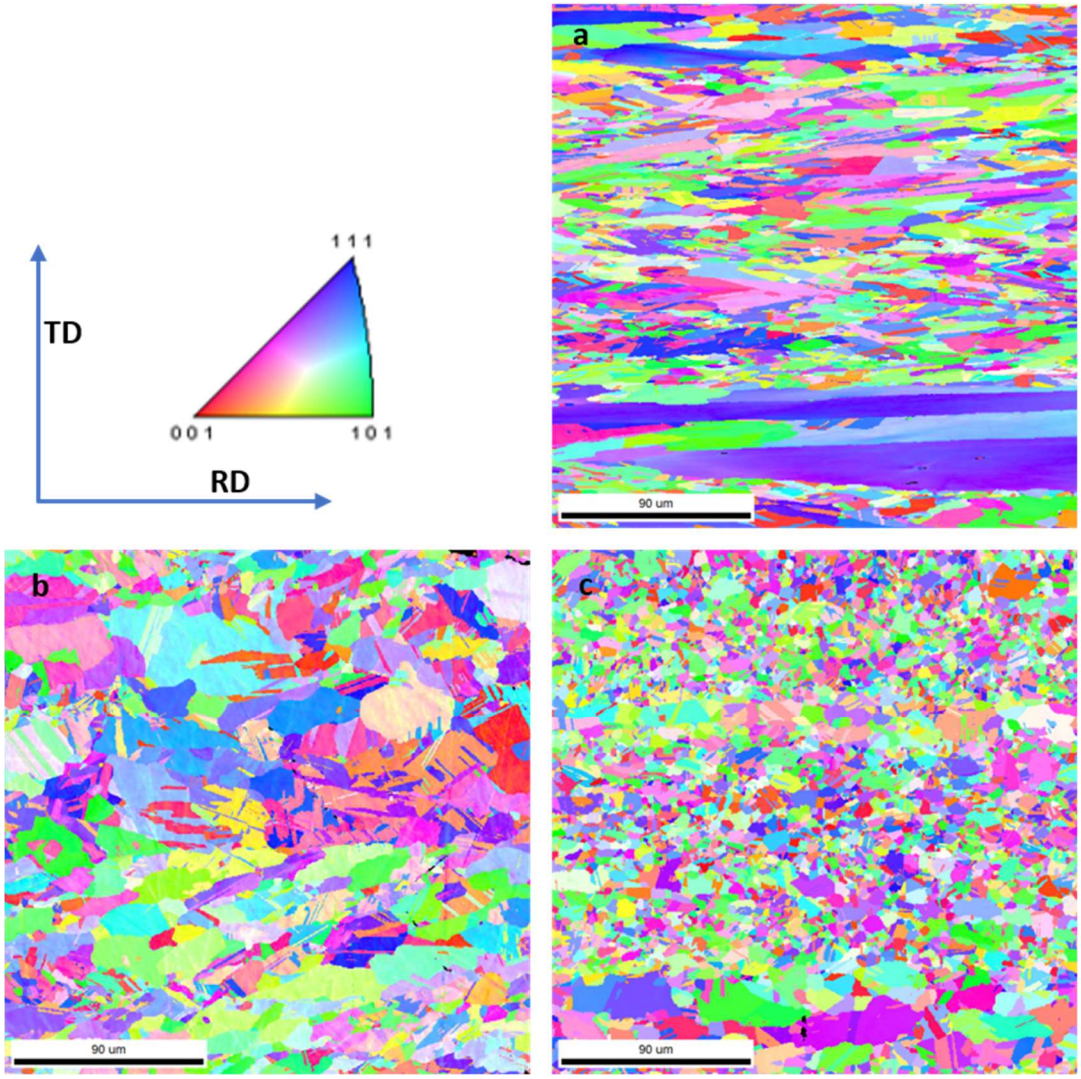

Figure 5.12: IPF maps of: a) 50%, b) 70%, and c) 80% reduced sheets following $0.7T_m$ annealing.

Figure 5.12 presents the EBSD results of 50%, 70%, and 80% cold-rolled and $0.7T_m$ annealed sheets. The IPF maps presented in the figure suggest that 70% and 80% cold-rolled sheets recrystallize during annealing at $0.7T_m$. In 50% cold-reduced sheet majority of the grains are fine, elongated and recrystallized. However, a few grains remained uncrystallized suggesting that this is the onset of recrystallization. The grain-boundary maps presented in Figure 5.13 confirm that more than 95% of the recrystallized grains have high-angle grain-boundaries.

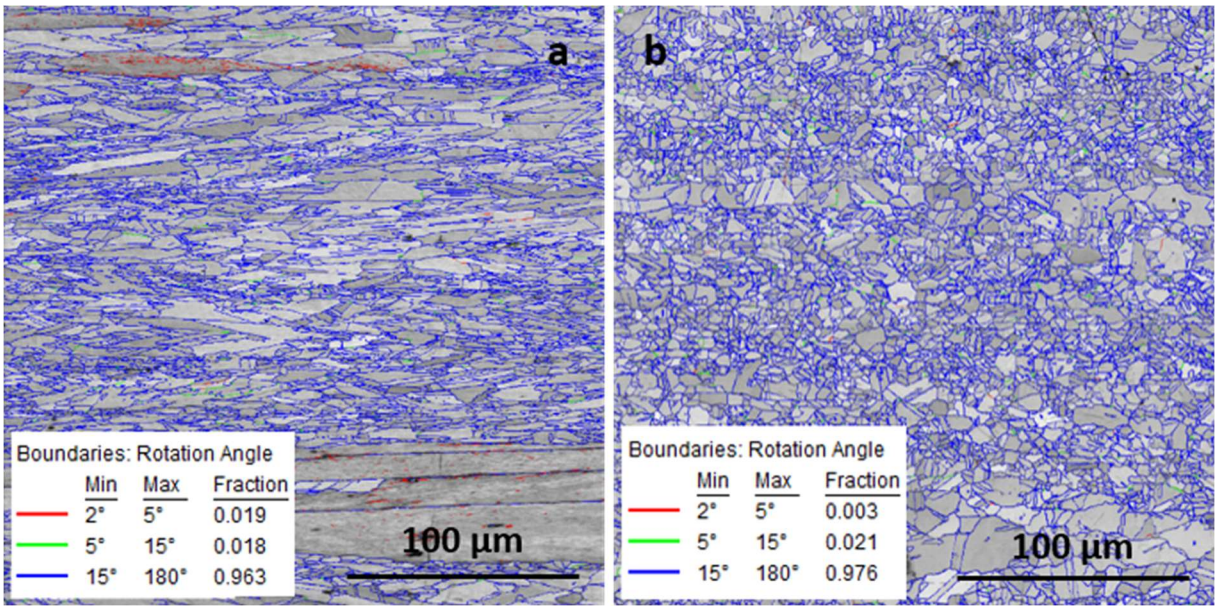

Figure 5.13: Grain boundary maps of: a) 50%, and d) 80% reduced sheets following $0.7T_m$ annealing.

5.3. Discussion

The cold-rolling and annealing experiments, the mechanical testing, and the structural characterization carried out in the present investigation yield the following key results. (a) Prior-coldworked sheets consistently display increasing-decreasing trend in both strength and hardness of the alloy with increasing isothermal annealing temperature, (b) The 50% cold-rolled sheet, on isothermal exposure at $0.7T_m$ produces fine-recrystallized grains with high aspect ratio along the rolling direction.

The first key-result confirms that the peak-hardening of prior-coldworked sheets occurs during low-temperature annealing. On higher temperature exposures the alloy softens due to recovery and recrystallization. This non-monotonic trend is consistent irrespective of the degree of prior-coldworking. The mechanism involved in this peak-hardening is not clear as the microstructural details and XRD analysis neither show any phase-transformation nor precipitation of any hard-particles occurring during low-temperature annealing. However, considering that IN 601 contains carbon as the interstitial solute and the sheets were prior-coldworked, it is most likely that the alloy is displaying hardening due to solute-pinning effect of dislocations and this phenomenon can be identified as ‘strain-aging’.

Advanced characterization techniques including TEM and atom-probe analyses should confirm the peak-hardening mechanism. However, it is challenging to characterize and analyze heavily deformed specimens considering that densely populated dislocation network would clutter the images. In-situ loading-unloading type tension tests at low strain-rates should also reveal the strain-hardening effect on the yielding. Discontinuous yielding is considered indicative of strain-aging by interstitial solute-pinning of dislocations (Cribb and Reed-Hill 1977; De et al. 1999; Hong et al. 1996; Stahl et al. 2001). In the present work, there are indications that annealed IN 601 display discontinuous yielding. From the tensile behaviour tests in Figure 5.9, the raw data of tension tests especially of $0.6T_m$ and $0.7T_m$ exposed specimens do show discontinuous yielding as shown in Figure 5.14. Thus, the current investigation supports the solute-pinning mechanism of strain-aging in IN 601.

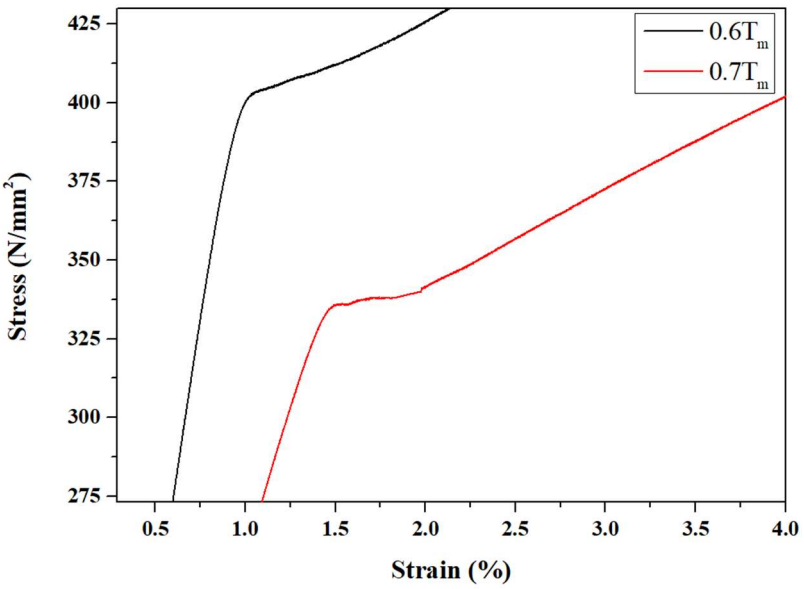

Figure 5.14: Stress-Strain curve of $0.6T_m$ and $0.7T_m$ exposed specimen showing discontinuous yielding.

It is important to consider that the alloy contains significant amount of chromium that may form chromium-carbides in most part. However, a small fraction of interstitial carbon is sufficient to cause strain-aging (De et al. 1999). From Figure 5.8, it is clear that the higher the degree of prior-coldworking the lower is the peak-hardening

temperature. This suggests that the peak-hardening is a diffusion-controlled phenomenon. As the dislocation density increases with increasing cold-working, the diffusion distance between evenly distributed solute and highly populated dislocations should decrease significantly and 'solute-pinning' should occur rather quickly even at a lower thermal activation. On exposure to higher temperatures, higher mobilities of dislocations and atoms should cause recovery-softening followed by recrystallization. Thus, the strain-aging effect for heavily deformed sheets should be higher at lower temperature exposures and the same should diminish as the sheets are exposed to higher temperatures.

This phenomenon is recognized and reported to occur in IN 601 (Cui et al. 2012; Gopinath et al. 2009). However, prior-straining was either limited or the dynamic-strain-aging at elevated temperature was reported. The negative effects of strain-aging of IN 601 components is also reported (Stahl et al. 2001). The present work provides a comprehensive picture that irrespective of the degree of prior-coldwork the alloy displays strain-aging during low-temperature exposure. The hardness profiles, engineering stress-strain curves, and the microstructural results presented in this work suggest that there are multiple stages in the annealing behaviour of IN 601 including strain-aging, recovery, and recrystallization as the annealing temperature increases. To have a comprehensive picture on the thermomechanical processing of the alloy, a 'Thermomechanical Processing Map' is proposed as shown in Figure 5.15.

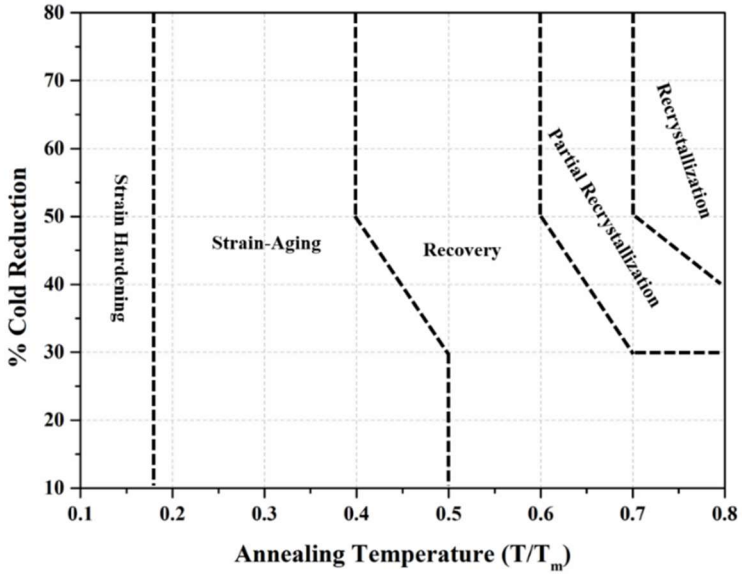

Figure 5.15: Thermomechanical Processing Map of IN 601.

Since the map is constructed out of the limited experimental results, the trajectories are shown as splines rather than smooth contours. The map can be refined in future with more experimental results and using theorical modelling so that splines may be replaced with smooth-contours. This map will be significant for designing thermomechanical processing sequences of the alloy as various fields of metallurgical phenomenon corresponding to key processing parameters are shown.

It is important to recognize that 50% cold-reduced IN 601, on 1h isothermal annealing at $0.7T_m$ produces quite an unusual microstructure as confirmed by the EBSD results shown in Figure 5.12 and 5.13. The fine recrystallized grains are elongated along the rolling direction and arranged themselves as a pan-cake like structure. The reason for developing such a unique microstructure in IN 601 is not clear at this stage. However, from the EBSD IPF maps shown in Figure 5.12 that $0.7T_m$ annealing temperature for 50% prior-coldworked IN 601 should be onset of recrystallization. The corresponding EBSD map shows that there are a few un-recrystallized grains along with the recrystallized grains. It is likely that during the onset of recrystallization, discretely formed nuclei grew along slip-bands to form the unique microstructure. This should be thermodynamically favourable condition for the growth of the grains. More work has to be carried out to understand the evolution of this unique microstructure. However, at this stage, it is important to recognize that this is a unique microstructure for a wrought

alloy and it resembles the directionally solidified grain-structures in cast-superalloys for turbine blading applications. Considering that the grains in the IN 601 are fine and that the effective transverse grain-boundary distance is quite large in the rolling direction, this microstructure should provide both fatigue and creep resistance.

6. RESULTS AND DISCUSSION OF SS 304

This section presents the results and associated analysis of cold-rolling experiments, annealing experiments, hardness measurements, tensile tests, XRD analysis, EBSD analysis. The section provides a comprehensive summary of the thermomechanical processing of the second experimental material, SS 304 and proposes a Recrystallization Map based on the experimental results.

6.1 Effect of Cold-Reduction

Figure 6.1 presents longitudinal microstructures of as-received and cold-rolled SS 304 sheets. The as-received sheet in mill-annealed condition shows fine-equiaxed grains and presence of finely distributed grains. The average grain size of the material is found to be about 25 μm. Microstructures of cold-rolled 304 sheets show grains becoming more and more elongated/ flattened along the rolling-direction with an increase in the cold-reduction. Figure 6.2 presents the effect of cold-reduction on the grain aspect ratio (GAR) and hardness. It is clear from the figure that both the GAR and hardness of the material increase monotonically with increasing cold-reduction. It is interesting to note that the GAR increases non-linearly from 1:1 for mill-annealed condition to about 8:1 for 70% reduction. However, unlike IN 601, the increase in the hardness between 10% and 70% reduction is quite linear for SS 304. This suggests that SS 304 hardens slightly differently from IN 601. It is likely that the Strain-Induced Martensitic Transformation (SIM) that is known to occur in SS 304 is influencing the hardening behaviour.

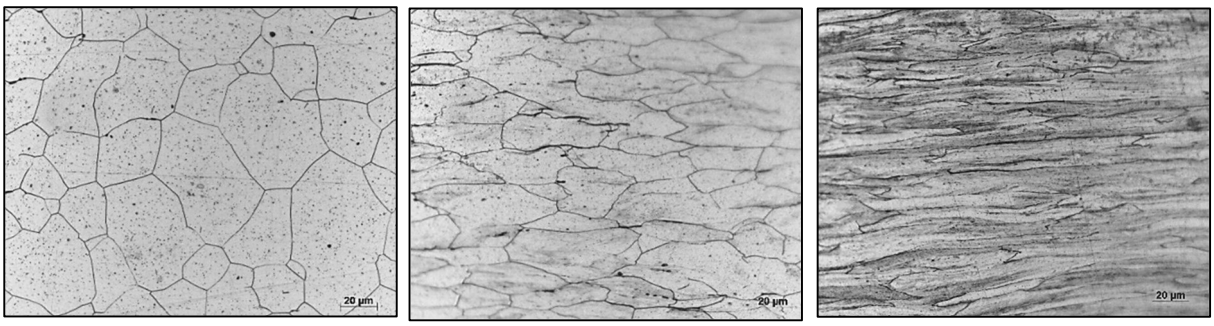

Figure 6.1: Longitudinal microstructures of SS 304 sheets showing flattening of equiaxed grains during cold-rolling; (a) as-annealed, (b) 50% cold-rolled, and (b) 70% cold-rolled.

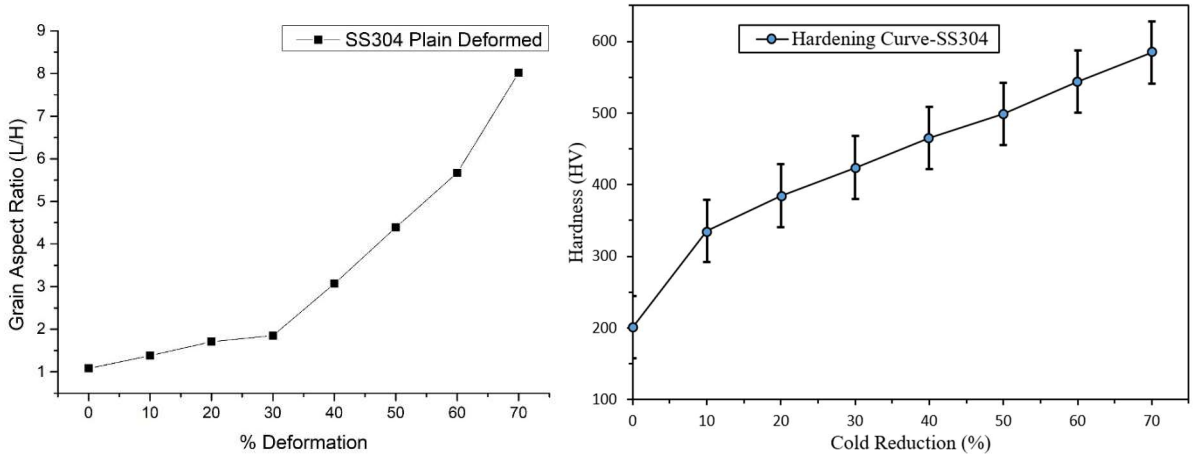

Figure 6.2: Curves showing variations in, (a) grain aspect ratio, and (b) hardness, of cold-rolled SS 304 sheets with increasing degree of cold reduction.

It is possible that the phase-fraction of martensite may correlate linearly with increase in the cold-reduction and corresponding increase in the hardness of SS 304. It is likely that the higher the dislocation density, the higher is the formation of strain induced martensite (SIM) contributing to increase in the hardness from 200 HV for as-received sheet to 584 HV for 70% cold-reduced sheet. XRD analysis and EBSD analysis should provide more information regarding the SIM.

Figure 6.3 shows XRD profiles of the as-received and cold-rolled SS 304 sheets. As-received sheet shows the typical FCC XRD pattern for an austenitic stainless steel characterized by $(111)_\gamma$, $(200)_\gamma$, $(220)_\gamma$ and $(311)_\gamma$ peaks. Considering that SS 304 is a single-phase m-type material, there is no indication of any other phase in the XRD profile of as-received sheet. However, strain-induced phase-transformation of SS 304 by the formation of α′-martensite is characterised by $(110)_{\alpha'}$ peaks. These peaks are detected for cold-reductions of 10% and above. With increasing cold-reduction the intensity of α′-Martensite peaks is increasing while intensity of austenite peaks is gradually decreasing. This suggests that the strain-induced martensitic transformation increases with an increase in the cold-reduction of SS 304. Additionally, the relative peak intensities of the primary (γ) phase are varying with increased degree of cold-reduction suggesting that there is a strong crystallographic texturing during cold-rolling of SS 304 sheets.

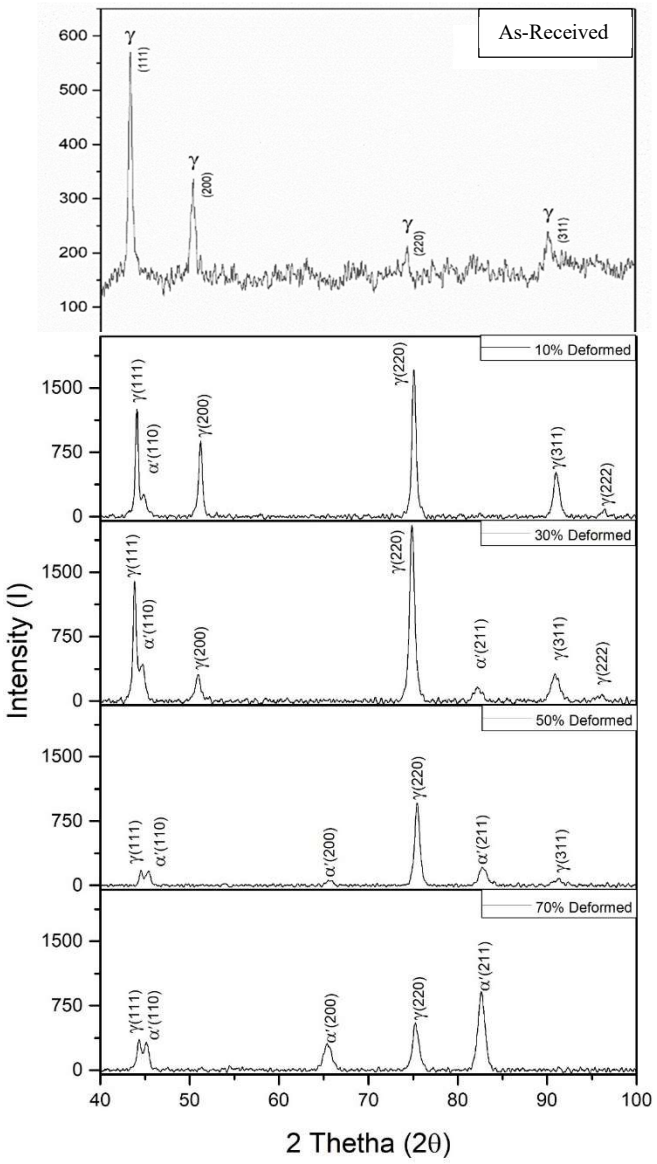

Figure 6.3: XRD profiles of as-received and 10% to 70% cold-reduced SS 304 showing crystallographic texturing and increased SIM with increased reduction.

Figure 6.4 and Figure 6.5 present EBSD Inverse Pole Figure (IPF) Maps and EBSD phase-fraction maps respectively for cold-rolled SS 304. It is clear from the IPF maps that the grain show (101) and (111) orientations dominantly along the rolling direction when cold-rolled up to 50% reduction. However, the grains are severely deformed during higher cold-reductions. These EBSD results confirm the indications of hardening behaviour and the XRD analysis. SS 304 shows increased SIM and increased texturing with increased cold-reduction.

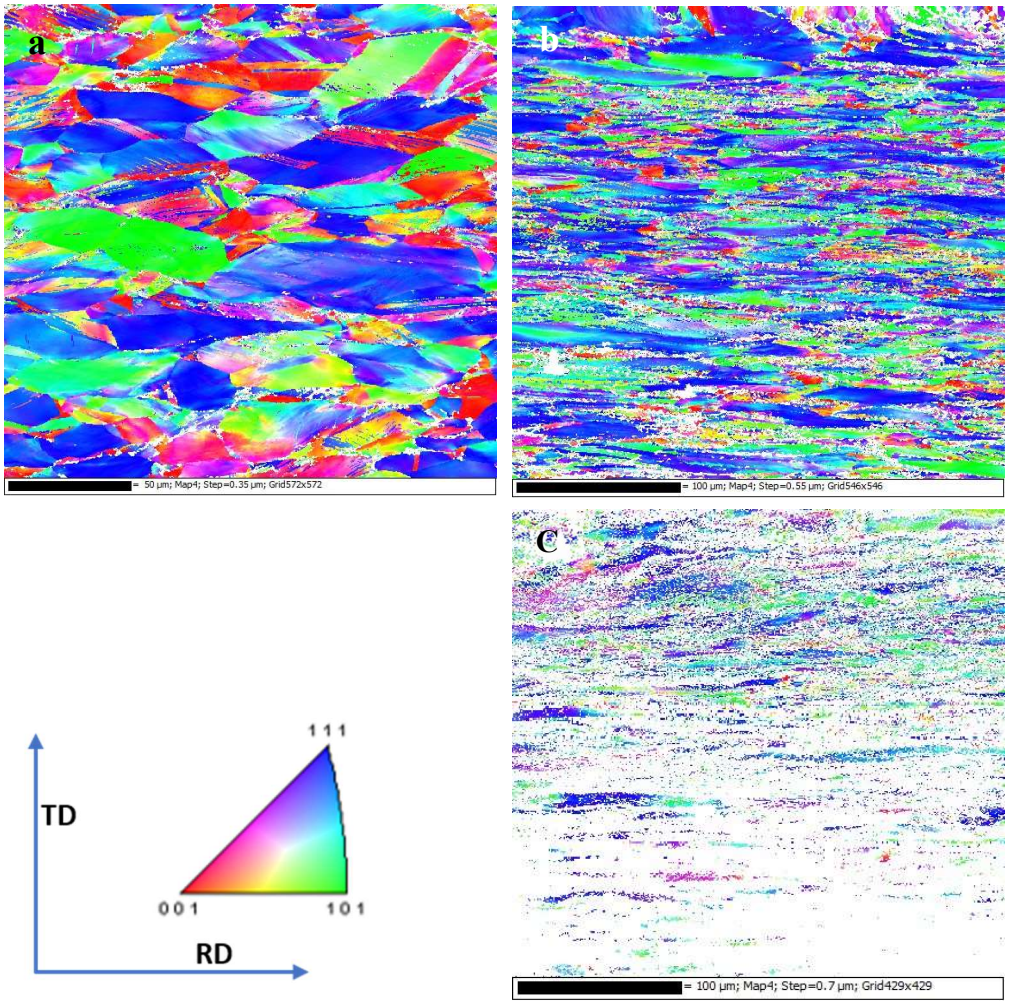

Figure 6.4: IPF maps of SS 304 sheets cold-rolled to: a) 30%, b) 50%, and c) 70%, showing crystallographic-orientations relative to Rolling Direction (RD) and Transverse Direction (TD).

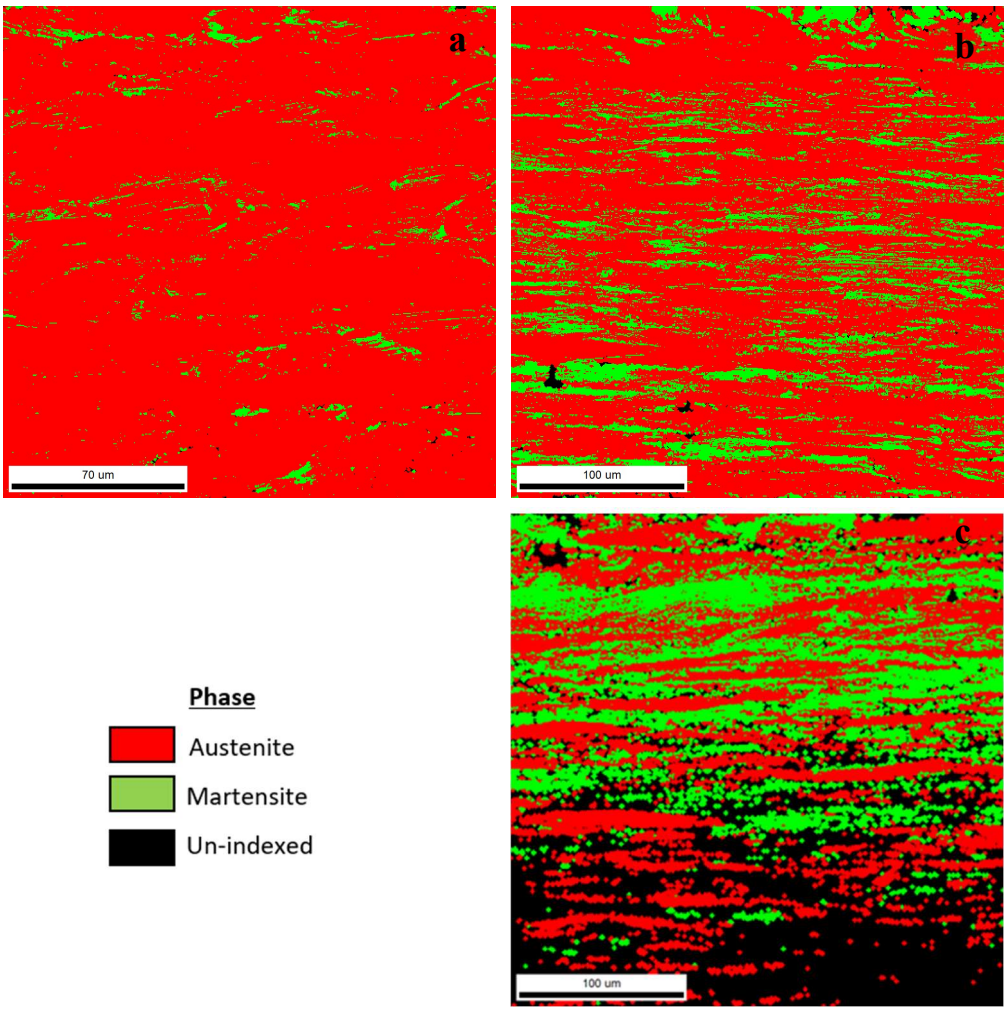

Figure 6.5: EBSD Phase Fraction Maps of cold-rolled SS 304 sheets showing increased SIM with increased reduction; a) 30%, b) 50%, and c) 70%.

6.2 Effect of Annealing

Figure 6.6 shows microstructural matrix of cold-rolled and annealed sheets. The figure provides a comprehensive picture of annealing behaviour of SS 304 that is subjected to wide range of cold-working (10% to 70% reduction) followed by isothermal annealing at wide range of temperatures ($0.3T_m$ to $0.7T_m$). For low annealing temperatures of $0.3T_m$ (244 °C) and $0.4T_m$ (416 °C) the microstructures appear dark, with shear bands appearing dark within the grains. For temperatures of $0.5T_m$ (590 °C) the shear bands appear more prominently compared to the grain boundaries, possibly indicating reversion of martensite. From the literature, it is known that above 400 °C α′-martensite is unstable and begins undergoing reversion and completely reverts to austenite at

750°C (Padilha et al. 2003; Singh 1985). It is clear from the microstructures that, irrespective of degree of cold-working, SS 304 does not recrystallize on thermal exposure up to $0.5T_m$ (588 °C). Microstructures for $0.6T_m$ (760 °C) at 20% shows partial recrystallization with grains nucleating within the shear bands and for strains above 20% new fine grains are formed indicating recrystallization of the deformed structure. The sheets annealed to $0.7T_m$ (933 °C) show equiaxed and large grains compared to as-received sheets indicating that recrystallization followed by grain growth has occurred. This result indicates that recrystallization temperature for this material is $0.6T_m$ for a threshold cold working of 20%.

It is understandable that the higher the cold-working, the greater is the energy stored in the material and hence higher is the driving force for recrystallization during annealing. Thus, when highly cold-worked material is exposed to recrystallization annealing, large number of nuclei would nucleate and grow to impinge upon each other to form fine-grained structure. Simply put, higher the strained sample, finer is the size of recrystallized grain. The converse must be true to produce coarse recrystallized grains in materials that are cold-worked to lesser degree. This suggests that, grain-size can be controlled by suitably controlling the nucleation kinetics during static recrystallization. It is evident from the microstructures that with higher activation energy during annealing at $0.7T_m$ (930 °C), recrystallization is complete followed by grain coarsening within one hour of exposure. These microstructural results confirm that the cold-rolling and annealing experiments performed in this work comprehensively cover recovery, recrystallization and grain growth phenomena of SS 304.

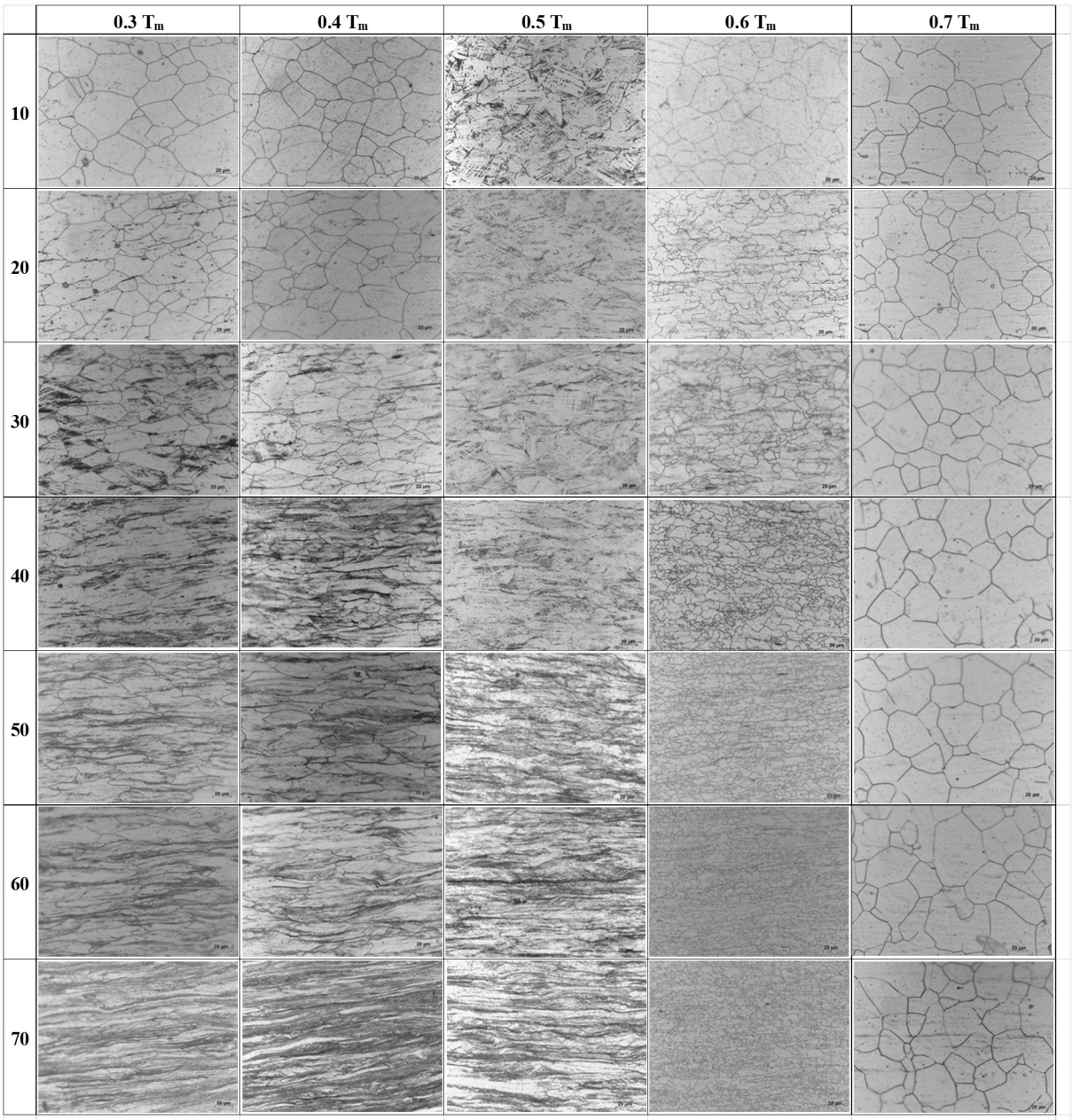

Figure 6.6: Microstructural matrix of SS 304 that is cold rolled by 10 % to 70 % reductions (shown in rows) followed by isothermal annealing for 1 hour at 0.3Tm to 0.7Tm (shown in columns).

Hardness profiles of cold-reduced and annealed SS 304 as a function of annealing temperature are presented in Figure 6.7. Hardness (HV) values increase linearly with increasing strain for cold rolling at room temperature. However, there is an increasing-decreasing trend in the hardness of cold-rolled sheets as the annealing temperature increases. Irrespective of the degree of cold-reduction, peak-hardening is observed in SS 304 for low-temperature annealing at $0.3T_m$ and $0.4T_m$. Similar phenomena have

been reported in the literature and they have attributed it to increase of α′-martensite amount for low annealing temperatures(Padilha et al. 2003). This work endorses the above observation. However, hardness values for specimens annealed at $0.5T_m$ drops below levels of cold rolled sheets. It is known that the strain induced martensite α' is unstable for temperatures above 400 °C and undergoes reversion to form austenite. The complete reversion to austenite may occur when the annealing temperature increases to about 750 °C (Padilha et al. 2003; Singh 1985). The hardness profiles when corroborated with the microstructural matrix indicate that at $0.6T_m$ (761 °C) the hardness of specimen drops substantially due to recrystallization.

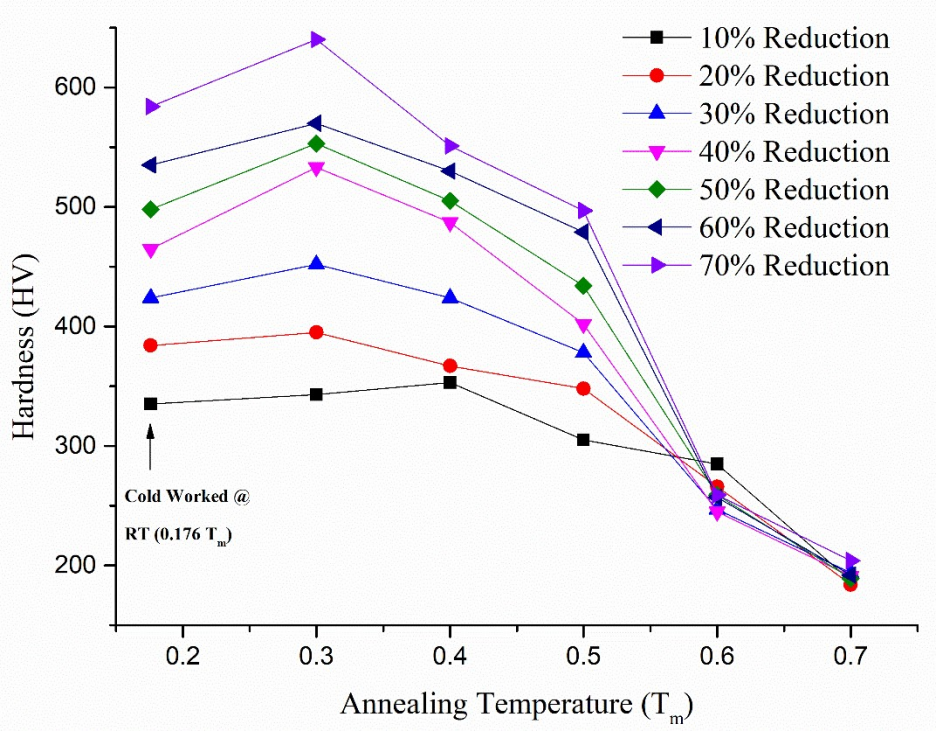

Figure 6.7: Hardness-profiles of cold-rolled SS 304 sheets with annealing temperature.

Engineering stress-strain curves of cold-reduced and annealed SS 304 are presented in Figures 6.8 and 6.9. Variation in the tensile behaviour of 10% reduced is quite gradual as a function of annealing temperature as shown in Figure 6.8. However, for 30%, 50% and 70% reduced sheets this is dramatic. There is a demarcation between the tensile behaviour of the material that is annealed below $0.5T_m$ and above $0.5T_m$. When this behaviour is corroborated with the microstructural matrix shown in Figure 6.6 and the

hardness profiles shown in Figure 6.7, it is clear that $0.6T_m$ is the recrystallization temperature of SS 304. These results also suggest that the threshold cold-reduction for the static-recrystallization to occur is 20%. However, irrespective of the degree of prior-coldworking, SS 304 displays an increasing-decreasing trend in the tensile-strength and the yield-strength.

The mechanical properties of prior-coldworked SS 304 following isothermal annealing-treatment are presented comprehensively in Figure 6.10. Variations in tensile-strength and yield-strength of the annealed sheets match well with the hardness profile. The ductility of SS 304 also varies accordingly. This mechanical behaviour of SS304 is previously reported by Kestenbach 1977; Yang and Spruiell 1982. Among the austenitic stainless steel (ASS) grades, SS304 being a low stack-fault energy (SFE) alloy has lower recrystallization temperatures as compared to SS 316 and SS 321 ASS. Recovery is believed to have small effect in restoration of hardness while recrystallization is the main softening process(Padilha et al. 2003). This work confirms the above reports and shows that at $0.7T_m$ (933 °C) the hardness values reduce below the hardness of as-received specimen due to grain-coarsening as indicated by the microstructural matrix presented in Figure 6.6.

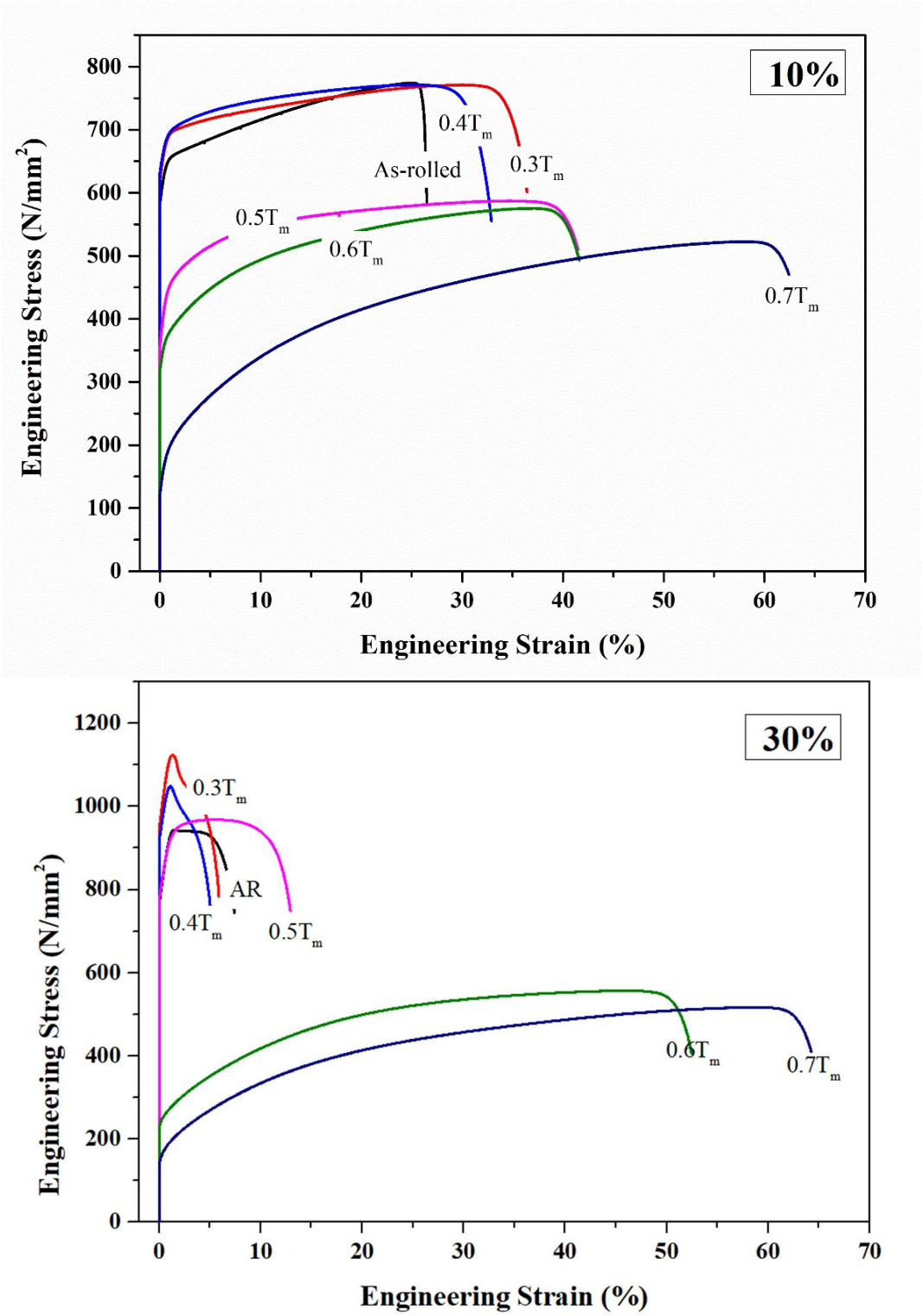

Figure 6.8: Engineering stress-strain curves of 10% and 30% reduced SS 304 after annealing at various temperatures; AR refers to as-rolled.

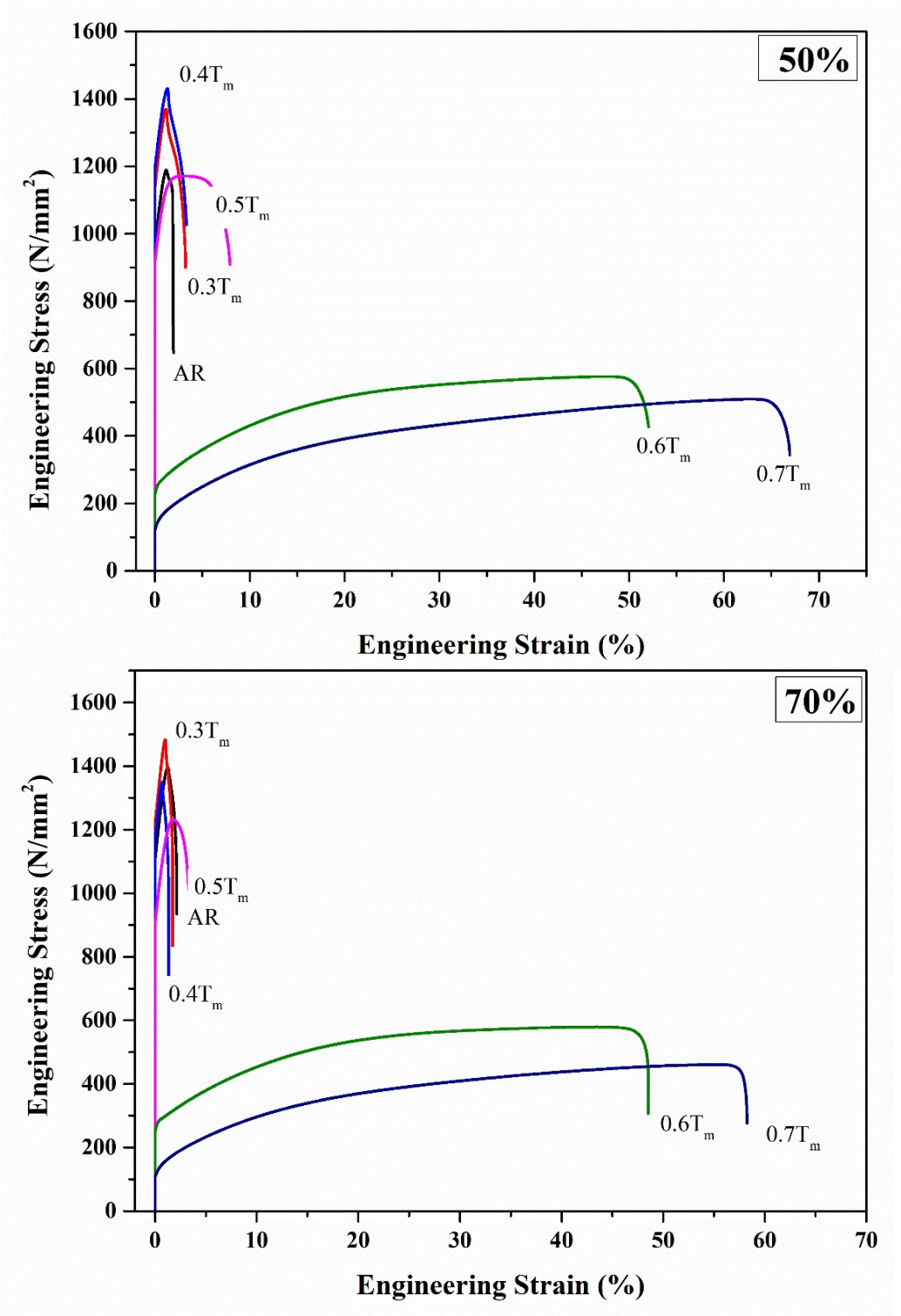

Figure 6.9: Engineering Stress-strain curves of 50% and 70% reduced SS 304 after annealing at various temperatures; AR refers to as-rolled.

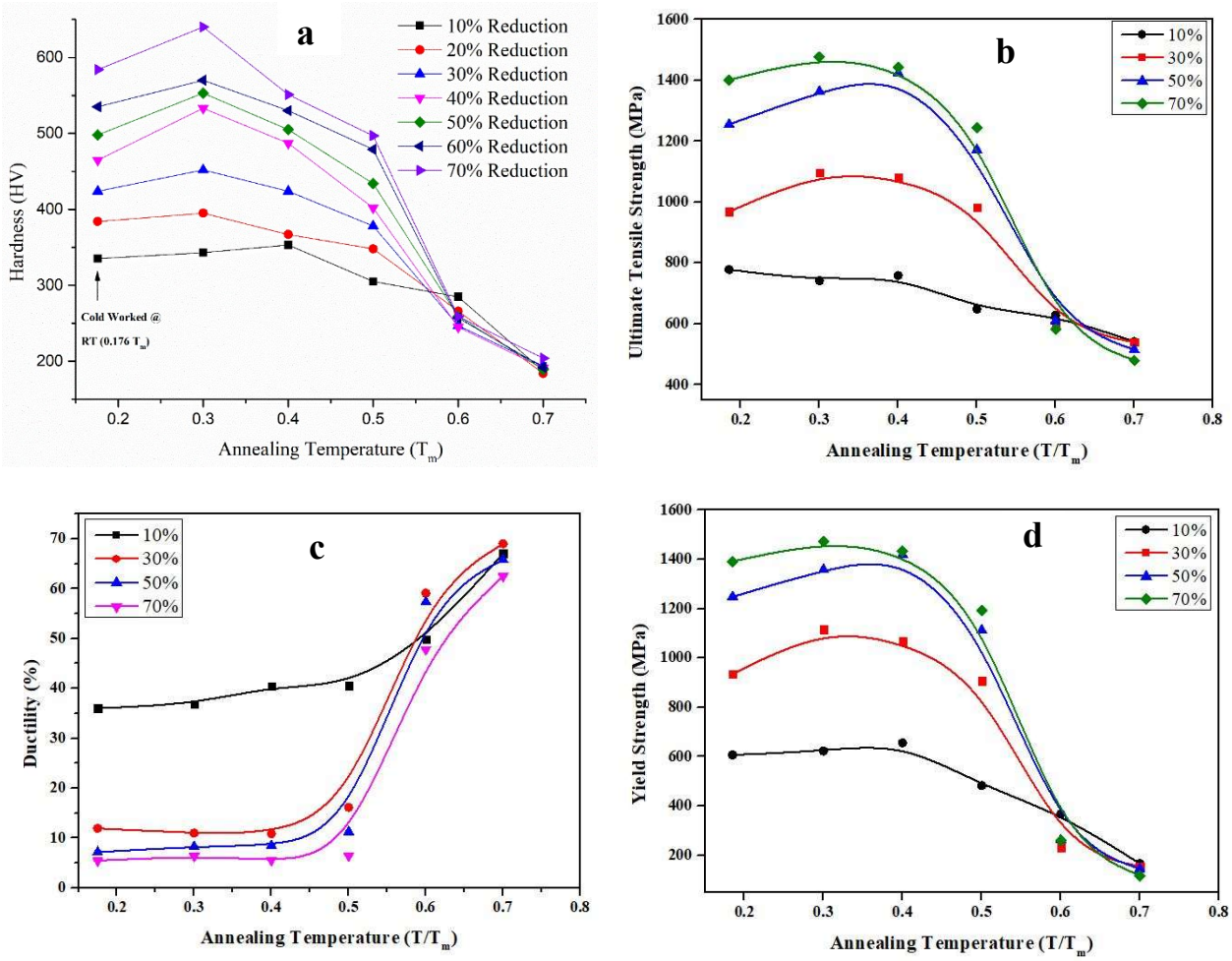

Figure 6.10: Mechanical properties of cold-rolled and annealed SS 304: a) hardness, b) tensile strength, c) ductility, and d) yield strength.

Figure 6.11 comparatively presents XRD profiles of as-rolled SS 304 sheets with that of $0.3T_m$ annealed sheets. Incremental variations in the relative peak-intensities of the primary γ phase and α′ martensite as shown in Figure 6.11a suggest that an increase in the cold-reduction increases strain-induced martensitic transformation. After annealing at $0.3T_m$ the α′martensite increases furthermore with highest increase observed for samples having highest deformation as shown in Figure 6.11b. However, 10% rolled sample does not show any significant change in α′martensite for $0.3T_m$ annealing.

Figure 6.12 presents XRD profiles of the rolled sheets that are annealed at $0.4T_m$, $0.5T_m$, $0.6T_m$, and $0.7T_m$. Here, α′martensite shows decreasing with increased annealing temperature. This suggests that at temperatures above $0.4T_m$ the strain-induced

martensite is unstable and starts reverting to the primary FCC γ-phase. For annealing temperatures of $0.5T_m$ and $0.6T_m$ the reversion is rapid with α′martensite observed only for samples rolled to high reduction. For $0.7\ T_m$ annealed samples it can be considered that the α′martensite is almost completely reverted to the primary austenite phase.

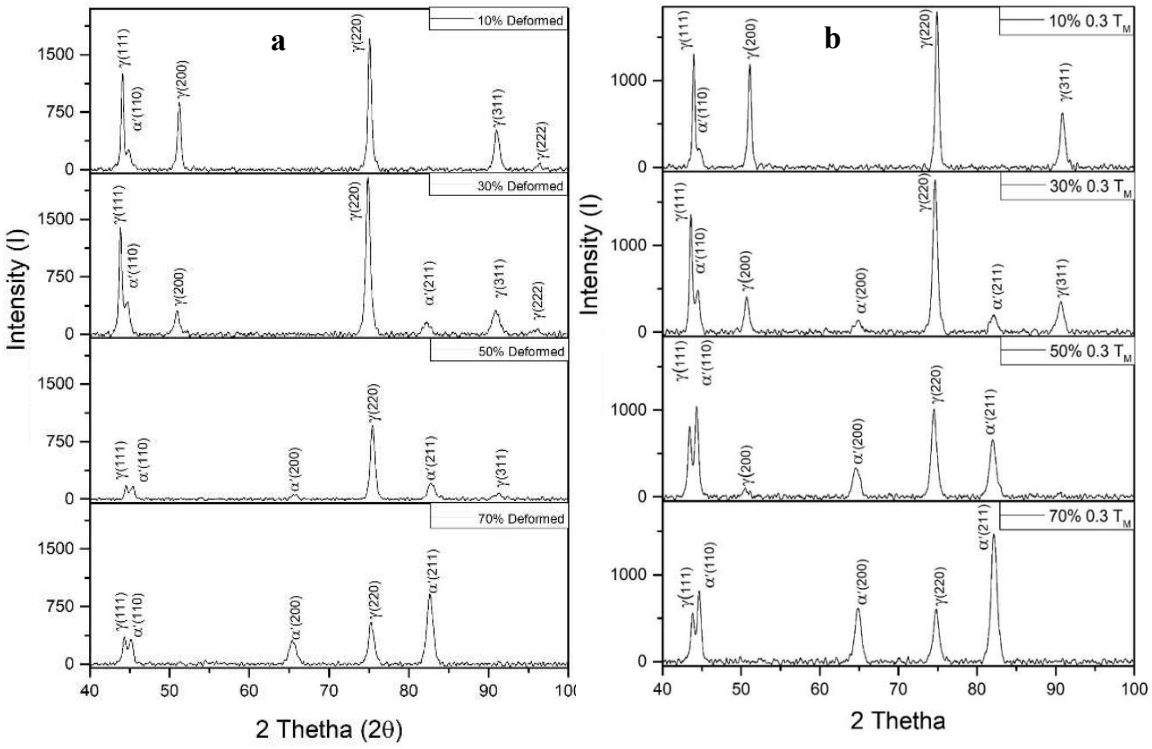

Figure 6.11: XRD profiles of 10%, 30%, 50%, and 70% deformed SS 304 sheets; a) before annealing, and b) after annealing at $0.3T_m$.

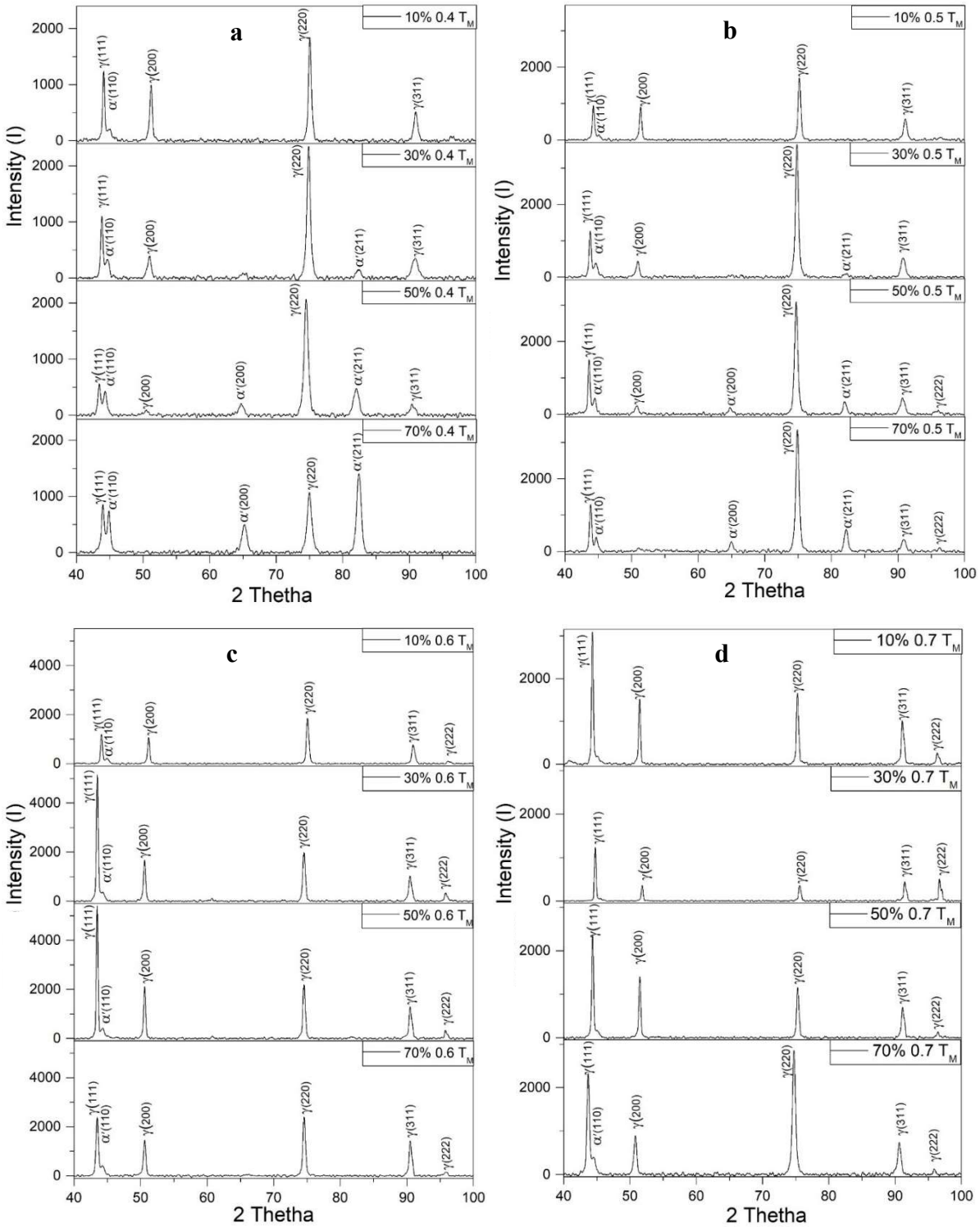

Figure 6.12: XRD profiles of 10%, 30%, 50%, and 70% deformed SS 304 sheets; a) after annealing at $0.4T_m$, b) after annealing at $0.5T_m$, c) after annealing at $0.6T_m$ and b) after annealing at $0.7T_m$.

Quantitative phase-fraction analysis for strain induced martensite (SIM) for different annealing temperatures was carried out by Gaussian peak-fitting method using the XRD profiles. The result of the analysis is presented in Table 6.1. The α′ phase-fraction profiles are presented in Figure 6.13. The phase-fraction profiles match with corresponding hardness profiles presented in Figure 6.7. This suggests that the hardening and softening behaviour during thermomechanical processing of SS 304 is predominantly due to the strain-induced martensitic transformation and reversion.

Table 6.1: Gaussian α′ phase-fraction (%) analysis of as-rolled and annealed SS 304.

Reduction	As-rolled	Annealed				
		$0.3T_m$	$0.4T_m$	$0.5T_m$	$0.6T_m$	$0.7T_m$
10%	7.5	6.1	6.6	5.0	5.0	0
30%	16.5	21.6	12.5	9.7	5.5	0
50%	31.3	54.6	30.8	16.6	7.2	0
70%	67.6	75.0	60.2	21.0	7.7	5.7

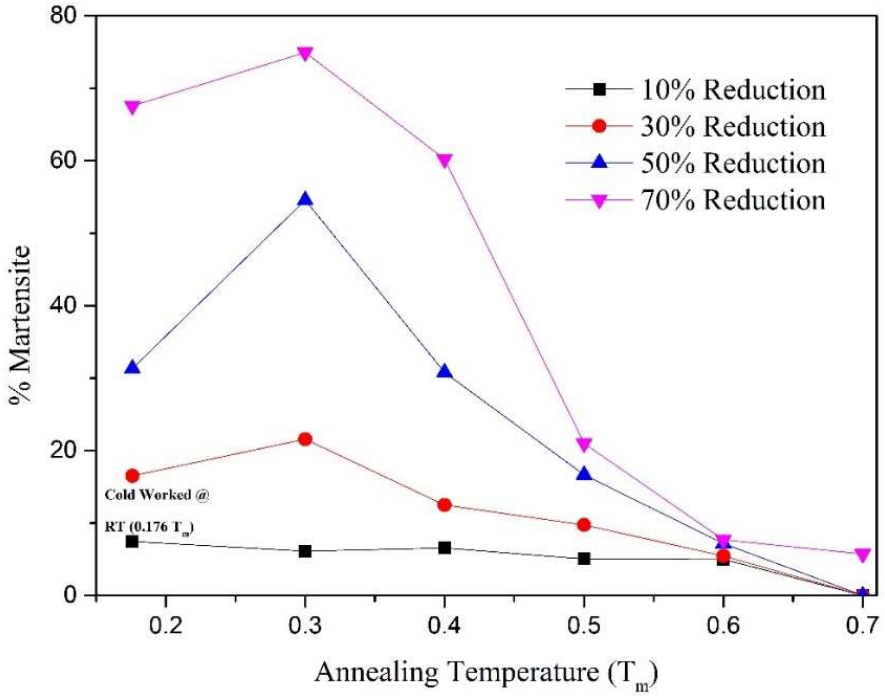

Figure 6.13: Gaussian α′ phase-fraction profiles of SS 304.

If XRD profile of mill-annealed as-received specimen is taken as the reference, the following key observations can be made.

1. Relative peak intensities of primary (γ) phase in as-rolled specimens vary monotonically with increased degree of cold-reduction suggesting that there is a strong texturing during cold-rolling. However, the XRD profiles of recrystallized specimens revert-back to that of mill-annealed condition suggesting that influence of texturing on the nucleation and growth of recrystallized grains is insignificant.
2. Peak intensities of secondary phase (α′) increase monotonically with increased degree of cold-reduction suggesting that strain-induced martensitic transformation in SS 304 is a function of degree of straining.
3. α′ peak intensities of cold-rolled specimens increase furthermore after annealing at $0.3T_m$ and decrease after annealing at higher temperatures. This suggests that transformation of γ into α′ occurs during low-temperature annealing of prior-coldworked SS 304. On exposure to higher temperatures, α′ reverts back to the primary γ phase.
4. Quantitative phase-fraction analysis based on Gaussian XRD peak-fitting analysis clearly demonstrates that there is an increasing and decreasing trend in α′ fraction of cold-reduced SS 304 as a function of annealing temperature.
5. The increasing-decreasing α′ martensite phase-fraction trend perfectly matches with the hardness profiles suggesting that the strain-induced martensitic transformation is attributed to the mechanical properties of thermomechanically processed SS 304.

EBSD Phase Fraction Maps are shown in Figure 6.14 and corresponding quantitative phase-fraction data is shown in Table 6.2. The EBSD phase-fraction analysis indicates increasing-decreasing trend in the α' martensitic phase-fraction confirming the phenomena of strain-induced transformation and reversion in cold-rolled and annealed SS 304.

Figure 6.15 presents EBSD IPF Maps of cold-reduced and annealed SS 304 sheets. Analogous to the microstructural matrix presented in Figure 6.6, here cold-reductions (10%, 30%, 50%, 70%) are arranged as rows and annealing temperatures (Room-

Temperature, $0.3T_m$ and $0.6T_m$) are arranged as columns. Essentially, this EBSD IPF matrix covers as-rolled condition, low-temperature annealing, and high temperature annealing effects for 10%-70% reduced SS 304.

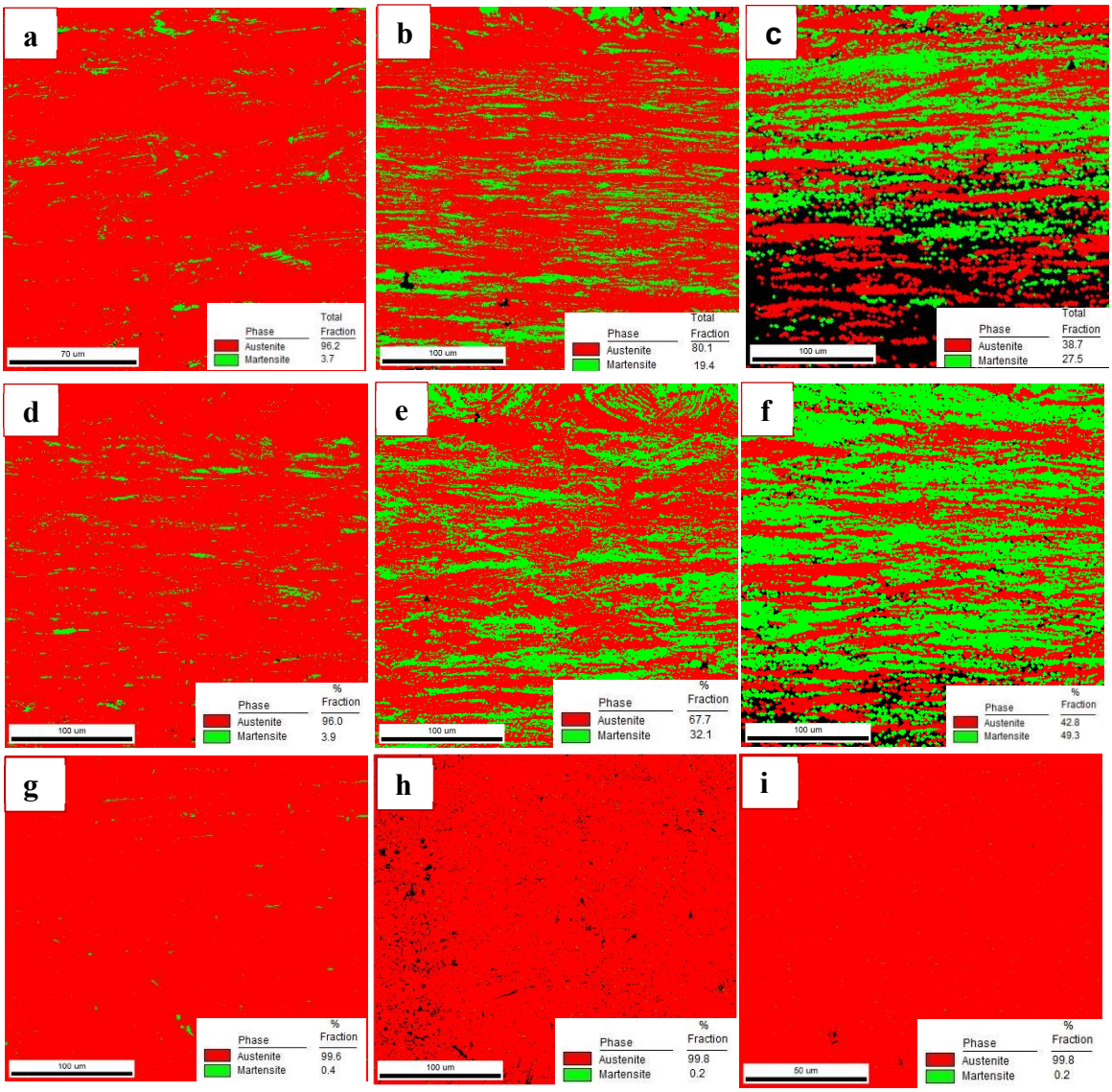

Figure 6.14: EBSD Phase Fraction Maps of SS 304 sheets that are cold-rolled to: 30%, 50%, and 70% (a, b, and c), followed by annealing at $0.3T_m$ (d, e, and f) and $0.6T_m$ (g, h, and i) showing strain-induced martensitic transformation and reversion.

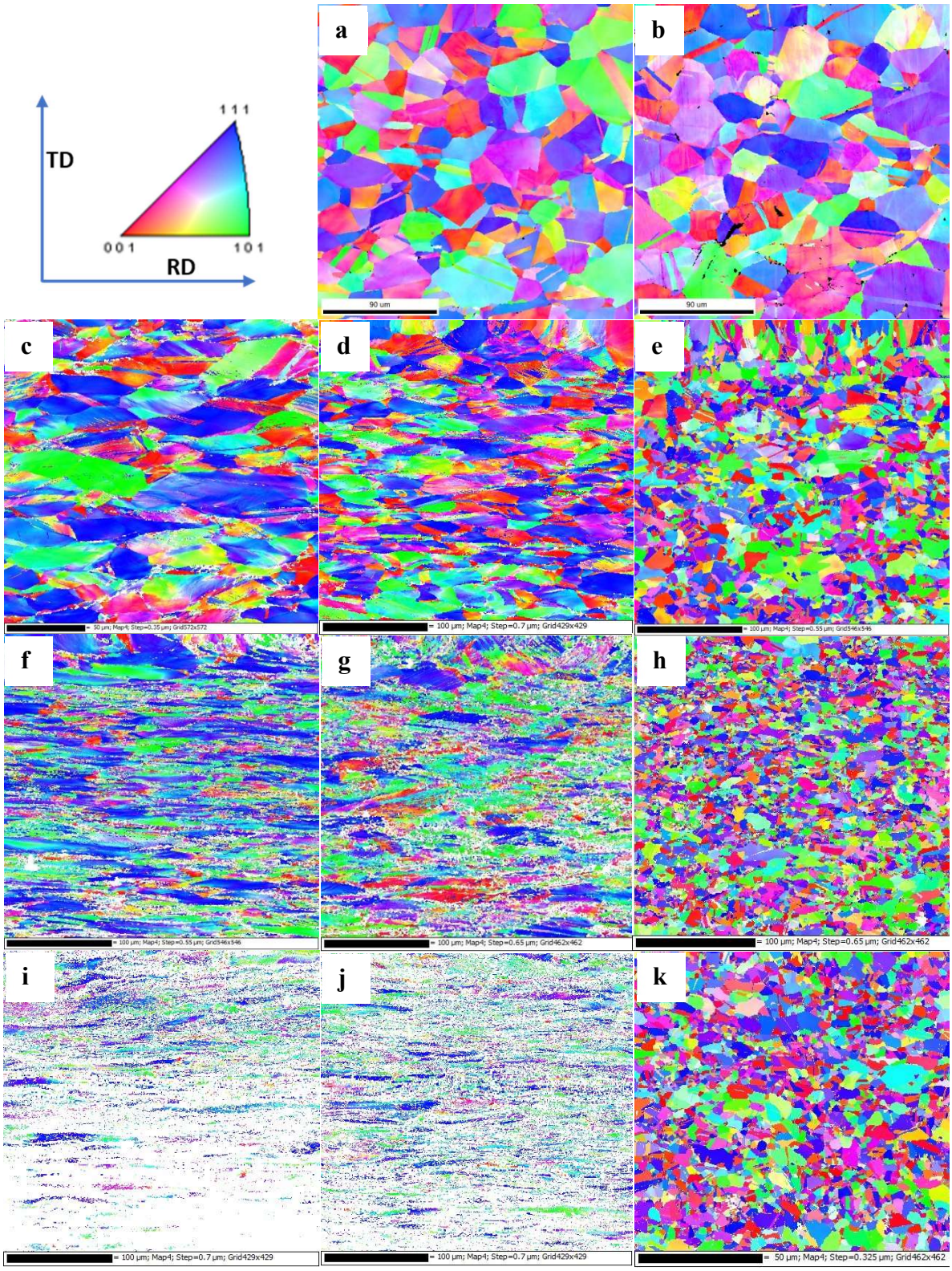

Figure 6.15: EBSD IPF Maps of 10%, 30%, 50% and 70% cold-rolled SS 304 that are annealed at room temperature (as-rolled), $0.3T_m$, and $0.6T_m$; cold-reductions are arranged as rows and annealing temperatures are arranged as columns; (RD, TD) rolling and transverse directions.

Table 6.2: EBSD Phase fraction (%) analysis of α′-martensite in cold-rolled and annealed SS 304.

Cold Reduction	As-Rolled	Annealed	
		$0.3T_m$	$0.6T_m$
30%	3.7	3.9	0.4
50%	19.4	32.1	0.2
70%	27.5	49.3	0.2

The first column represents the room-temperature annealing or as-rolled (AR) condition for 30%, 50% and 70% (c, f, i) reduced sheets. The second column represents $0.3T_m$ annealed condition for 10%, 30%, 50% and 70% (a, d, g, j) reduced sheets. Similarly, the third column represents $0.6T_m$ annealed condition for (0%, 30%, 50% and 70% (b, e, h, k) reduced sheets. This way, the grain-shapes of thermomechanically processed SS 304 are scanned over wide ranges of reduction and annealing temperature. The first and the second columns do not show any indication of recrystallization. The third column confirms that SS 304 recrystallizes when 30%, 50% and 70% cold-reduced sheets are exposed to $0.6T_m$. However, the coarse-equiaxed grains in figure 6.15b confirms that 10% cold-reduced SS 304 does not recrystallize even when exposed to $0.6T_m$. This observation endorses that the threshold cold-reduction of the recrystallization of SS 304 is 20% and the recrystallization temperature for the alloy is $0.6T_m$.

From the grain-shape point of view, this result is disappointing as there is no indication of recrystallized elongated grains having high aspect ratio along the rolling direction. Instead, SS 304 shows formation of fine-equiaxed grains during the recrystallization. Thus, unlike IN 601, the possibility of producing creep-resistant microstructure in SS 304 appears bleak.

6.3 Discussion

The experimental materials chosen for this work are similar in terms of the simple single-phase microstructure, FCC crystal structure, and composition. The methodology for processing, testing, and characterization applied in this work for IN 601 and SS 304 is also same. The hardening behaviour during cold-working and the softening behaviour during annealing are also comparable. Both the materials show an increasing-decreasing trend in the strength and hardness with an increase in the annealing temperature. Both the materials show peak-hardening during low-temperature annealing. Yet, only IN 601 shows tendency to form fine-elongated grains along the rolling-direction especially during the on-set of recrystallization. However, the microstructural analysis corroborated with the EBSD IPF maps confirm that SS 304 does not show any tendency to form elongated grains during recrystallization.

It is important to consider that there is a fundamental difference between IN 601 and SS 304. Being a Ni-based alloy, IN 601 possesses a high stacking fault energy (>35mJ/m^2). Thus, the tendency to form twins during cold-working or annealing is low in IN 601. However, SS 304 being a Fe-based alloy possess a low stacking fault energy (<20mJ/m^2). Thus, SS 304 should easily form twins during thermomechanical processing. The microstructures of SS 304 do not reveal twinning during cold-working (Figure 6.1) and annealing (Figure 6.2) as a grain-boundary etchant was used for revealing the variations in the shape and size of the grains. However, the EBSD IPF maps do show numerous twins oriented randomly especially in 10% rolled SS 304 (Figure 6.15a, 6.15b). At higher degrees of rolling there should be increased twinning. However, high dislocation densities, slipping, and the strain-induced martensitic transformation do not reveal the influence of twinning in the EBSD maps (Figures, 6.15c, 6.15f, 6.15i). But on recrystallization, a highly refined microstructure is obtained in SS 304. With increased cold-reduction and annealing temperature, the grain-refinement increases as confirmed by the microstructural matrix shown in Figure 6.2. The XRD quantitative analysis (Table 6.1) and EBSD phase-fraction maps (Figure 6.14) indicates that the strain-induced martensitic transformation has to occur at highly at regions of high dislocation density and may interfere with slip-bands and twins. Thus, multiple interfaces at the grain-boundaries as well as within the grains act as preferred nucleation sites for the recrystallization of SS 304. As a result, discretization of

nucleation and controlling the nucleation kinetics becomes difficult for such materials. This situation defeats the very idea proposed in this work. The same result was obtained in another high stacking fault energy material, silver in fine-equiaxed grains formed despite performing highly refined cold-reduction and annealing experiments (Kumar I. 2019). This suggests designing recrystallized elongated grains in low SFE materials is almost impossible.

As seen in IN 601, for high SFE materials, nucleation sites are limited to slip-bands and grain-boundaries since twinning is minimal. This should help in discretizing the nucleation by controlling the degree of cold-reduction and thermal exposures. During on-set of recrystallization, the discretely formed nuclei would typically grow along the slip-bands as indicated in the EBSD IPF map shown in Figure 5.12a. The grain-boundary map shown in Figure 5.13 indicates the same. This map shows that there are a few un-recrystallized grains present along with fine-elongated recrystallized grains suggesting that the on-set of recrystallization is the ideal condition for obtaining such microstructure. If the degree of cold-reduction or the thermal exposure is higher, densely formed nuclei, quick recrystallization should form fine-equiaxed grains as indicated in Figure 5.13b. Thus, it should be relatively easy for high SFE materials such as, Aluminium, Platinum and Nickel based alloys, to design fine-elongated recrystallized grains by carefully controlling the degree of cold-working and the annealing temperature.

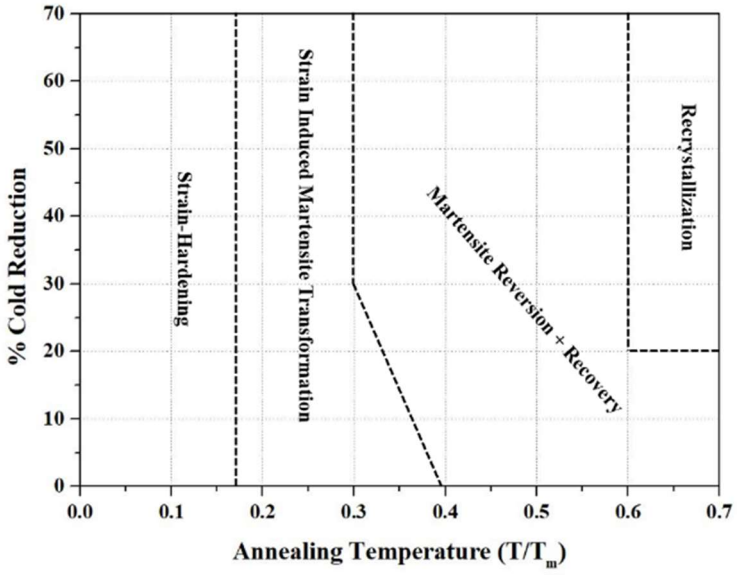

Figure 6.16: Thermomechanical Processing Map of SS 304.

Based on the experimental analysis carried out involving hardness profiles, engineering stress-strain curves, and the microstructural results presented in this work suggest that there are multiple stages in the annealing behaviour of SS 304 which includes strain-hardening, SIM transformation, Martensite Reversion and recovery, and recrystallization as the annealing temperature increases. To have a comprehensive picture on the thermomechanical processing of the alloy, a 'Thermomechanical Processing Map' is proposed as shown in Figure 6.16.

7. SUMMARY AND CONCLUSION

This section presents the summary and conclusions derived from the results and associated analysis of experimental work carried on Inconel 60 and SS 304 sheets. The contribution of this research works in the field of thermomechanical processing of IN 601 and SS 304 are highlighted and emphasized.

This work comparatively studied various metallurgical phenomena and associated variations in the structure and properties occurring during the thermomechanical processing of two commercially important M-type wrought materials, Inconel 601 and Stainless-Steel 304. By tracking the microstructural variation with the processing parameters, this work searched for an opportunity to produce elongated-recrystallized grains in wrought-alloys analogous to the columnar-grains in directionally solidified cast-alloys. When the hardness of the experimental materials was tracked with the processing steps, the work stumbled upon the static strain-ageing phenomenon occurring in both the materials that shows peak-hardening during low-temperature annealing irrespective of the degree of cold-reduction. Interestingly, the hardening and softening profiles during the work-hardening and annealing of both the materials are similar. However, peak-hardening in IN 601 is found to be due to the strain-ageing caused by the dislocation-pinning of interstitial carbon, while peak-hardening in SS 304 is found to be predominantly due to increased strain-induced martensitic transformation.

The work explored the possibility of controlling the shape of the grains in wrought materials by tracking the thermomechanical processing parameters to obtain a processing-window for producing fine-elongated grains in recrystallized form for improving the creep-properties relative to their equiaxed counterparts. Using microstructural analysis and EBSD analysis, the work demonstrated that, by carefully controlling the nucleation and recrystallization kinetics, it is possible to produced fine-elongated grains in IN 601. However, elongated grains could not be produced in SS 304 sheets. Considering that SS 304 is a low stacking fault energy material with high twinning tendency, fine equiaxed grains were produced. Using microstructural analysis,

mechanical testing, XRD analysis and EBSD analysis, this work presented isothermal annealing behaviour of prior-coldworked IN 601 and SS 304 sheets and the following are the conclusions based on the experimental results obtained.

1. Cold-Rolling of IN 601 from 0% to 80% reduction causes increased grain aspect ratio from 1:1 to 18:1, increased hardness from 220 to 486 HV, and increased tensile strength from 580 MPa to 1086 MPa in the rolling direction. Increase in the grain-aspect ratio with the cold-reduction found to be non-linear while increase in the hardness and the tensile strength found to be quite linear. Cold-Rolled SS 304 displays similar trends. However, SS 304 shows better work-hardening tendency as 0% to 80% cold-reduced SS 304 shows an increase in the hardness from 200 HV to 586 HV.
2. Irrespective of the degree of prior-coldwork, IN 601 displays strain-aging during low-temperature annealing preceded by recovery and recrystallization. Thus, the mechanical strength and the hardness of the prior-coldworked IN 601 sheets shows an increasing-decreasing trend with increasing annealing temperature. Similar trend is observed during the annealing of prior-coldworked SS 304. The peak-hardening in IN 601 is found to be due to dislocation-pinning by interstitial carbon while peak-hardening in SS 304 is found to be predominantly due to increased strain-induced martensitic transformation.

3. Static recrystallization of cold-worked and isothermally annealed sheets is quite complex as there is neither a definite threshold degree of cold-working nor a threshold temperature for the recrystallization of the material. Instead, the recrystallization temperature depends on the degree of cold-working; the higher the cold-reduction, the lower is the recrystallization temperature. Similarly, temperatures for peak-aging, and static-recovery depend on the degree of cold-reduction. Therefore, experimental thermomechanical processing maps for both IN 601 and SS 304 are proposed that identify various stages of annealing corresponding to the processing parameters.

4. Elongated recrystallized grains are produced successfully in IN 601. The EBSD analysis confirms that fine-elongated grains having aspect ratio up to 3:1 along the rolling direction are obtained by suitably controlling the recrystallization kinetics. The recrystallization rate is controlled by providing minimal driving force and activation energy. For IN 601 the processing-window for producing elongated grains is 50% cold-reduction followed by annealing at 0.7 T_m (880°C).

5. Based on the above findings, the work suggests that precipitation-free and dispersion-free M-type alloys having high stacking fault energy should promote the formation of fine-elongated grains during the on-set of recrystallization by carefully controlling the degree of cold-working and the annealing temperature. Conversely, the materials having low stacking fault energy would promote random twinning and hence causes the polygonization of grains. Thus, it is not possible to control the grain-shape of such materials by thermomechanical processing.

SCOPE FOR FUTURE WORK

The present work demonstrated that, by applying the thermomechanical processing method, fine-elongated grains in recrystallized form can be produced in a high stacking fault energy material, IN 601. This peculiar grain-morphology is ideal for fatigue-creep resistance. However, the potential advantages of this grain-morphology should be verified experimentally. The repeatability of the process should be checked by processing IN 601 to produce fine-elongated grains along the rolling direction. Once the repeatability is established, the process should be fine-tuned by applying subtle variations in the processing-parameters such that the grain-morphology is optimized. Following the process-optimization, the potential advantages of the elongated-grains should be quantitatively recorded by performing standard creep and fatigue tests. The work can be extended to confirm and validate the advantages of fine-elongated grains in other M-type high stacking fault energy materials such as, platinum, platinum-rhodium alloys, commercial aluminium-alloys, other wrought nickel-based superalloys, etc.

REFERENCES

Aboulfadl, H., Deges, J., Choi, P., and Raabe, D. (2015). "Dynamic strain aging studied at the atomic scale." *Acta. Mater.*, 86, 34–42.

Ahmad, S., and Channa, I. A. (2013). "Mathematical Relationship between Ferritic, Pearlitic and Average Grain Size of Steel." *J. Mod. Sci. Technol.,* 1(1), 1–18.

Al-Fadhalah, K. J. (2015). "Strain-Induced Martensite Formation and Recrystallization Behavior in 304 Stainless Steel." *J. Mater. Eng. Perform.*, 24(4), 1697–1709.

Armstrong, R. W. (1970). "The influence of polycrystal grain size on several mechanical properties of materials." *Metall. Trans. B,*1, 1169–1176.

Arzt, E., and Singer, R. F. (1984). "The effect of grain shape on stress rupture of the oxide dispersion strengthened Superalloy Inconel MA 6000." *Proc.,* Superalloys *1984: The Fifth Intl. Symp. on Superalloys, Metallurgical Society of AIME, PA., USA,* 367–376.

Asadi, M., Guillot, D., Weck, A., Hegde, S. R., Koul, A. K., Sawatzky, T., and Saari, H. (2012). "Constructing a Validated Deformation Mechanisms Map Using Low Temperature Creep Strain Accommodation Processes for Nickel-Base Alloy 718." *Proc., Pressure Vessels and Piping Conference*, *Vol. 2: Computer Technology and Bolted Joints,* ASME, Toronto, ON., Canada. 65–73.

Babu, S. S. (2022). "Thermo-Mechanical Processing." *Encyclopedia of Materials: Metals and Alloys*, Elsevier, 27–38.

Biswas, S., Ramachandra, S., Hans, P., and Kumar, S. P. S. (2022). "Materials for Gas Turbine Engines: Present Status, Future Trends and Indigenous Efforts." *J. Indian Inst. Sci.*, 102(1), 297–309.

Burgel, R., Grossmann, J., Lusebrink, O., Mughrabi, H., Pyczak, F., Singer, R. F., and Volek, A. (2004). "Development of a New Alloy for Directional Solidification of Large

Industrial Gas Turbine Blades." *Proc., Superalloys 2004: The Tenth Intl. Symp. on Superalloys*, TMS, PA., USA, 25–34.

Buscail, H., Perrier, S., and Josse, C. (2011). "Oxidation mechanism of the Inconel 601 alloy at high temperatures." *Mater. and Corr.*, 62(5), 416–422.

Calcagnotto, M., Ponge, D., and Raabe, D. (2010). "Effect of grain refinement to 1μm on strength and toughness of dual-phase steels." *Mater. Sc. and Eng. A*., 527(29-30), 7832-7840.

Chukhleb, A. N., and Martynov, V. P. (1959). "The change in phase composition of 18-8 type steels with temperature and plastic deformation." *Metal Sc. and Heat Treatment of Metals*, 1(9), 43–45.

Clemens, H., and Scheu, C. (2008). "Microstructure and Properties of Engineering Materials." *Neutrons and Synchrotron Radiation in Engineering Materials Science*, Wiley-VCH Verlag GmbH & Co. KGaA, 1–20.

Coleman, T. H., and West, D. R. F. (1976). "Deformation-induced martensite and its reversion to austenite in an Fe-16Cr-12Ni alloy." *Metals Technol.*, 3, 49–53.

Cottrell, A. H., and Bilby, B. A. (1949). "Dislocation Theory of Yielding and Strain Ageing of Iron." *Proc. Phys. Soc. A*, 62(1), 49–62.

Cribb, W. R., and Reed-Hill, R. E. (1977). "Static strain-aging in nickel 200 between 373 and 473 K." *Metall. Trans. A*, 8(1), 71–76.

Cui, C. Y., Tian, C. G., Zhou, Y. Z., Jin, T., and Sun, X. F. (2012). "Dynamic Strain Aging in Ni Base Alloys with Different Stacking Fault Energy." *Proc., Superalloys 2012: The 12th Intl Symp. on Superalloys*, Wiley, TMS, PA., USA 715–722.

Davis, J. R. (1997). *ASM Specialty Handbook: Heat-Resistant Materials*. ASM International, Materials Park, OH., USA.

Davis, J. R. (Ed.). (1998). *Metals Handbook Desk Edition*. ASM International, Materials Park, OH., USA.

De, A. K., Vandeputte, S., and Cooman, B. C. De. (1999). “Static strain aging behavior of ultra low carbon bake hardening steel.” *Scr. Mater.*, 41(8), 831–837.

Dieter, G. E., and Bacon, D. (1988). “Strengthening Mechanisms.” *Mechanical Metallurgy. SI Metric Edition*. McGraw-Hill Book Company, New York, USA, 184-240.

Donachie, M. J., and Donachie, S. J. (2002). *Superalloys: A Technical Guide*. ASM International.

Fischer, B., Freund, D., Brömel, T., and Völkl, R. (2001). “Practical Experience with New Oxide Dispersion Hardened Platinum Materials.” Proc., *25th International Precious Metals Conference*, Tucson, AZ., USA 1–22.

Fuchs, G. E. (2005). “High Temperature Alloys.” *Kirk-Othmer Encyclopedia of Chemical Technology*, John Wiley & Sons, Ltd, NY., USA.

Gauzzi, F., Montanari, R., Principi, G., and Tata, M. E. (2006). “AISI 304 steel: anomalous evolution of martensitic phase following heat treatments at 400°C.” *Mater. Sc. and Eng. A*, 438-440, 202-206.

Geddes, B., Leon, H., and Huang, X. (2010). *Superalloys: Alloying and Performance,* ASM International, Materials Park, OH., USA, 2-57.

Glenny, R. J. E., Northwood, J. E., and Burwood-Smith, A. (1975). “Materials for Gas Turbines.” *Intl. Metall. Rev.*, 20(1), 1–28.

Gopinath, K., Gogia, A. K., Kamat, S. V., and Ramamurty, U. (2009). “Dynamic strain ageing in Ni-base superalloy 720Li.” *Acta Mater.*, 57(4), 1243–1253.

Hadji, M., and Badji, R. (2002). “Microstructure and mechanical properties of austenitic stainless steels after cold rolling.” *J. Mater. Eng. Perform.*, 11(2), 145–151.

Hähner, P. (1993). “Modelling the spatiotemporal aspects of the Portevin-Le Châtelier effect.” *Mater. Sc. and Eng. A*, 164(1–2), 23–34.

Hähner, P., and Rizzi, E. (2003). “On the kinematics of Portevin–Le Chatelier bands: theoretical and numerical modelling.” *Acta Mater.*, 51(12), 3385–3397.

Hall, E. O. (1970). “Yield Point Phenomena and their Theoretical Background.” *Yield Point Phenomena in Metals and Alloys*. Springer, Boston, MA., US, 1-64.

Hänninen, H., Seifert, H.P., Yagodzinskyy, Y., Ehrstén, U., Tarasenko, O., and Aaltonen, P. (2003). “Effect of Dynamic Strain Aging on Environment-Assisted Cracking of Low Alloy Pressure Vessel and Piping Steels.” *Proc., VTT Symp. on Plant Life Management,* VTT Technical Research Centre of Finland, 199–221.

Hansen, N. (2004). “Hall-Petch Relation and Boundary Strengthening.” *Scr. Mater*., 51(8), 801-806.

Heckel, R. W. (1997). “Introduction to the Effects of Composition, Processing, and Structure on Materials Properties.” *Materials Selection and Design*, ASM Handbook, Vol 20, ASM International, Materials Park, OH., USA, 331-335.

Hedayati, A., Najafizadeh, A., Kermanpur, A., and Forouzan, F. (2010). “The effect of cold rolling regime on microstructure and mechanical properties of AISI 304L stainless steel.” *J. Mater. Process Technol.*, 210(8), 1017–1022.

Hong, S.H., Kim, H. Y., Jang, J. S., and Kuk, I. H. (1996). “Dynamic strain aging behavior of Inconel 600 alloy.” *Proc., Superalloys 1996: The Eighth Intl. Symp. on Superalloys,* Wiley, TMS, PA., USA 715-722, 401-408.

Jeong, S. W., Kang, U. G., Choi, J. Y., and Nam, W. J. (2012). “Comparative study of hardening mechanisms during aging of a 304 stainless steel containing α′-martensite.” *J. Mater. Eng. Perform.*, 21(9), 1937–1942.

Karjalainen, L. P., Taulavuori, T., Sellman, M., and Kyröläinen, A. (2008). “Some Strengthening Methods for Austenitic Stainless Steels.” *Steel. Res. Int.*, 79(6), 404–412.

Kassner, M. E., & Kassner, M. (2015). “Fundamentals of creep in materials.” *Fundamentals of creep in metals and alloys, 3rd edition,* Butterworth-Heinemann, Boston, USA, 1-6.

Kawasaki, M., and Langdon, T. G. (2013). “The many facets of deformation mechanism mapping and the application to nanostructured materials.” *J. Mater. Res.*, 28(13), 1827–1834.

Kestenbach, H. J. (1977). “Influence of dislocation substructure on recrystallization in type 304 stainless steel.” *Metall. Trans. A*, 8(1), 213–216.

Kishawy, H. A., and Hosseini, A. (2019). “Superalloys.” *Machining Difficult-to-Cut Materials. Materials Forming, Machining and Tribology*. Springer, Cham, 97-137.

Koyama, M., Akiyama, E., and Tsuzaki, K. (2013). “Factors affecting static strain aging under stress at room temperature in a Fe-Mn-C twinning-induced plasticity steel.” *ISIJ International*, 53(6), 1089-1096.

Kumar, B. R., Singh, A. K., Das, S., and Bhattacharya, D. K. (2004). “Cold rolling texture in AISI 304 stainless steel.” *Mater. Sc. and Eng.*, 364, 132-139.

Kumar I., R. (2019). “Recrystallization Behaviour of Silver.” *M. Tech Thesis*, National Institute of Technology Karnataka, Surathkal.

Lai, George. L. (2007). “Oxidation.” *High-Temperature Corrosion and Materials Applications*, ASM International, Materials Park, OH., USA, 5-66.

Lasalmonie, A., and Strudel, J. L. (1986). “Influence of grain size on the mechanical behaviour of some high strength materials.” *J. Mater. Sci.*, 21(6), 1837–1852.

Lee, S. H., Lee, J. C., Choi, J. Y., and Nam, W. J. (2010). “Effects of deformation strain and aging temperature on strain aging behavior in a 304 stainless steel.” *Metals and Materials International*, 16(1), 21–26.

Lee, S. I., Lee, S. Y., Lee, S. G., Jung, H. G., and Hwang, B. (2018). “Effect of Strain Aging on Tensile Behavior and Properties of API X60, X70, and X80 Pipeline Steels.” *Metals and Materials International*, 24(6), 1221–1231.

Malakondaiah, G., and Rama Rao, P. (1985). “Effect of Grain Size, Grain Shape and Subgrain Size on High Temperature Creep Behavior.” *Def. Sci. J.*, 35(2), 201–217.

Mangonon, P. L., and Thomas, G. (1970a). “Structure and Properties of Thermal-Mechanically Treated 304 Stainless Steel.” *Metall. and Mater. Trans.*, 1(6), 1587–1594.

Mangonon, P. L., and Thomas, G. (1970b). “The Martensite Phases in 304 Stainless Steel.” *Metall. and Mater. Trans.*, 1(6), 1577–1586.

McGuire, M. F. (2008). “Austenitic Stainless Steels,” *Stainless Steels for Design Engineers*. ASM International, Materials Park, OH., USA, 69-90.

Mehta, K. K., Mukhopadhyay, P., Mandal, R. K., and Singh, A. K. (2014). “Mechanical properties anisotropy of cold-rolled and solution-annealed Ni-based Hastelloy C-276 alloy.” *Metall. Mater. Trans. A Phys. Metall. Mater. Sci.*, 45(8), 3493–3504.

Meyers, M. A., and Chawla, K. K. (2008). “Creep and Superplasticity.” *Mechanical Behavior of Materials*. (2nd ed.) Cambridge: Cambridge University Press, 653-687.

Milad, M., Zreiba, N., Elhalouani, F., and Baradai, C. (2008). “The effect of cold work on structure and properties of AISI 304 stainless steel.” *J. Mater. Process Technol.*, 203(1–3), 80–85.

Mittemeijer, E. J. (2011). “Mechanical Strength of Materials.” *Fundamentals of Materials Science*. Springer, Berlin, Germany, 497-581.

Morris, D., and McGrath, R. (2013). “ZGS platinum materials for improved glass manufacturing equipment and laboratory ware.” *Platin. Met. Rev.*, 57(3), 230-232.

Morris, J. W., Jr. (2001). “The influence of grain size on the mechanical properties of steel.” *Technical Report by Lawrence Berkeley National Laboratory,* University of California, Berkeley, CA, USA, 1-8.

Mukherjee, A. K. (2002). “An examination of the constitutive equation for elevated temperature plasticity.” *Mater. Sc. and Eng. A.*, 322(1-2), 1–22.

Mukhopadhyay, C. K., Jayakumar, T., Kasiviswanathan, K. V., and Raj, B. (1995). "Study of ageing-induced α′-martensite formation in cold-worked AISI type 304 stainless steel using an acoustic emission technique." *J. Mater. Sci.*, 30(18), 4556–4560.

Nabarro, F. R. N. and Villiers, F. De (1995). "The phenomenology of creep." *The physics of Creep and Creep-resistant alloys*. Taylor and Francis, London, 15-45.

Naghizadeh, M., and Mirzadeh, H. (2016). "Microstructural Evolutions During Annealing of Plastically Deformed AISI 304 Austenitic Stainless Steel: Martensite Reversion, Grain Refinement, Recrystallization, and Grain Growth." *Metall. Mater. Trans. A.,* 47, 4210-4216.

Nowotnik, A. (2016). "Nickel-Based Superalloys." *Reference Module in Materials Science and Materials Engineering*, Elsevier, 6154-6155.

Padilha, A. F., Plaut, R. L., and Rios, P. R. (2003). "Annealing of cold-worked austenitic stainless steels." *ISIJ International*, 43(2), 135–143.

Rathbun, R. W., Matlock, D. K., and Speer, J. G. (2000). "Strain aging behavior of austenitic stainless steels containing strain induced martensite." *Scr. Mater.*, 42(9), 887–891.

Ravi Kumar, B., Das, S. K., Mahato, B., and Ghosh, R. N. (2010). "Role of strain-induced martensite on microstructural evolution during annealing of metastable austenitic stainless steel." *J. Mater. Sci.*, 45(4), 911–918.

Reed, R. C. (2006). "The physical metallurgy of nickel and its alloys." *The Superalloys: Fundamentals and Applications*, Cambridge University Press, Cambridge, 33-120.

Reed, R. C., and Rae, C. M. F. (2014). "Physical Metallurgy of the Nickel-Based Superalloys." *Physical Metallurgy: Fifth Edition*, Elsevier B.V, 2215-2290.

Reed, R. P. (1962). "The spontaneous martensitic transformations in 18% Cr, 8% Ni steels." *Acta Metall.*, 10(9), 865–877.

Schramm, R. E., and Reed, R. P. (1975). “Stacking fault energies of seven commercial austenitic stainless steels.” *Metall. Trans. A*, 6(7), 1345–1351.

Segal, V. (2005). “Equal-Channel Angular Extrusion.” *ASM Handbook Volume 14A, Metalworking: Bulk Forming*, ASM International, Materials Park, OH., USA, 528–536.

Semiatin. S. L. (Ed.). (2005). “Recovery, Recrystallization, and Grain-Growth Structures.” *ASM Handbook Volume 14A, Metalworking: Bulk Forming,* ASM International, Materials Park, OH., USA, 552–562.

Shen, Y. F., Li, X. X., Sun, X., Wang, Y. D., and Zuo, L. (2012). “Twinning and martensite in a 304 austenitic stainless steel.” *Mater. Sc. and Eng. A*, 552, 514–522.

Singh, J. (1985). “Influence of deformation on the transformation of austenitic stainless steels.” *J. Mater. Sci.*, 20(9), 3157–3166.

Singh, R. K., and Sahu, J. K. (2019). “Yield strength anomaly and dynamic strain ageing behaviour of recently developed advanced ultra-supercritical boiler grade wrought Ni-based superalloy IN 740H.” *Materials at High Temperatures*, 36(3), 220-231.

Sourabh, K., and Singh, J. B. (2022). “Tensile Behavior of Alloy 690 in the Dynamic Strain Aging Regime.” *J. Mater. Eng. Perform*.

Spencer, K., Embury, J. D., Conlon, K. T., Véron, M., and Bréchet, Y. (2004). “Strengthening via the formation of strain-induced martensite in stainless steels.” *Mater. Sc. and Eng. A*, 387–389(1-2), 873–881.

Stahl, H., Smith, G., and Wastiaux, S. (2001). “Strain-age Cracking of Alloy 601 Tubes at 600 °C.” *J. Failure Analysis and Prevention*, 1(1), 51–54.

Staudhammer, K. P., Murr, L. E., and Hecker, S. S. (1983). “Nucleation and evolution of strain-induced martensitic (b.c.c.) embryos and substructure in stainless steel: A transmission electron microscope study.” *Acta Metall.*, 31(2), 267–274.

Stewart, G. R., and Jonas, J. J. (2004). “Static and Dynamic Strain Aging at High Temperatures in 304 Stainless Steel.” *ISIJ International*, 44(7), 1263–1272.

Sundara Raman, S. G., and Padmanabhan, K. A. (1994). “Tensile deformation-induced martensitic transformation in AISI 304LN austenitic stainless steel.” *J. Mater. Sci. Lett.*, 13(5), 389–392.

Talonen, J., and Hänninen, H. (2004). “Damping properties of austenitic stainless steels containing strain-induced martensite.” *Metall. Mater. Trans. A.,* 35 A (8), 2401–2406.

Teichmann, K., Liebscher, C. H., Völkl, R., Vorberg, S., and Glatzel, U. (2011). “High temperature strengthening mechanisms in the alloy platinum-5% rhodium DPH.” *Platin. Met. Rev.*, 55(4), 217–224.

Verlinden, B., Driver, J., Samajdar, I., and Doherty, R. D. (2007). *Thermo-mechanical processing of metallic materials*. Pergamon Materials Series, Cahn, R., W., ed., Elsevier, 1-528.

Wang, Z., and Gong, B. (2002). “Residual stress in the forming of materials.” *Handbook of residual stress and deformation of steel*, ASM International, Materials Park, OH., USA, 141-149.

Wesselmecking, S., Song, W., and Bleck, W. (2022). “Dynamic and Static Strain Aging in a High-Manganese Steel.” *Steel Res. Int.*, 93(7).

Wilcox, B. A., and Clauer, A. H. (1972). “The role of grain size and shape in strengthening of dispersion hardened nickel alloys.” *Acta Metallurgica*, 20(5), 743-757.

William, C. H., Chester, T., and Norman, S. S. (1987). *Superalloys 2: High-Temperature Materials for Aerospace and Industrial Power*. J. Wiley & Sons.

Yang, S. W., and Spruiell, J. E. (1982). “Cold-worked state and annealing behaviour of austenitic stainless steel.” *J Mater Sci*, 17(3), 677–690.

Zhao, W., Chen, M., Chen, S., and Qu, J. (2012). “Static strain aging behavior of an X100 pipeline steel.” *Materials Science and Engineering: A*, 550, 418–422.

Zhao, Y., Yao, H., Song, X., Jia, J., and Xiang, Z. (2018). “Predicting creep strengths and lifetimes of creep resistant engineering alloys.” *Metals and Materials International*, 24(1), 51–59.

PATENT AND PUBLICATIONS

1. "Method and System for Producing Elongated Grain in Wrought Metals with Superior Creep Resistance". **Indian Patent No: 465865**, granted on 06-11-2023. Authors: Subray R. Hegde & Preetish C. Dsilva.

2. "Annealing Behaviour of Cold Rolled Inconel 601". **Preetish C. Dsilva**, Basavaraj Padasale, Jitesh Vasavada, Sushil Mishra & Subray R. Hegde, Journal of Materials Engineering and Performance (2023). https://doi.org/10.1007/s11665-023-08681-z

3. "Role of δ-Phase on Recrystallization Behavior of Inconel 718"; Basavaraj Padasale, **Preetish Dsilva**, Lokendra Potphode, Subray Hegde; Materials Science and Technology, 2024; 40(2), 120-140. doi:10.1177/02670836231212617

4. "Recrystallization Behavior of Inconel 601 Sheets". Intl. Conference on Advances in Materials & Processing: Challenges & Opportunities, at IIT Roorkee, November 30-Decemeber 2, 2017. (Conference Papers Presented).

5. "Recrystallization Studies of Inconel 601 and Stainless Steel 304 Sheets". The 7th National Conference on Processing and Characterization of Materials (NCPCM) at NIT, Rourkela. (Conference Papers Presented).

6. "Failure of Soap Extruder Bolt Assembly"; J. K. Rakshan Kumar, Natesh Mogra, Basavaraj Padasale, **Preetish C. Dsilva**, Pavankumar Sondar & Subray R. Hegde; Failure Analysis and Prevention, 23, 1469–1483 (2023). DOI:10.1007/s11668-023-01708-6

7. "Creep cavitation damage of K-type thermocouples"; J.K. Rakshan Kumar, Debalina Bhattacharjee, **Preetish Dsilva**, R. Praveen, Subray R. Hegde,

Engineering Failure Analysis, Volume 143, Part A, 2023, s106846, DOI: 10.1016/j.engfailanal.2022.106846.

8. “Biodegradation of PEEK Piston Rings”; Preethi Shetty, **Preetish Dsilva**, Pavankumar Sondar, B. Ganesh Kumar, Subray Hegde, Polymer Degradation and Stability, Volume 191, 2021, 109666, DOI: 10.1016/j.polymdegradstab.2021.109666.

9. “Failure Analysis of Reciprocating CO2 Compressor”; **Preetish C. Dsilva**, Preethi Shetty, Pavankumar R. Sondar, B. Ganesh Kumar & Subray R. Hegde, Journal of Failure Analysis and Prevention, 21, 595–603 (2021), DOI: 10.1007/s11668-020-01109-z.

10. “Premature failure of superheater tubes in a fertilizer plant”; **Preetish C. Dsilva**, Sadhana Bhat, Jagadish Banappanavar, Krishnaraja G Kodancha, Subray R. Hegde, Engineering Failure Analysis, Volume 121, 2021, 105152,), DOI: 10.1016/j.engfailanal.2020.105152.

11. “Catastrophic failure of urea Prill-tower fan”; Subray R. Hegde, J.K. Rakshan Kumar, Pavankumar Sondar, **Preetish C. Dsilva**, Engineering Failure Analysis, Volume 121, 2021, 105207, DOI: 10.1016/j.engfailanal.2020.105207.

12. “Failure of a Cooling Water Pump Shaft”; Pavankumar R. Sondar, J. K. Rakshan Kumar, Sanjay Chawla, **Preetish C. Dsilva** & Subray R. Hegde, Journal of Failure Analysis and Prevention, Volume 21, 149–159 (2021), DOI: 10.1007/s11668-020-01043-0.

BIODATA

Name: Preetish Crimson Dsilva

Father's name: Louis Dsilva

Mother's name: Lydia Dsilva

Nationality: Indian

Contact details:

Mobile: +91 9916416479

Email id: pritish.dsilva@gmail.com

Permanent Address:

D/No: 2-78/5(5), Flat No: G3,

Carmel View Apartments,

Jayanagar Road, Near St. Joseph Monastery,

Jayashree Gate, Kulshekar,

Mangalore- 575005

Karnataka, India.

Present Address:

Element- Metallurgical Services Pvt Ltd.

Mehta House, Ashok Silk Mills Lane, Off,

Lal Bahadur Shastri Marg, Ghatkopar

West, Mumbai- 400086,

Maharashtra, India.

Educational Qualifications:

Course	Institute	University	Year
M. Tech (Process Metallurgy)	National Institute of Technology Karnataka, Surathkal.	National Institute of Technology Karnataka, Surathkal.	2011-2013
B.E (Mechanical Engg.)	St. Joseph Engineering College, Mangalore.	Visvesvaraya Technological University, Belagavi.	2003-2007